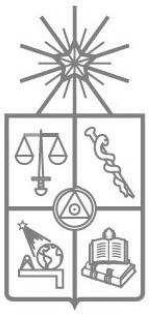

UNIVERSIDAD DE CHILE
FACULTAD DE CIENCIAS FÍSICAS Y MATEMÁTICAS
DEPARTAMENTO DE ASTRONOMÍA

SEARCH FOR UNSEEN PLANETS USING TRANSIT TIMING VARIATIONS

TESIS PARA OPTAR AL GRADO DE DOCTOR EN CIENCIAS, MENCIÓN ASTRONOMÍA

SANTIAGO DE CHILE
ENERO 2012

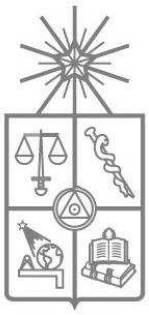

UNIVERSIDAD DE CHILE
FACULTAD DE CIENCIAS FÍSICAS Y MATEMÁTICAS
DEPARTAMENTO DE ASTRONOMÍA

SEARCH FOR UNSEEN PLANETS USING TRANSIT TIMING VARIATIONS

TESIS PARA OPTAR AL GRADO DE DOCTOR EN CIENCIAS, MENCIÓN ASTRONOMÍA

SERGIO DAVID HOYER MIRANDA

PROFESOR GUÍA:
PATRICIO ROJO RUBKE
PROFESOR CO-GUÍA:
MERCEDES LÓPEZ MORALES

MIEMBROS DE LA COMISIÓN:
DANTE MINNITI
MARIO HAMUY WACKENHUT
RENE MENDEZ BUSSARD

SANTIAGO DE CHILE
ENERO 2012

Resumen

Observaciones de cambios en el periodo orbital de planetas extrasolares transitantes permite la detección de compañeros orbitales todavía *inadvertidos* en el sistema. Con esta técnica, conocida como Variaciones Temporales de Tránsitos (TTVs por sus siglas en ingles), es posible detectar perturbadores incluso en el regimen de masas terrestres, sobrepasando la sensibilidad de las actuales búsquedas de exoplanetas por medio de velocidades radiales. Esta Tesis ha iniciado un proyecto de más largo plazo: *TraMoS*: Transit Monitoring in the South (Monitoreo de Tránsitos en el Sur), que consiste en un cuidadoso y homogéneo monitoreo fotométrico de planetas extrasolares observables en el Hemisferio Sur, con el fin de buscar compañeros orbitales y potencialmente descubrir planetas con masas similares a la terrestre. Adicionalmente, la acumulación de las curvas de luz de estos exoplanetas ha permitido refinar parametros físicos, tales como su inclinación orbital, radio y por lo tanto, su masa total y densidad media. Todos estos parámetros son críticos a la hora de restringir modelos necesarios para entender la física de los interiores de exoplanetas y su evolución. La detección de estos exoplanetas via TTVs es clave, además, para determinar la arquitectura de los sistemas exoplanetarios, y por lo tanto, muy necesarios para discriminar entre diferentes modelos de formación y evolución de planetas extrasolares.

En esta tesis doctoral se presentan las observaciones de 29 tránsitos de 4 exoplanetas: OGLE-TR-111b, WASP-5b, WASP-4b y WASP-7b. Basados en el análisis de las curvas de luz, a todos estos exoplanetas se le refinaron las efemérides y parametros físicos. El análisis temporal de estos tránsitos no entregó evidencias de la presencia de posibles compañeros orbitales con masas mayores a $\sim 10\ M_{\oplus}$ y fue posible establecer límites muy estrictos en la masa de posibles *perturbadores* en estos sistemas especialmente en las resonancias orbitales de los planetas transitantes. Estos resultados apoyarían los modelos teóricos de formación que predicen la escacez de planetas adicionales en sistemas con planetas "*tipo Júpiter*".

Abstract

Observing the changes in the orbital period of transiting exoplanets produced by gravitational perturbations allows to detect *unseen* orbital companions in the system. With this technique, known as Transit Timing Variations (TTVs), it is possible to detect perturbers down to Earth-like masses, overcoming the limits of current Radial Velocity searches. This PhD thesis has led to a long term project: Transit Monitoring in the South (*TraMoS*) project, which consists in a methodical and homogeneous monitoring of transiting exoplanets observable from the Southern Hemisphere with the goal of searching for orbital companions, and potentially finding Earth-mass planets. Aditionally, the cumulative light curves provide improved values of the physical parameters of the planets, such as orbital inclination and radius, and from those absolute mass and mean planetary density, which are critical to our model understanding of the physics of exoplanetary interiors and their evolution. Also, establishing the presence or absence of other planetas helps determine the architecture of multi-planetary systems, and therefore is key to discriminate between different models of formation and evolution of exoplanets.

In this Thesis I present the observations and analysis of 29 transits of 4 exoplanets: OGLE-TR-111b, WASP-5b, WASP-4b and WASP-7b. Based on the analysis of the light curves of these exoplanets we refined the ephemeris and physical parameters of all these exoplanets. Based on the temporal analysis, we found no evidence of the presence of additional planets with masses larger than $\sim 10\ M_{\oplus}$ in those systems. We place strong limits in the mass of possible *perturbers* especially in the orbital resonances with the transiting planets. These results support the formation theories that predict a paucity of planetary companions to Jupiter-like planets.

Dedicado a mi mama, mamita wally y papito checho.

Agradecimientos

Quisiera agradecer a Pato y a Mercedes, por la confianza, motivación, consejos y guía. Y por supuesto por su amistad. Quisiera agradecer a **todo** *Cerro Calan* (profesores, funcionarios y estudiantes) que me dejó ser parte de su comunidad, me acogió y me permitió desarrollar este proyecto y vivir un tiempo inolvidable. Gracias a todo el *staff* de Tololo y Pachón (administrativos, choferes, cocineros, janitors, técnicos y asistentes de observación) por su ayuda en todas jornadas de observación, por el buen '18' y la última Navidad. En especial quisiera agradecer a Ximena Herreros, Curita Gómez, Alberto Pastén, Patito Ugarte y Mauricio Rojas.

Gracias también para mi amigos y compañeros de oficina Zeus (Andrés Guzman), Matias Jones, Felipe Santana, Celia Verdugo, Thomas De Jaeger y todos con los que compartí durante estos años. Sin su ayuda y jugo no habría sido posible sobrevivir un doctorado.

Muchas gracias a mi polola Bárbara Rojas Ayala, por su amor y por dejarme ser su fan#1.

Finalmente quisiera agradecer por sobretodo a mi familia, por su cariño y apoyo en los momentos precisos, por estar siempre cerca incondicionalmente.

Contents

List of Figures

List of Tables

Chapter 1

Introduction

Since the discovery of the first extrasolar planet around the solar-like star 51 Peg by radial velocities (Mayor & Queloz 1995) and the dicovery of the first transiting planet around the nearby solar-type star HD 209458 (Charbonneau et al. 2000, Henry et al. 2000) a number of systematic extrasolar planetary searches have spread adopting a variety of techniques: radial velocities, transits, microlensing, astrometry and imaging, among others. As a combined results of such techniques, the number of discovered exoplanets (currently are about 700 confirmed objects) keeps growing at a stunning rate, as shown in Figure 1.1.

The radial velocity (RV) technique, based in *Doppler* measurements of the reflex motion of the host star induced by the orbital motion of the planet, is the most prolific approach. To date, over two thirds of the known exoplanets have been discovered via this technique[1].

The transit surveys are currently the second most successful with the detection of more than 200 planets. When a planet crosses in front of a star (in our line of sight), it blocks part of the light emitted by the star, tipically of the order of a few percent. The detection of this star's brightness drop is the aim of the transit searches.

Given the large number of ongoing ground-based surveys (e.g. OGLE, SuperWASP, HatNet, MEarth, TrES) and space-based surveys (e.g. MOST, CoRoT, Kepler) the number of transiting planets is expected to continue increasing rapidly. In fact, the Kepler Space mission has released a list of ~ 1200 exoplanet candidates (Borucki et al. 2011). They are cataloged as *candidates* since they show transit-like signatures in Kepler data but have not yet passed all the consistency tests of the *Kepler Science Team* and/or are not yet confirmed by means of precise RV measurements, TTVs or other methods. Most of the about 200 confirmed transiting exoplanets correspond to *Hot Jupiters*, defined as Jupiter-mass objects orbiting their host star with periods of few days (see Figure 1.2 and 1.3).

From the transit light curves it is possible to measure/infer, among other parameters, the depth of the transit, δ, the impact parameter, b, and the transit duration (time between the first and fourth contact), T (see Figure 1.4). Not considering limb darkening effects we have the following simple relationships:

[1] exoplanet.eu

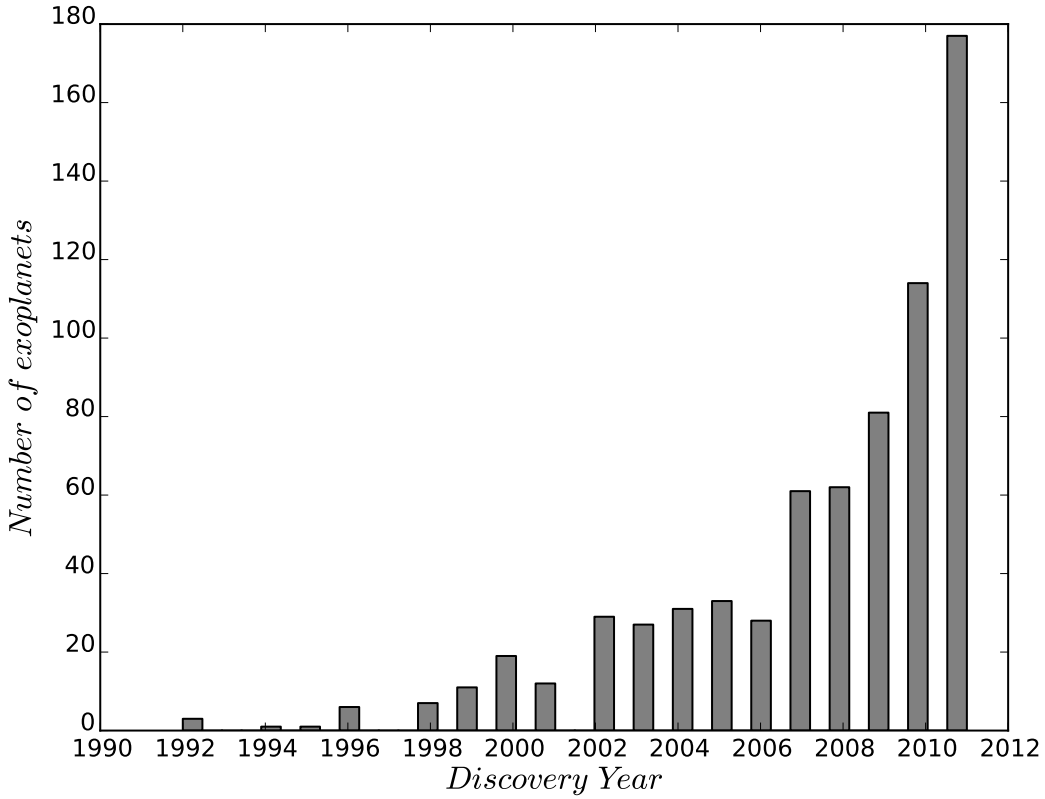

Figure 1.1 Distribution of the number of exoplanets detected ($\sim$ 700 objects) as a function of its year of discovery. Compiled with data from the on-line exoplanet encyclopaedia: exoplanet.eu as of 2011-12-04.

$$\delta \approx \frac{R_{planet}^2}{R_{star}^2}, \tag{1.1}$$

$$b = \frac{a \cos i}{R_{star}} \left(\frac{1 - e^2}{1 + e \sin \omega} \right), \tag{1.2}$$

$$T = \frac{P R_{star}}{\pi a} \sqrt{\left(1 + \frac{R_{planet}}{R_{star}}\right)^2 - \left(\frac{a}{R_{star}} \cos i\right)^2} \tag{1.3}$$

where P, a, i, e and ω are the orbital period, semi-major axis, inclination with respect of the line of sight, eccentricity and the periastron longitude, respectively. R_{star} and R_{planet} represent the radius of the host star and the transiting planet (for details see e.g. Seager & Mallén-Ornelas 2003, Winn 2010).

The transit technique is indeed the only way to measure the planet-to-star radius ratio and the orbital inclination. Combined with RV measurements, which give estimations of the *minimum mass* of the planet ($M_P \sin i$), it allows the determination of the mass and

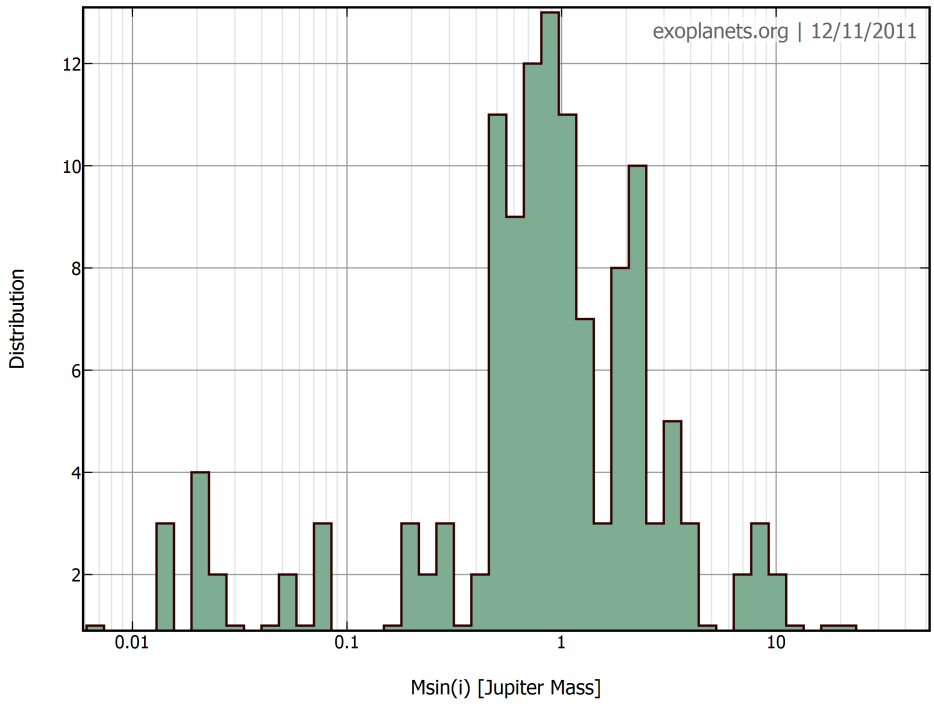

Figure 1.2 Histogram of the mass of the $\sim$ 180 detected transiting exoplanet. The peak of the distribution is around $\sim 1\ M_{JUP}$, but the detection limit is decreasing significatively with the improvement of the search techniques. From the Exoplanet Orbit Database and the Exoplanet Data Explorer at exoplanets.org as of 2011-11-12.

consequently, the mean density of the planet, all of them critical quantities to study the physics of exoplanetary interiors and the exoplanet's formation and evolution.

Moreover, transiting planets enable several other studies such as the determination of the projected spin-orbit angle (Figure 1.5), i.e. the projection on the sky of the angle between the star's rotation axis and the planet's orbital axis, through the measurement of the Rossiter-McLaughlin effect (Rossiter 1924, McLaughlin 1924). The study of star spots can also be done with transiting planets, identifying protuberances or bumps in the transit light curves (e.g. Silva-Valio 2008, Sanchis-Ojeda et al. 2011). These light curve anomalies permit the modeling of the spot sizes and its distribution and therefore, the activity, rotation period and rotation angle of the star can also be estimated.

Additionally the transiting planets, specially those that orbit bright stars due to signal-to-noise considerations, permit the study of the exoplanet atmospheres when the planet is transiting, a fraction of the stellar light crosses the exoplanet atmosphere and gets imprinted with absorption signatures in the stellar spectrum (e.g. Vidal-Madjar et al. 2004, Bean et al. 2010). Moreover, detections of the planetary emission itself can be detected via infrared secondary eclipse observations (Deming et al. 2005, Charbonneau et al. 2005, Sing & López-Morales 2009, Cáceres et al. 2011, Désert et al. 2011).

Arguably, one of the most exciting aspects of the current research on transiting planets is the possibility of detecting unseen orbital companions in the system. These detections can be achieved via the Transit Timing Variations (TTV) technique. This PhD thesis focuses on this technique and consists in the monitoring of a large sample of transiting planets observable

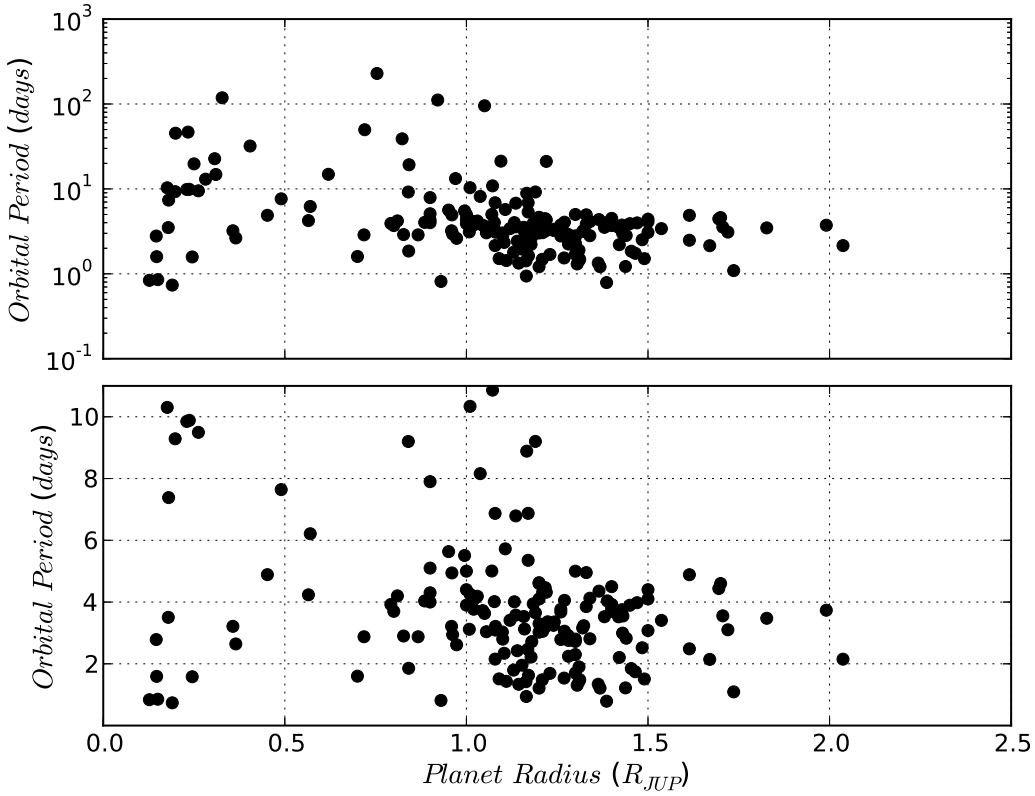

Figure 1.3 Top panel: Distribution of the radius and orbital period of $\sim$ 180 transiting exoplanets. Bottom panel: a close view of the distribution shows that most of the exoplanets detected so far have sizes similar to Jupiter with periods of a few days. Data from the on-line exoplanet encyclopaedia: exoplanet.eu as of 2011-12-04.

from the Southern Hemisphere with the goal of detecting variations in transit parameters (orbital inclination, transit depth, transit duration, etc.) and, in particular, in the central time of the transits, that can be attributed to the gravitational perturbations induced by an additional planet in the transiting system.

In Chapter 2, I describe in detail the TTV technique to search for planets and its more relevant recent results. In Chapter 3 I present the transit monitoring project (*TraMoS*) developed as part of this Ph.D. thesis. I present the first results of this project in Chapters 4, 5, 6 and 7, to finalize with my conclusions in Chapter 8.

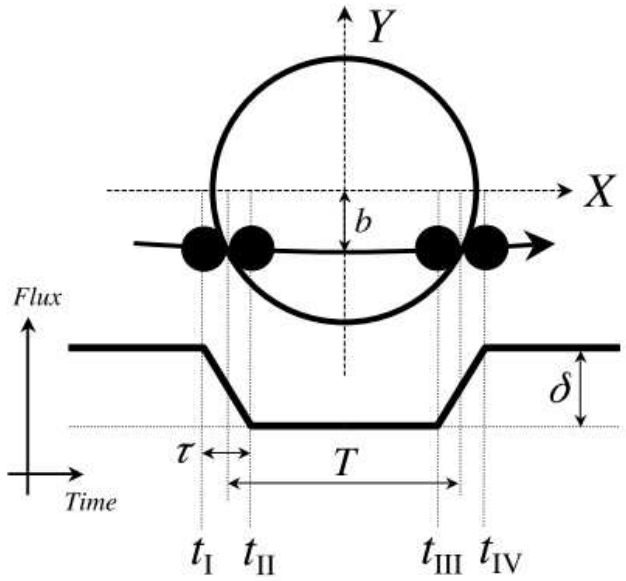

Figure 1.4 Illustration of a transit light curve (Figure 2 from Winn 2010). Based on a transit observation it is possible to measure, among other parameters, the depth (δ) and the impact parameter (b) and therefore the ratio R_p/R_s and the orbital inclination (i). With this information combined with RV measurements it is possible to estimate the mass and the mean density of the planet. The duration of the transit (T) and ingress (τ), toghether with the time of the first, second, third and fourth contact (t_I, t_{II}, t_{III} and t_{IV}, respectively) are also shown.

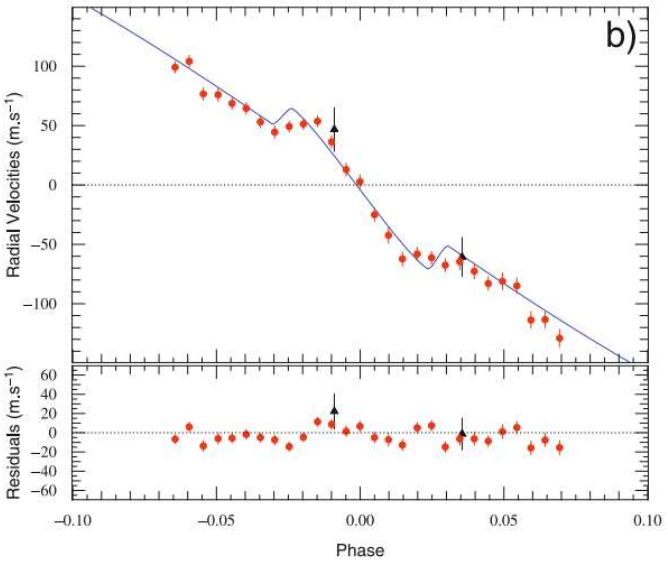

Figure 1.5 Measurement of the Rossiter-McLaughlin effect in the host star of the exoplanet WASP-5b (Figure 4 from Triaud et al. 2010).

Chapter 2

The Transit Timing Variation (TTV) Technique

One of the parameters that is measured from the transit light curves is the central time of the transit,or transit mid-time, T_c

$$T_c = \frac{1}{2}\left(t_{IV} + t_I\right), \tag{2.1}$$

where t_I and t_{IV} are the time of the first and fourth contact of the transit, respectively (see Figure 1.4).

If a planet is moving around a star without companions in a keplerian orbit, its transit mid-times will be well predicted using an ephemeris equation with a constant orbital period:

$$T_c = T_0 + P \times E, \tag{2.2}$$

where P is the orbital period and E the number of epochs since the reference time T_0. An additional orbital companion in the system will produce departures from a Keplerian orbit, changing in particular, the orbital period of the transiting body, resulting in deviations in the measured central time of the transits.

In the following section 2.1, I will describe the context of the Transit Timing Variation (TTV) technique at the time of this PhD project started (year 2008). In particular, I will enunciate the theoretical works that proposed TTV as a potential method to find planets in transiting systems and the preliminary candidates for TTVs at that time. In section 2.2, I will enumerate recent observational and theoretical TTVs results, particularly those coming from the Kepler Space Mission.

2.1 Transit Timing Variation Technique in 2008.

As mentioned, the method of Transit Timing Variations (TTVs) has been proposed by several theoretical works as of great potential to detect additional planets, down to Earth-mass objects, in transiting exoplanetary systems and even exomoons.

Variations of other light curve parameters, such as the depth or duration of the transits, can also indicate the presence of additional planets in those systems. These changes are produced, in particular, by the precession of the orbital plane and the periastron of the transiting planet as a result of the pertubations of a second planet in the system(Miralda-Escudé 2002). Agol et al. (2005) performed an analytical study of the perturbations in the timing of the transits induced by a second planet in the system. They found that perturbations are larger in the Mean Motion Resonances (MMRs) (would be fully detectable by the precision of ground-based observations) and that TTVs can be used to measure the absolute radii and mass of the host stars. Holman & Murray (2005), based on analytical and numerical studies proposed that depending on the system configuration, Earth-mass planets can be detected and found a semi-analytical expression to compute the temporal variations (Δt) between successive transits:

$$\Delta t \simeq \frac{45\pi}{16}\left(\frac{M_2}{M_*}\right) P_1 \alpha_e^3 (1-\sqrt{2}\alpha_e^{3/2})^{-2}, \tag{2.3}$$

where M_2 refers to the mass of the perturber, M_* is the star mass, P_1 is the orbital period of the transiting body and $\alpha_e = a_1/[a_2(1-e_2)]$ is a constant that relates the semi-major axis of the planets (where $a_1 > a_2$) and the perturber's eccentricity (e_2). Figure 2.1 shows Δt as a function of the distance for the transits of Jupiter induced by a perturber of 1, 5 and 20 $M_\oplus$ orbiting a star of $1M_\odot$ in a circular orbit ($e_2 = 0$).

TTVs can also potentially be used to find exomoons. Sartoretti & Schneider (1999) calculated that the expected variation between transits induced by a satellite of mass M_s and orbital radius a_s orbiting a planet of mass M_p, period T_p with and orbital radius, a_P, is

$$\Delta t \sim 2a_s \frac{M_s}{M_p} \times \frac{T_p}{2\pi a_p} \tag{2.4}$$

As example, Figure 2.2 shows the Δt of the transits of Jupiter as a function of the distance induced by a satellite of mass 1, 2 and 20 $M_\oplus$.

In addition, Ford & Holman (2007) describe the possibility of detecting Earth-mass Trojan planets (those bodies that share with the transiting planet the same or a very similar orbital distance from its host star) using TTVs.

Another application of the TTV technique is the detection of long-term orbital period variations produced by tidal interactions between the star and the planet, star oblateness and general relativity. Those effects are predicted to introduce changes in the orbital periods of the transiting planets with amplitudes of the order of 0.3-10 ms/yr (Miralda-Escudé 2002, Heyl & Gladman 2007, Jordán & Bakos 2008) and would be detectable in 10-20 years timescales given the precision of the current instruments.

All of these theoretical predictions have prompted the work of several observational groups, who in the past few years have started to monitor various transiting exoplanets from the ground.

At the time of the beginning of this project in 2008, most of the observational efforts were still preliminary. For instance, preliminary results include the hints of transit duration and orbital inclination variations in the hot Neptune Gliese 436b system reported by Coughlin

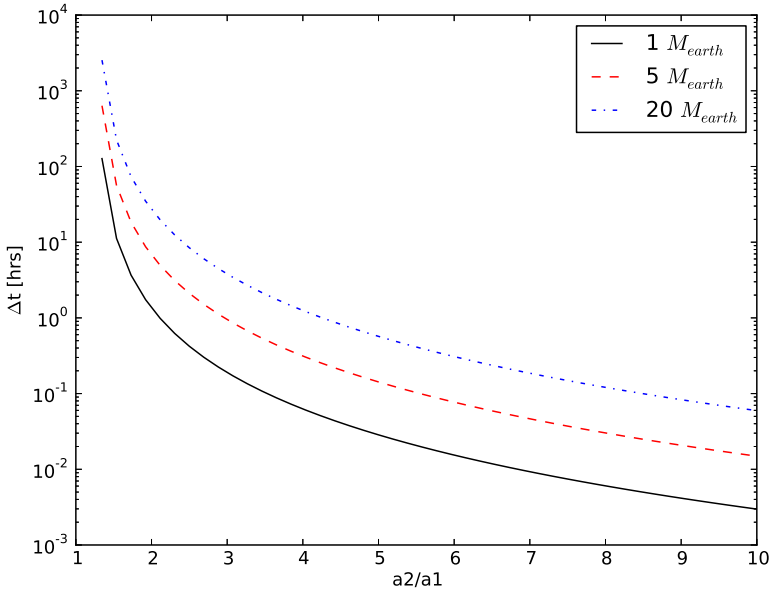

Figure 2.1 Temporal variations between consecutive transits (following equation 2.3) of a Jupiter-like planet induced by a perturber of a mass of 1, 5 and 20 $M_{\oplus}$ represented by the solid (black), dashed (red) and point-dashed (blue) lines. The planets move around a central star of $1M_{\odot}$ in circular orbits.

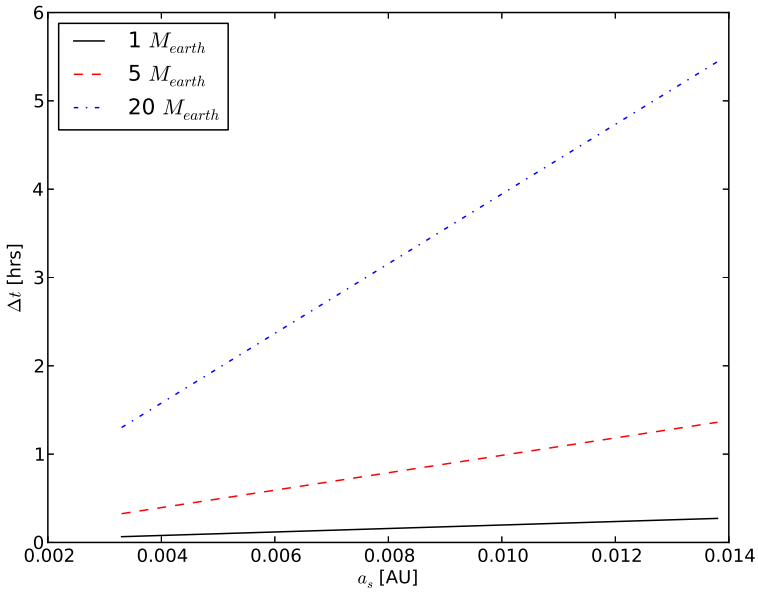

Figure 2.2 Temporal variations between consecutive transits (following equation 2.4) of a Jupiter-like planet induced by a satellite of a mass of 1, 2 and 20 $M_{\oplus}$ represented by the solid (black), dashed (red) and point-dashed (blue) lines.

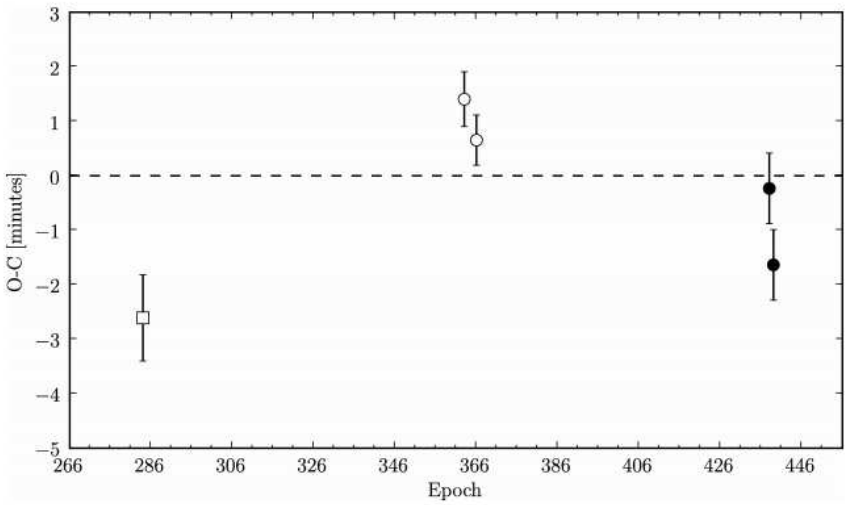

Figure 2.3 The Observed *minus* Calculated (O−C) diagram of the transits of OGLE-TR-111b as reported by Díaz et al. (2008). Deviations as large as 2.5 minutes were suggested in the central times of the transits of this exoplanet.

et al. (2008) and the shift of about 3σ difference in the orbital period of XO-2b reported by Fernandez et al. (2009) when compared with previous published values.

On the other hand, there are systems which have been monitored without showing any clear evidence of TTVs, e.g. Steffen & Agol (2005) found no evidence of a second planet using timing data of eleven transits of TrES-1b, and Agol & Steffen (2007) ruled out Earth-mass planets in low order resonances in the HD 209458b system. In a later work, Miller-Ricci et al. 2008b,a found no TTVs with amplitudes larger than 45 seconds on the transits of HD 209458b and HD 189733b based on *MOST* satellite data.

One of the most promising results at that time was that of Díaz et al. (2008), who reported suggestive shifts of up of 2.5 minutes in the times of transits of the OGLE-TR-111b exoplanet (Figure 2.3). This result led to list this exoplanet as one of our priority targets to be monitored, in order to confirm or rule out the TTV signal, in the framework of this thesis (see Chapter 4).

2.2 TTVs today: recent results

In parallel to the observational works, a big effort in analytical and theoretical studies has been developed in the TTV field. TTVs and Transit Duration Variations (TDVs) can be used also to detect earth-mass exomoons (Kipping 2009a,b). Inversion method, used to recover physical parameters of the transiting system from TTVs, are in development to detect and characterize perturbing planets (Nesvorný & Morbidelli 2008, Nesvorný 2009, Nesvorný & Beaugé 2010, Meschiari & Laughlin 2010).

TTVs have not only given an impulse to the development of physical and dynamical theoretical studies. Because the high precision achieved by transit observations in the central

times of the transit and, because in general, the transits of a single exoplanet are observed by different telescopes and/or instruments, it was necessary to establish a precise time reference that allows direct comparison between the values widely reported in the literature. Before TTVs, and when the reported exoplanet transits were just starting to accumulate in the literature, the T_c of the transits were reported using different time frameworks: *Julian Days*, *Baricentric Julian Days*, *Heliocentric Julian Days* were used indistinctly, without indicating under wich time standard were calculated (e.g. Alonso et al. 2004, Udalski et al. 2008). In the past, only subfields in Astronomy such as the study of pulsars have needed of very precise time recording. More recently, because of the transits and in particular TTV studies, a large part of the exoplanet community has started to pay close attention to the need of a timing system as accurate as possible, and that is how the *Baricentric Julian Day* expressed in Terrestrial Dynamical Time has been adopted as time reference standard. In Eastman et al. (2010) it is possible to find an excellent summary of the different time definitions and reference frames currently used. To illustrate how this ambiguity can affect the timing when the frame reference is not specified I show in Figure 2.4 the time shifts between the International Atomic Time (TAI) and the Coordinated Universal Time (UTC) produced by the leap seconds added when the UTC deviates more than 0.9 seconds from the Universal Time (UT1). Also represented in Figure 2.4 is the shift of 32.184 seconds between Terrestrial Time (TT) and TAI. If these terms are not taken into account transit times can have offsets of $\sim$ 1 minute. It is common to have time stamps in astronomical images expressed in UTC. In the bottom panel of Figure 2.4 I show the difference between the BJD(TDB) and the UTC that can be obtained for observations of the exoplanet WASP-4b. In this example, the difference can be as large as $\sim$ 7 minutes, and consequently if the transit times are not corrected it is possible to introduce significant but false TTV signals in the analysis.

TTVs is a very important tool for discovering new exoplanets because of its higher sensitivity to low mass planets when compared to other techniques, but even the non detection of companions via TTVs is of scientific interest, since with the information provided by the lack of TTVs it is possible to determine with high accuracy the architecture of the exoplanetary systems, giving critical insights to discriminate between different models of formation and evolution of exoplanets (Lin et al. 1996, Kozai 1962, Rasio & Ford 1996).

In the last few years several TTV studies have been reported. Intense monitoring of transiting exoplanets from ground-based telescopes have been published, but despite of having good TTV candidates, there were no conclusive results.

Several systems show no evidence of TTVs. Among these kind of objects we can find TrES-3b (Gibson et al. 2009), HAT-P-3b (Gibson et al. 2010), OGLE-TR-56b (Adams et al. 2011b), OGLE-TR-132b (Adams et al. 2011a), TrES-4b (Chan et al. 2011), XO-5b (Maciejewski et al. 2011c), GJ436b and XO-1b (Cáceres et al. 2009).

Examples of these works include the potential detection of TTVs with amplitudes of up to 3 min for the hot Jupiter WASP-3b, which could be explained by the presence of a $\sim$ 15 $M_{\oplus}$ planet near the outer 2:1 mean motion resonance (Maciejewski et al. 2010), and the also preliminary detection of a -60 ± 15 ms/yr orbital period decay of the hot Jupiter OGLE-TR-113b by Adams et al. (2010b).

The exoplanet WASP-12b was discovered in 2009 (Hebb et al. 2009). Just recently, almost two simultaneous publications announced the observations of four additional transits

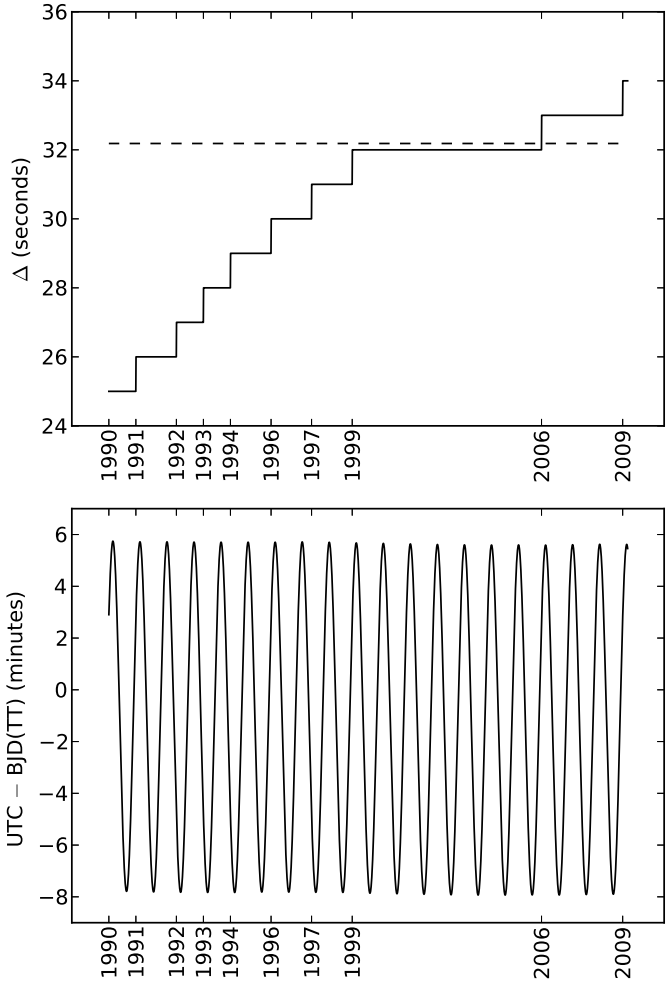

Figure 2.4 Differences between some of the time references frames. Top Panel: The discontinuity (leap seconds) of the Coordinate Universal Time with respect of the Atomic Time is represented by the solid line and the constant shift of 32.184 seconds between Terrestrial Time and the International Atomic Time is shown with the dashed line. Bottom Panel: The difference between the Baricentric Julian Day (expressed in Terrestrial Time) and the UTC can be as large as ~ 7 minutes in the case of WASP-4b.

(Maciejewski et al. 2011a, Chan et al. 2011) that seem to hint possible TTVs (Figure 2.5).

Also, it has been reported that the WASP-10b exoplanet shows a TTV signal (Maciejewski et al. 2011d) that can be explained by a perturber of $0.1 M_{Jup}$ in a 5.23 day orbit, close to the 5:3 MMR with WASP-10b. Another work (Maciejewski et al. 2011b) added four new epochs claiming a periodic variation in the mid-times of the transits, but a linear ephemeris can not be ruled out with the available information (see Figure 6 in Maciejewski et al. 2011b).

HAT-P-13 was the first detected double-planet system with a transiting planet (Bakos et al. 2009). Payne & Ford (2011), based on N-body simulations, showed that TTV observations

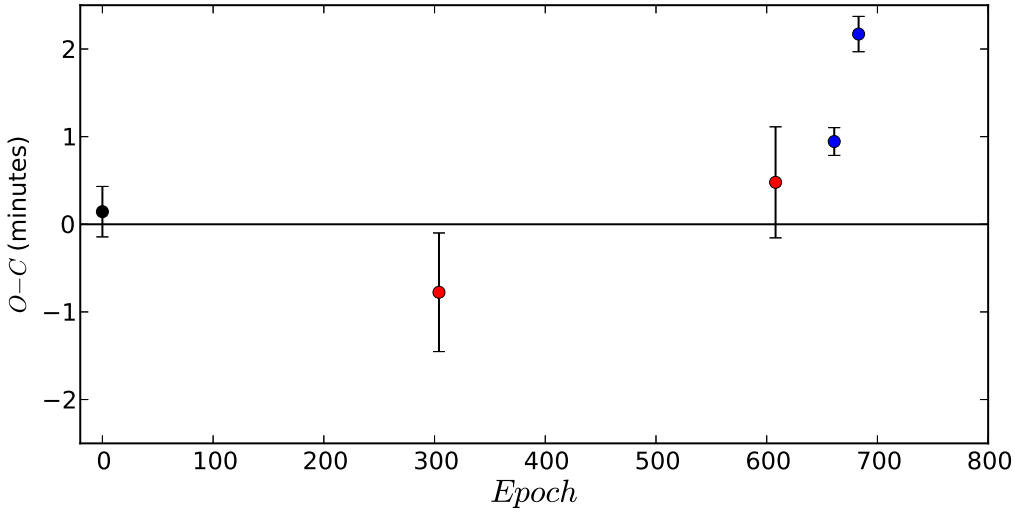

Figure 2.5 The Observed *minus* Calculated Diagram of the central times of the transits of the exoplanet WASP-12b. Black, red and blue points correspond to the epochs reported by Hebb et al. (2009), Chan et al. (2011) and Maciejewski et al. (2011a), respectively (compared with the predicted times of the ephemeris equation from Maciejewski et al. (2011a)).

can strongly constrain the eccentricity and inclination of the outer perturber. Also, with the timing information already obtained for this planet they claimed that there is high probability that the outer planet can also transit. Intense follow-up of this transiting planet has been carried-out during the past few years (Szabó et al. 2010, Pál et al. 2011, Nascimbeni et al. 2011, Fulton et al. 2011). Despite the large scatter in the Observed *minus* Calculated (O−C) diagram of the transits there is an open debate regarding if the transits follow a linear ephemeris (Fulton et al. 2011, see Figure 2.6) or if there is a periodic TTV signal (Nascimbeni et al. 2011, see Figure 2.7).

One explanation for the lack of firm TTV detections, from ground-based surveys, has been proposed by García-Melendo & López-Morales (2011) where they claim that most of the transit surveys can be missing the detection of objects with TTVs due to the current algorithms used to discard *false positives*: systems presenting transit-like periodic signal such as binary system blended with a background bright star. In consequence, the selection criteria of planet candidates must be revisited.

Just recently, space missions dedicated to exoplanets studies, in particular for transiting planets, have came into the play: CoRot (Barge et al. 2008) and Kepler (Borucki et al. 2010). These missions have started to collect high duty cycle and long-term monitoring data which especially beneficial to TTV studies. These missions have delivered a huge amount of very precise data, which allows the generation of high quality transit light curves and therefore, to obtain very accurate measurements of the central times of the transits, among other parameters. TTVs of exoplanets such as CoRoT-1b (Bean 2009, Csizmadia et al. 2010), TrES-2b (Kipping & Bakos 2011), HAT-P-11b (Deming et al. 2011) have been discarded using these *space* data.

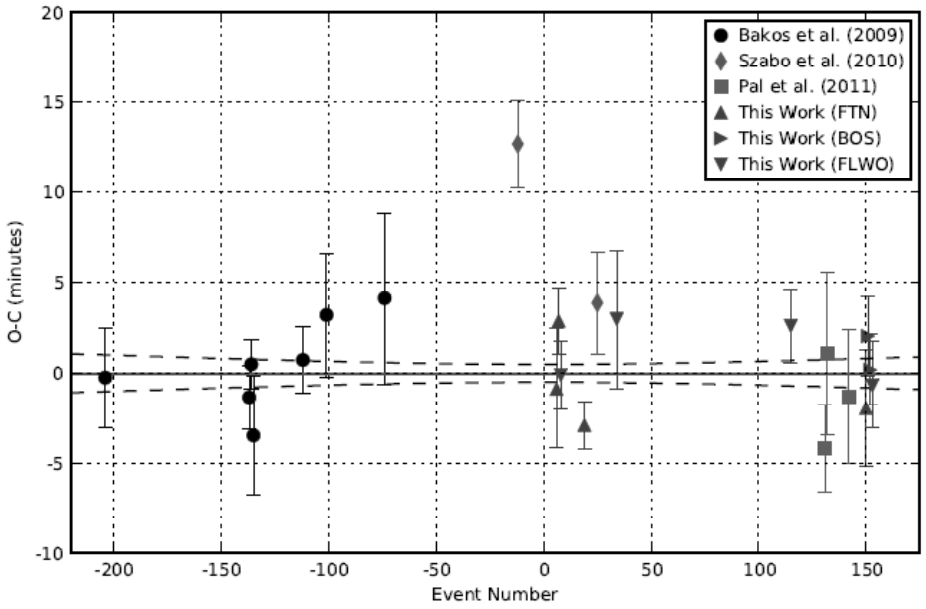

Figure 2.6 The Observed *minus* Calculated diagrams of the central times of the transits of the exoplanet HAT-P-13b as presented in Fulton et al. 2011. With the new epochs observations they claim that a linear ephemeris can not be ruled-out.

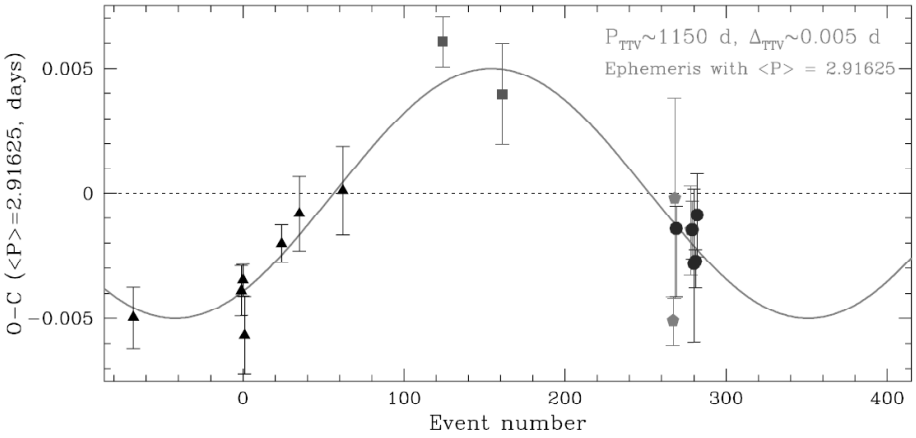

Figure 2.7 The Observed *minus* Calculated diagram of the central times of the transits of the exoplanet HAT-P-13b as presented in Nascimbeni et al. 2011. A periodic TTV signal is shown by the solid line.

But the most important contributions to TTVs studies have been obtained using Kepler data. Steffen et al. (2010) identified 5 Kepler stars which show transits of multiple exoplanet candidates. Detectable TTV signal of those multiple systems can be used to confirm the exoplanetary nature of these candidates.

The first unquestionable empirical result of TTVs was the discovery of a planetary system with two Saturn-like exoplanets, both transiting their host star (Holman et al. 2010). This remarkable finding allowed to record the mid-times of transit of the two planets showing that

both presented TTVs of amplitudes of tens of minutes. Shortly after, Lissauer et al. (2011) reported a system with six transiting planets, all of them with TTVs. Dynamical analysis based on the TTV information allowed the determination of the masses of the 6 exoplanets without the need of RV measurements. Using TTVs it was also possible to confirm the detection of three planets in the system Kepler-18 (Cochran et al. 2011) and an additional body in the transiting system Kepler-19 (Ballard et al. 2011). All these exoplanets have masses in the range of 2 to 80 $M_{\oplus}$, confirming the potential of the TTV technique to find companions in the Earth mass regime. In Kepler-16 system, the first exoplanet transiting a binary star, was reported by Doyle et al. (2011). The variations in the time and the duration of the eclipses helped to determine without ambiguity the mass of both of the stars and the exoplanet ($0.333 \pm 0.016\ M_{JUP}$).

A statistical analysis of all the Kepler planet candidates suitable for TTV analysis show that between 11%-20% present some evidence of TTVs (Ford et al. 2011). The detectability of Earth-sized planets in the habitable zone of low mass stars using TTVs with Kepler data was tested by Haghighipour & Kirste (2011). Relying in the information obtained from N-body simulations with the Mercury Code (Chambers 1999), they showed that perturbers in low order MMRs with the transiting planets are more likely to present detectable TTV signals.

With the extremely large number of transiting exoplanets being discovered around bright stars, small telescopes can be exploited to monitor those exoplanets and obtain high precision photometry during the transit events. That is the main goal of the *TraMoS* project, which is presented in Chapter 3.

Chapter 3

The *TraMoS* Project

Since the second semester of 2008, I have conducted a homogeneous monitoring program of known transiting planets observable from the Southern Hemisphere, the pilot sample for the **Tra**nsit **Mo**nitoring in the **S**outh (*TraMoS*) project, in search for variations in their light curve parameters, i.e. duration and/or depth of the transits and their orbit's inclination, and in particular, for changes in the mid-times of the transits, which can be indicative of the presence of an *unseen* companion.

The *TraMoS* project's aim is both to detect additional planets via short-term TTVs (that can be detected by observations of consecutive transits) and/or long-term or secular variations (which can be detected with only few observations over a time span of years). Our monitoring consists in collecting very accurate light curves of transits in the I_c or z' filters to diminish limb darkening effects (see Knutson et al. 2007). The aim of our project is to take advantage of the fastest available CCDs cameras in order to obtain high cadence observations (between 20 and 50 seconds) and thus determine the mid-time of the transits with precision of up to a few tens of seconds. Besides the high sampling observations, for the purpose of minimizing systematics and reducing uncertainties of the parameters, I follow the strategy of using the same telescope/instrument setups in all of our observations.

3.1 Observations

Under the *TraMoS* project I have chosen the fastest cameras available to the Chilean community. Depending on the targets magnitudes I used: the FOcal Reducer and Spectrograph (FORS1 and FORS2) at ESO Very Large Telescope (VLT), Gemini Multi-Object Spectrograph (GMOS) in Gemini South Observatory, SOAR Optical Imager (SOI) in the Southern Astrophysical Research (SOAR) Telescope at Cerro Pachón Observatory and the Y4KCam in the SMARTS 1-m Telescope at Cerro Tololo Inter-american Observatory (CTIO). All these instruments have binning modes that allow one to reduce significantly the observation overheads, i.e. the time elapsed during the readout, writing and transfer of each image frame, therefore optimizing the sampling (duty cicle) of the observations, which is one of the key parameters for TTVs work. A detailed description of each instrument is presented in the corresponding observation sections of Chapter 4, 5 and 6.

I monitored a total of 19 transiting hot Jupiters (orbital periods between 1.8 and 8 days) discovered by the OGLE and SuperWASP surveys, and also the recently discovered hot Neptune GJ-1214b (Charbonneau et al. 2009). The names of all the targets are listed in Tables 3.1 and Table 3.2.

The Optical Gravitational Lensing Experiment (OGLE) Survey (Udalski et al. 1997) was designed to search for dark matter via the microlensing effect. The OGLE survey observes in general very crowded fields and therefore, a large number of stars are observed searching for photometric variability allowing to develop a great number of studies, including the detection of exoplanetary transits. In general, the confirmed OGLE's exoplanets orbit relative faint stars ($14 \leq I \leq 16$). From here the need to employ large telescopes such as VLT/UT4 and GEMINI-South Telescope to monitor the OGLE planets. Big apertures telescopes allows to us to achieve good Signal-to-Noise values and good Point-Spread-Functions (PSF) which are critical for the photometry I need to perform in such crowded fields. OGLE fields are ideally suited for observations in large telescopes, since they contain many nearby comparison stars that can be simultaneously observed in the generally small Field-of-View (FoV) of large telescopes instruments.

On the contrary, the SuperWASP-South (Super Wide Angle Search for Planets) project uses a network of small telescopes to detect transit signatures and therefore its targets correspond to relative bright stars, making it ideal for the use of the SOAR and SMARTS 1-m Telescopes for our follow-up. Smaller apertures help to avoid saturation and large FoVs facilitate the inclusion in the images of suitable (similar brightness) comparison stars.

The transit observations are in nature time critical. In the planning of the observation, the variables that need to be taken into account are (1) the transit duration, (2) an adequate bracketing before and after the transits (since these data are needed to efficiently model the transit and correct for systematics),(3) the elevation of the star during the night, among other variables. Figure 3.1 is an example of a type of plot I use to search for the best observable transits of an exoplanet (in this case WASP-25b) in terms of the airmass and time coverage during the night. Once the best transits are identified I proceed to predict the times of start/end of the transit and calculate how much time I can observe the targets with airmasses smaller than 1.8-2.0. An example of these calculations is shown in Figure 3.2. These plots are used extensively in the planning and execution of each observation.

For the *TraMoS* project I have observed 19 exoplanets, 7 objects with more than 5 transits each, and most of them with more than 2 years of monitoring. In Table 3.1 and Table 3.2 I show the number and date of the transits already observed to date for the WASP and OGLE exoplanets respectively, and in Table 3.3 I show a summary of the properties of their host-stars. Also I show the observation of a transit of GJ1214b, which was observed taking advantage of the opportunity to monitor it using SOAR's unallocated time via a Director Discretionary Time (DDT) proposal.

In the remaining of the chapter I detail the data analysis process. In Chapters 4, 5, 6 and 7 I present the analysis of 29 transits of the exoplanets: OGLE-TR-111b, WASP-5b, WASP-4b and WASP-7b, which constitute the bulk of this thesis work. I also have 46 additional transits observed for the remaining planets whose analysis and publication plans are described in Chapter 8.

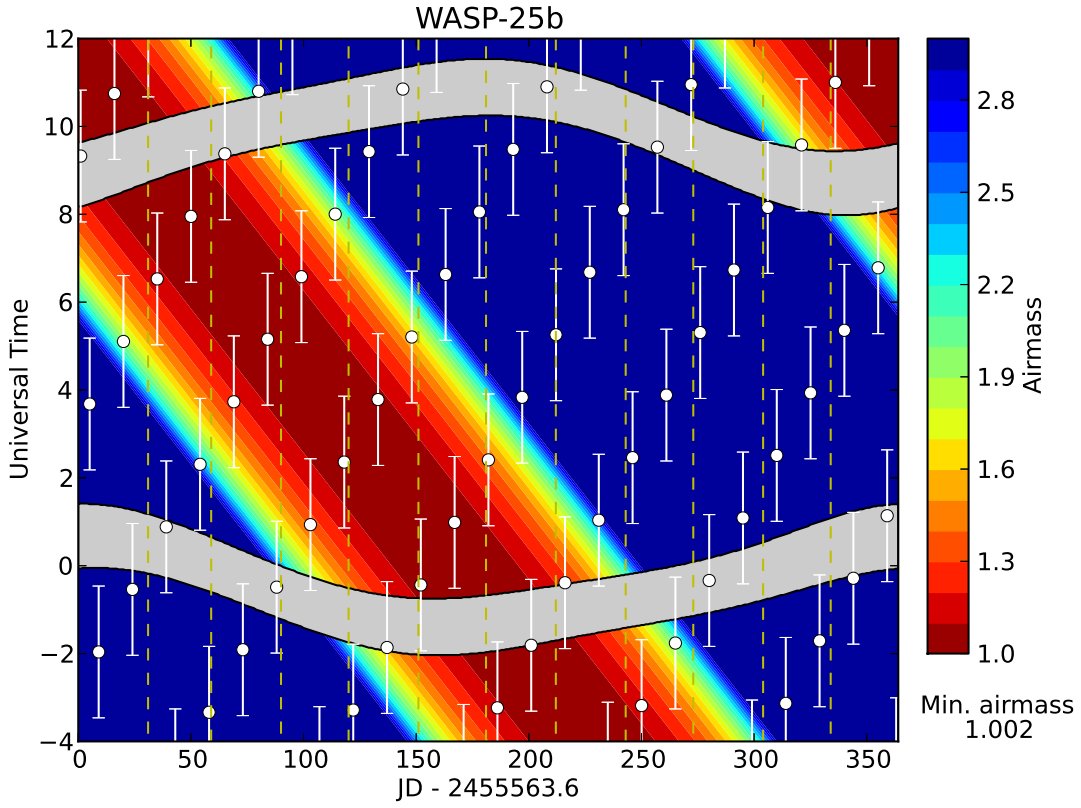

Figure 3.1 Example of observable series of transits for WASP-25 during 2011, as seen from telescopes at CTIO. White circles indicate the center of transit events, vertical error bars indicate transit span. White regions show morning and evening twilight and dashed vertical lines represent month boundaries. The airmass is represented by the color code as is indicated to the right (Adapted from Rojo 2006).

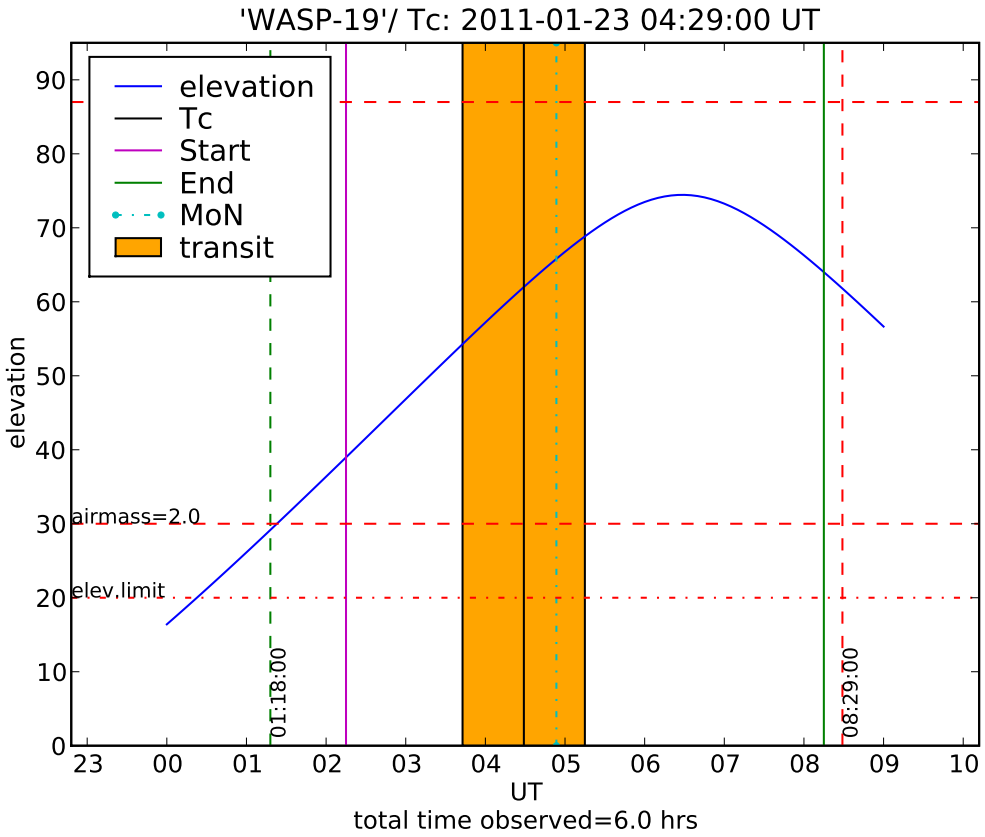

Figure 3.2 Example of the transit observation plot of WASP-19b during the night of 2011-01-22. The orange region indicates the predicted duration of the transit event. The blue solid line represent the elevation of the star during the night. Dashed lines mark the time of the end/start of the afternoon/morning twilight respectively. The point-dashed line indicates the Middle-of-the-Night (MoN) time and the horizontal lines represent some important elevation limits. Magenta and green solid vertical lines represent the times when the observation can be started/finished giving a total time of 6 hours of follow-up.

Table 3.1. Dates of the observed transits of WASP exoplanets by the *TraMoS* project.

Planet	Date	Telescope	Planet	Date	Telescope
WASP-4b	2008-08-22	SMARTS 1-m	WASP-5b	2008-08-20	SMARTS 1-m
	2008-08-22	SOAR		2008-08-28	SMARTS 1-m
	2008-08-26	SMARTS 1-m		2008-09-20	SMARTS 1-m
	2008-09-18	SMARTS 1-m		2008-10-22	SOAR
	2008-09-22	SMARTS 1-m		2008-11-04	SOAR
	2008-09-30	SMARTS 1-m		2008-11-16	SMARTS 1-m
	2009-07-28	SOAR		2009-06-22	SOAR
	2009-09-21	SOAR		2009-08-05	SOAR
	2009-10-27	SMARTS 1-m		2009-10-24	SMARTS 1-m
	2010-09-28	SMARTS 1-m		2010-10-09[a]	SOAR
WASP-7b	2009-06-07	SMARTS 1-m	WASP-2b	2009-06-03	SOAR
	2009-06-12	SMARTS 1-m		2009-07-26	SOAR
	2009-10-14[a]	SMARTS 1-m		2009-08-23	SOAR
	2011-07-20	SMARTS 1-m		2009-09-20	SOAR
				2010-08-26	SMARTS 1-m
WASP-18b	2009-10-28	SMARTS 1-m	WASP-8b	2010-08-12	SMARTS 1-m
	2009-10-29	SMARTS 1-m		2010-09-30	SMARTS 1-m
	2009-10-30	SMARTS 1-m		2011-09-24	SMARTS 1-m
	2010-08-29	SMARTS 1-m			
	2011-10-05	SMARTS 1-m			
	2011-10-06	SMARTS 1-m			
WASP-15b	2010-05-10	SMARTS 1-m	WASP-16b	2010-04-14	SMARTS 1-m
	2011-04-05	SMARTS 1-m		2010-05-09	SMARTS 1-m
	2011-06-23	SMARTS 1-m		2011-05-12	SMARTS 1-m
WASP-17b	2010-04-27	SMARTS 1-m	WASP-19b	2011-04-18	SMARTS 1-m
	2010-05-11	SMARTS 1-m		2011-04-22	SMARTS 1-m
	2011-06-26	SMARTS 1-m			
WASP-22b	2010-10-09	SMARTS 1-m	WASP-26b	2010-09-11	SMARTS 1-m
	2010-11-24	SOAR		2010-10-03	SMARTS 1-m
	2011-12-07	SMARTS 1-m			
WASP-29b	2010-09-13	SMARTS 1-m			

[a]These data were discarded due bad weather or telescope technical failures.

Table 3.2. Dates of the observed transits of OGLE planets and the GJ-1214b exoplanet by the *TraMoS* project.

Planet	Date	Telescope	Planet	Date	Telescope
OGLE-TR-111b	2008-04-26	VLT	OGLE-TR-113b	2008-12-19	Gemini-S
	2008-04-30	VLT		2008-12-29	Gemini-S
	2008-05-04	VLT		2009-01-21	Gemini-S
	2008-05-12	VLT		2009-02-20	Gemini-S
	2008-05-20	VLT		2009-02-23	Gemini-S
OGLE-TR-132b	2009-12-25	Gemini-S	OGLE2-TR-L9	2009-12-18	Gemini-S
	2010-01-16	Gemini-S		2009-12-28	Gemini-S
	2010-01-21	Gemini-S			
	2010-02-12	Gemini-S			
	2010-03-16	Gemini-S			
OGLE-TR-56b	2009-04-28	Gemini-S	OGLE-TR-10	2009-09-06	Gemini-S
GJ 1214b	2010-04-28	SOAR			

3.2 Data Reduction and Analysis

I have generated custom-made pipelines specifically developed for each instrument to reduce and analyze the data. In Figure 3.3, I summarize all the steps of the process from the reduction, photometry, generation of the light curves and final modeling of the transits. The majority of these steps are performed using my custom Python-based pipelines. It is worth mentioning that these pipelines can be easily modified to be used with data from different instruments/telescopes. In fact, we are currently adapting these codes to use it with data coming from small telescopes like TRAPPIST and REM at La Silla Observatory, and SARA telescope at CTIO. These small-size telescopes (0.6 meter) are being used in the next phase of *TraMoS*, taking advantage of their remote and/or service mode observations. This type of observations will improve the coverage of the project since the planning, scheduling and logistic of the observations will be easier, keeping in mind that the number of potential targets of the project is increasing rapidly and that the observations are time critical.

In the following chapters a description of the reduction, photometry, light curve generation and its further detrending is provided for specific planet cases. I also show and explain in the Appendices some important features of the codes used in these steps.

Table 3.3. Properties of the host stars observed by the *TraMoS* project.

Star	Apparent Magnitude V [a]	Spectral Type [a]	Mass ($M_\odot$) [a]	Radius ($R_\odot$) [a]
WASP-4	12.6	G8	0.93 ± 0.05	1.15 ± 0.28
WASP-5	12.26	G5	1 ± 0.06	1.084 ± 0.041
WASP-7	9.51	F5	1.276 ± 0.06	1.432 ± 0.09
WASP-8	9.9	G6	1.033 ± 0.058	0.953 ± 0.058
WASP-15	10.9	F7	1.18 ± 0.12	1.477 ± 0.072
WASP-16	11.3	G3	1.022 ± 0.101	0.946 ± 0.054
WASP-17	11.6	F4	1.2 ± 0.13	1.38 ± 0.2
WASP-18	9.3	F6	1.24 ± 0.04	1.23 ± 0.045
WASP-19	12.3	G8	0.97 ± 0.02	0.99 ± 0.02
WASP-22	12	...	1.1 ± 0.3	1.13 ± 0.03
WASP-26	11.3	G0	1.12 ± 0.03	1.34 ± 0.06
WASP-29	11.3	K4	0.825 ± 0.033	0.846 ± 0.048
OGLE-TR-111	15.55	G/K	0.82 ± 0.15	0.831 ± 0.031
OGLE-TR-113	14.42	K	0.78 ± 0.02	0.765 ± 0.025
OGLE-TR-132	15.72	F	1.26 ± 0.03	1.34 ± 0.08
OGLE2-TR-L9	13.97[b]	F3	1.52 ± 0.08	1.53 ± 0.04
OGLE-TR-56	16.6	G/K	1.17 ± 0.04	1.32 ± 0.06
OGLE-TR-10	14.93	G/K	1.18 ± 0.04	1.16 ± 0.06
GJ-1214	14.71	M	0.153 ± 0.01	0.21 ± 0.0005

[a]Data from the on-line exoplanet encyclopaedia: *exoplanet.eu*, and references therein.

[b]This value corresponds to the apparent magnitude in the *I band*.

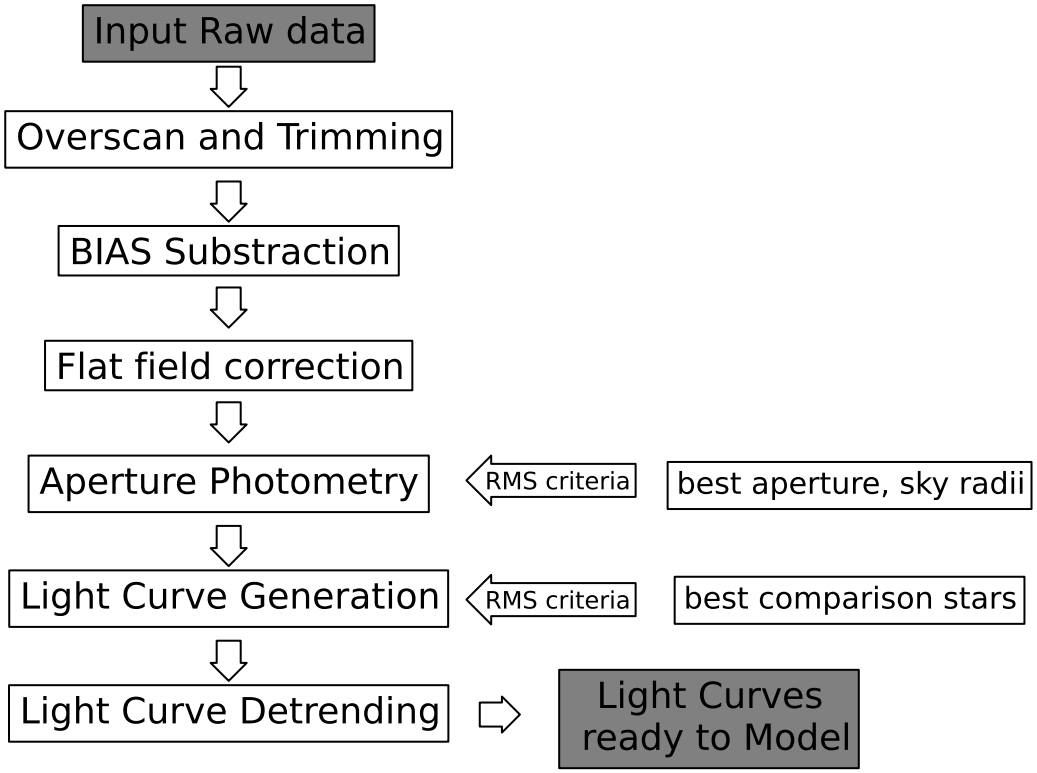

Figure 3.3 Diagram of the process followed for the reduction and light curve generation using our custom-made Python pipelines especifically developed for each instrument used in the *TraMoS* project.

3.3 Light Curve Modeling

For the modeling of the light curves I have used several third-party state-of-the-art codes that implement different approaches to derive light curve parameters. Among these is worth mentioning the JKTEBOP code (Southworth et al. 2004a) and Transit Analysis Package, TAP (Gazak et al. 2011).

In the modeling of the light curves it is necessary to take into account several elements that affect directly the derived value of the parameters and their uncertainties. A good fit not only depends on the Signal-to-Noise (SNR) of the photometry (i.e. the *root-mean-square (RMS)* of the points in the light curves) known as the uncorrelated or white noise. One of the most important elements that affect the light curve shape and its point dispersion is the correlated noise or *Red-Noise* (Pont et al. 2006).

But even more important than a good estimation of the red-noise is a reliable multi-parameter determination of the errors in the derived light curve's parameters. The Markov Chain Monte Carlo method (MCMC) is the most extensively method used to date in light curve fitting and estimate the confidence contours of the fitted parameters. The uncertainties estimations are critical when looking for variations in the light curve's parameters, especially in central times of the transits.

Deviations in strictly periodic transits are often calculated by using linear regressions, as described in sections 4.4, 5.4 and 6.5. Usually χ^2 indicators are used to estimate the significance of the deviations, where a $\chi^2_{red} \sim 1$ represents that the transit times are well predicted by the adopted ephemeris equation. Consequently, the underestimation of the errors can lead to erroneous TTV signals in the transits of an exoplanet. Carter & Winn (2009) showed a numerical example of this situation, and probably in the literature there are several cases where preliminary TTV candidates are identified based in a non-homogeneous analysis and underestimation of the errors in the transit's time; see for example the analysis of WASP-5b (section 5.4). There are different ways to estimate the red-noise and to take it into account in the modeling. Also, I have used different statistical approaches to estimate parameters errors from the light curves. A comprehensive comparison between these different methods is presented in sections 4.3 and 5.3.1. In Section 4.3, I present a discussion about the similarities/differences between the Levenberg-Marquardt Monte Carlo (LMMC) and the MCMC algorithms. In Section 5.3.1, I also discuss the advantages of the MCMC algorithm and the *wavelet method* (Carter & Winn 2009) implemented by TAP for error estimations.

Chapter 4

Analysis and Results of OGLE-TR-111b

FIVE NEW TRANSIT EPOCHS OF THE EXOPLANET OGLE-TR-111b

S. Hoyer[1], P. Rojo[1], M. López-Morales[2,3], R.F. Díaz[4,5], J. Chambers[3] and D. Minniti.[6,7]
The Astrophysical Journal, vol.733, p.53

[1]: Astronomy Department, Universidad de Chile, Casilla 36-D, Santiago de Chile, Chile.

[2]: Institut de Ciencies de l'Espai (CSIC-IEEC), Campus UAB, Facultat de Ciencies, Torre C5, parall, 2a pl, E-08193 Bellaterra, Barcelona, Spain.

[3]: Carnegie Institution of Washington, Department of Terrestrial Magnetism, 5241 Broad Branch Rd. NW, Washington, D.C. 20015, USA.

[4]: Institut d'Astrophysique de Paris, UMR7095 CNRS, Université Pierre & Marie Curie, 98bis boulevard Arago, 75014 Paris,France.

[5]: Observatoire de Haute-Provence, CNRS/OAMP, 04870 Saint-Michel-l'Observatoire, France.

[6]: Departamento de Astronomía y Astrofísica, Pontificia Universidad Católica de Chile, Casilla 306, Santiago 22, Chile.

[7]: Vatican Observatory, V-00120 Vatican City State.

Abstract

We report five new transit epochs of the extrasolar planet OGLE-TR-111b, observed in the *v-HIGH* and *Bessell I* bands with the FORS1 and FORS2 at the ESO Very Large Telescope, between April and May 2008. The new transits have been combined with all previously published transit data for this planet to provide a new Transit Timing Variations (TTVs) analysis of its orbit. We find no TTVs with amplitudes larger than 1.5 minutes over a 4-year observation time baseline, in agreement with the recent result by Adams et al. (2010a). Dynamical simulations fully exclude the presence of additional planets in the system with masses greater than 1.3, 0.4 and 0.5 $M_{\oplus}$ at the 3:2, 1:2, 2:1 resonances, respectively. We also place an upper limit of about 30 $M_{\oplus}$ on the mass of potential second planets in the region between the 3:2 and 1:2 mean-motion resonances.

Based on the work published in Hoyer et al. (2011b) and reproduced by permission of the AAS.

4.1 Introduction

OGLE-TR-111b was the first hot Jupiter for which tentatively significant TTVs were reported by Minniti et al. (2007), hereafter M07. The first two precision transit timing data points for this planet were published by Winn et al. (2007), W07. Shortly after, M07 published a third data point which deviated by about 5 minutes from the predicted W07 transit ephemeris. In a subsequent paper, Díaz et al. (2008) (D08) reported two new consecutive transits and combined their new data with the other three epochs to find TTVs with amplitudes of up to 2.5 minutes, which the authors suggested could be explained by the presence of a 1.0 $M_{\oplus}$ perturbing planet in an outer eccentric orbit to OGLE-TR-111b. The most recent TTVs analysis publication on this planet (Adams et al. 2010a, A10) reports six new transit observations and no TTVs for this planet with amplitudes larger than 71 ± 67 seconds.

In this new work we present five additional transits of OGLE-TR-111b observed between April and May 2008, and we perform a new homogeneous timing analysis of all available 16 epochs to further study the presence or absence of additional planets in this system. In section 4.2 we present the new observations and the data reduction. Section 4.3 describes the modeling of the light curves. In sections 4.4 and 4.5 we describe the timing and possible parameters evolution. In 4.6 we discuss the mass limits for a *unseen* perturber and finally in section 4.7 we present our conclusions.

4.2 Observations and data reduction

Between April and May 2008, we observed five transits of the exoplanet OGLE-TR-111b with FORS1 and FORS2 (Appenzeller et al. 1998) at the ESO Very Large Telescope. The first four transits were fully covered in phase. The fifth transit was only partially covered because the target reached the telescope's airmass limit, and is only complete between phases 0.97 and 1.01, which includes the out-of transit baseline before the transit, the ingress and most of the bottom of the transit (see Figure 4.1). The UT date of the mid-time of the transit, instrument, filter band, exposure time, airmass range and number of frames of each observation are summarized in Table 4.1. FORS1 and FORS2 are visual focal-reducer imagers composed of two 2048×4096 E2V/MIT CCD detectors mosaics with a pixel scale of 0.126 arcsec pixel^{-1} each (high resolution mode). The field of view (FoV) of each camera is therefore 4.25×4.25 arcminutes, large enough to include OGLE-TR-111 and several comparison stars. FORS1 and FORS2 have the same wavelength coverage (3000-11000 Å) but FORS1 is optimized for blue wavelengths (< 5000 Å) while FORS2 is for the red (> 6000 Å). Our first transit was observed with FORS1 using a *v-HIGH* filter ($\lambda_{eff} = 557$ nm) while the rest of the transits were observed with FORS2 using a *Bessell I* filter ($\lambda_{eff} = 768$ nm). A very close star appears partially blended with the target given the resolution of the instrument and the typical seeing conditions during the observations (Figure 4.2). The center of the field was selected so that OGLE-TR-111 and several good comparisons stars would fall on a single detector, while also locating a bright nearby star out of the field. However, diffraction spikes from that bright star moved across the field of view, occasionally reaching the location of the target, as illustrated in Figure 4.2. Our subsequent analysis revealed additional background noise in some of the images due to this effect. This problem was most evident in the 2008-05-03 light curve (Figure 4.3) where pronounced bumps were visible in the bottom of the light curve of

Table 4.1. Observational information of each transit of OGLE-TR-111b.

Transit Date	Instrument	Filter	Integration Time [s]	airmass range	# images[c]
2008-04-26	FORS1	v-HIGH	30	1.25 - 1.43	323
2008-04-30	FORS2	Bessell I	12	1.25 - 1.59	488
2008-05-04	FORS2	Bessell I	12	1.25 - 1.75	522(2)
2008-05-12[a]	FORS2	Bessell I	4	1.25 - 2.18	601(94)
2008-05-20[b]	FORS2	Bessell I	8	1.29 - 2.07	373

[a]This transit was also observed by Adams et al. (2010a).

[b]This transit has a incomplete phase coverage.

[c]The number of images descarted in the analisys is shown in parenthesis.

this night. Along the images obtained during this night, the diffraction spikes rotated trough the FoV reaching the comparison stars at different phases of the transit. The bumps also appeared in the light curves of these comparison stars. We use the peak of the larger bump in the light curve of the target to match in phase the bumps of all the other light curves (see Figure 4.3). We average the light curves of the comparison stars in a small region where the bumps were more evident (between the horizontal lines in Figure 4.3) and finally in order to remove the bumps, we substracted this average to the light curve of the transit. In the other nights it was not possible to identify clearly the bumps produced by the diffraction spikes, and therefore we could not reproduce the process mentioned before but we attributed some of the noise in the lights curve to this effect.

We worked with the processed data provided by the *VLT* pipeline which performs the bias and flatfield corrections. The times at the start of the exposure are recorded in the images headers, in particular we used the value of the *Modified Julian Day* keyword of each image and transformed it to *Barycentric Julian Day* (see section 4.4 for details).

Our photometric analysis was done with the Difference Image Analysis Package (DIAPL) written by Wozniak (2000) and recently modified by W. Pych[1]. The package is an implementation of the method developed by Alard & Lupton 1998, and is optimized to work with very crowded fields and/or blended stars, as is the case of OGLE-TR-111 (Figure 4.2). DIAPL models PSF variations along the X-Y coordinates, scales and subtracts the flux of the stars of a template image for each frame, among other calculations. One of the disadvantages of this code is the time required to complete the process, especially since it is not possible to verify the suitability of the input parameters and the quality of the products until the last steps (subtraction and/or photometry). In our case, due the large size of the frames and the large number of stars in the FoV, one iteration required up to 20 minutes. To eliminate a few nearby saturated stars in the field that hindered the photometry and to reduce considerably the processing time we worked on $\sim 500 \times 500$ pixel subframes. Working with these subframes, DIAPL estimations of the PSF, background and flux levels are more representative of the vicinity of our target in each frame and in the reference image; noise as well as obvious systematics in the final photometry are considerably reduced. Reference frames for each night were constructed by combining the 20-27 best images (in terms of seeing and signal-to-noise) depending on the night's conditions. We used aperture radii between 4 to

[1]The package is available at http://users.camk.edu.pl/pych/DIAPL/index.html

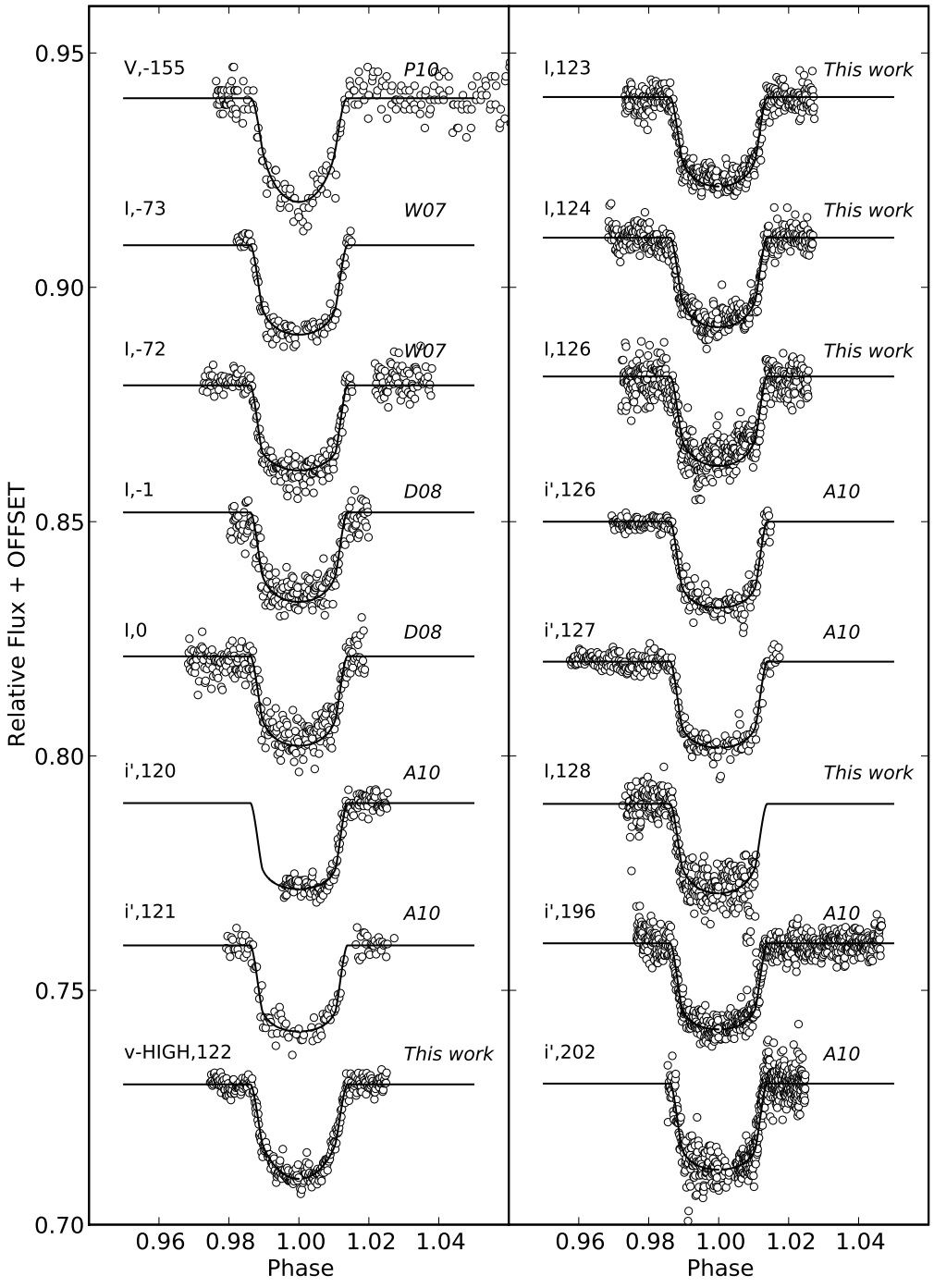

Figure 4.1 Light curves of all transits of OGLE-TR-111b. The solid lines show our best model fits produced by JKTEBOP (see section 4.3). The filter, epoch number and author of the light curve is also indicated.

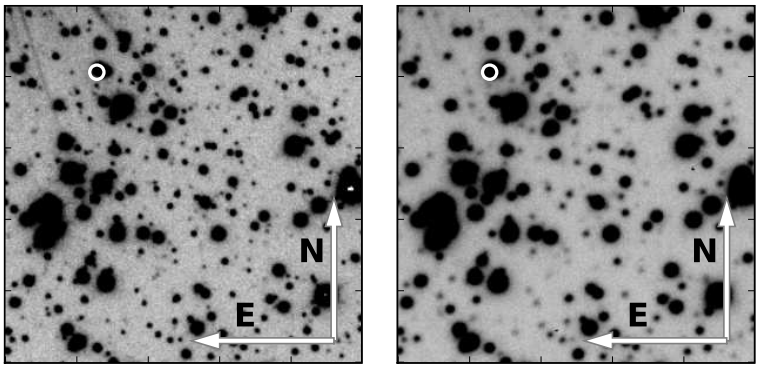

Figure 4.2 Portion of $0.5' \times 0.5'$ images of the night 2008-05-03 observed with FORS2 at VLT. The best image (FWHM$\sim 0.34''$) of the night is shown at the left panel and the worst image (FWHM $\sim 0.55''$) is shown at the right panel. The location of OGLE-TR-111 is marked by the circle. Due to the seeing and pixel scale our target appears blended with a nearby star. Also one of the diffraction spikes of a very bright star is visible at the upper left corner of the best seeing image. Ocassionally, these spikes reached the location of the target contaminating the photometry.

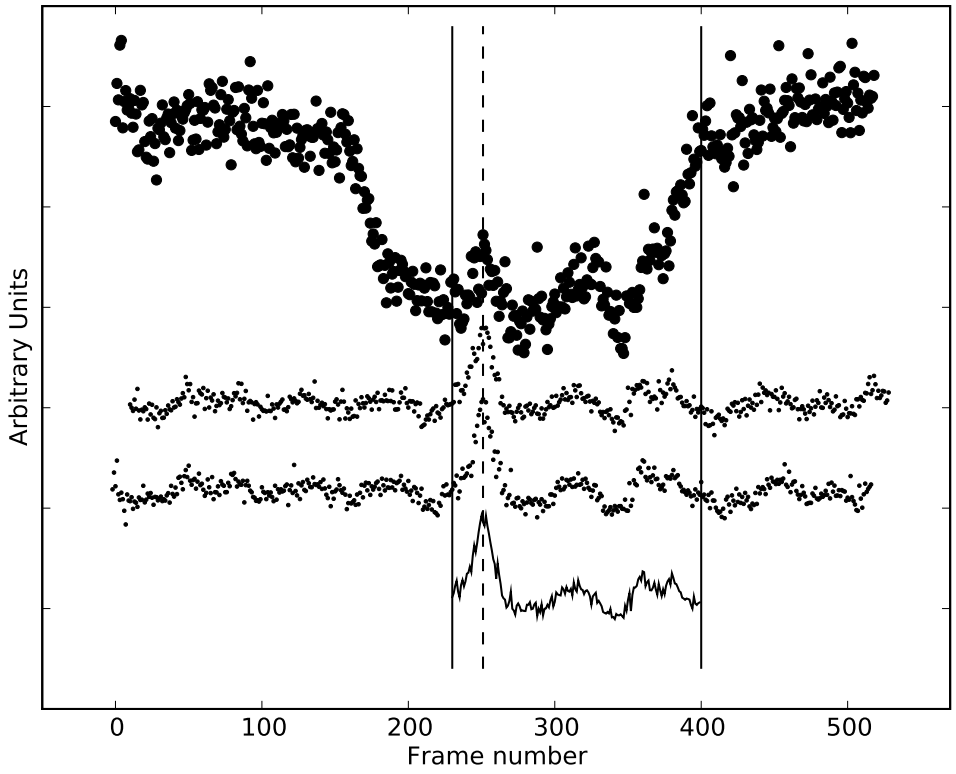

Figure 4.3 Light curve of OGLE-TR-111 (top) and two comparison stars (middle) of the night 2008-05-03 observed with FORS2 at VLT. The contamination produced by the diffraction spikes of a very bright star is evident in the region enclosed by the solid vertical lines. The average flux of the comparison stars (bottom) after aligning the peaks of the bumps (vertical dashed line) was substracted from the light curve of the transit to remove the contamination. This procedure was only applied to this transit.

10 pixels (in DIAPL's task *phot.bash*) to perform the relative photometry of the target and comparison stars (8 to 15 stars) on each subtracted frame.

To obtain an absolute normalization, we performed aperture photometry (DAOPHOT-ALLSTARS, Stetson 1987) in the reference frame of each night using a curve of growth analysis to select the ideal aperture radii.

The resultant light curve contains some remaining systematic variations, which we have modeled using linear regression fits of the out-of-transit data points against the airmass, average FWHM of the point spread function and/or background level around our target of each frame. Doing this we were able to achieve an *RMS* precision of $\sim 0.0013 - 0.0027$ *mag* in the light curves (almost reaching the Poisson noise level in the best nights or doubling it in the worst).

4.3 Modeling Light Curves

We fitted our five new light curves together with all the light curves previously published by W07, D08 and A10, using JKTEBOP[2] (Southworth et al. 2004a). The fit also includes the light curve by Pietrukowicz et al. (2010, P10 hereafter), obtained from the reanalysis of the VIMOS data published by M07. P10 found a problem with the times reported by M07, which results in a mid-transit epoch time difference of ~ 5 minutes. We only consider the P10 analysis of this transit from this point onwards.

Among the parameters fitted by JKTEBOP for each light curve are: the planet to star radii ratio (k), the inclination (i) and eccentricity (e) of the orbit, the out-of-transit baseline flux (F_b), the mid-time of transit (T_c), the quadratic limb darkening coefficients (u_1 and u_2), and the sum of the fractional radii, $r_p + r_s$. The terms r_p and r_s are defined as $r_p = R_p/a$ and $r_s = R_s/a$, where R_p and R_s are the absolute stellar and planetary radii, and a is the orbital semi-major axis. In the case of the limb darkening coefficients, we fixed u_2 to the values given by Claret (2000) and Claret (2004) for each observation's filter (for the *v-HIGH* filter we use the v coefficient) and only left u_{1x} as free parameter during the fitting process described below, where x denotes the filter band. We performed the same fitting method using a linear limb-darkening law obtaining basically the same final χ^2_{red} for each transit, which reveals that the photometric precision of the light curves is not sufficient to distinguish between limb darkening laws. Also, to minimize potential degeneracies between parameters, we fixed the eccentricity and the longitude of the periastron of the orbit to zero, and the planet to star mass ratio to $m_p/m_s = 0.00061$, adopting the mass values derived by Santos et al. (2006).

JKTEBOP also allows for a statistical determination of the error of each parameter, as well as an analysis of the impact of systematics in the light curves, via Monte Carlo simulations. We ran 10^4 Monte Carlo simulations adding random simulated gaussian noise to the input parameters to estimate the uncertainty of each parameter while also testing for potential correlations. When all the parameters described above are left free, there are clear correlations between k, i, and u_{1x}, and also between r_p+r_s and i, as illustrated in Figure 4.4. No significant correlation was observed between any of the other parameters.

[2]http://www.astro.keele.ac.uk/ jkt/codes/jktebop.html

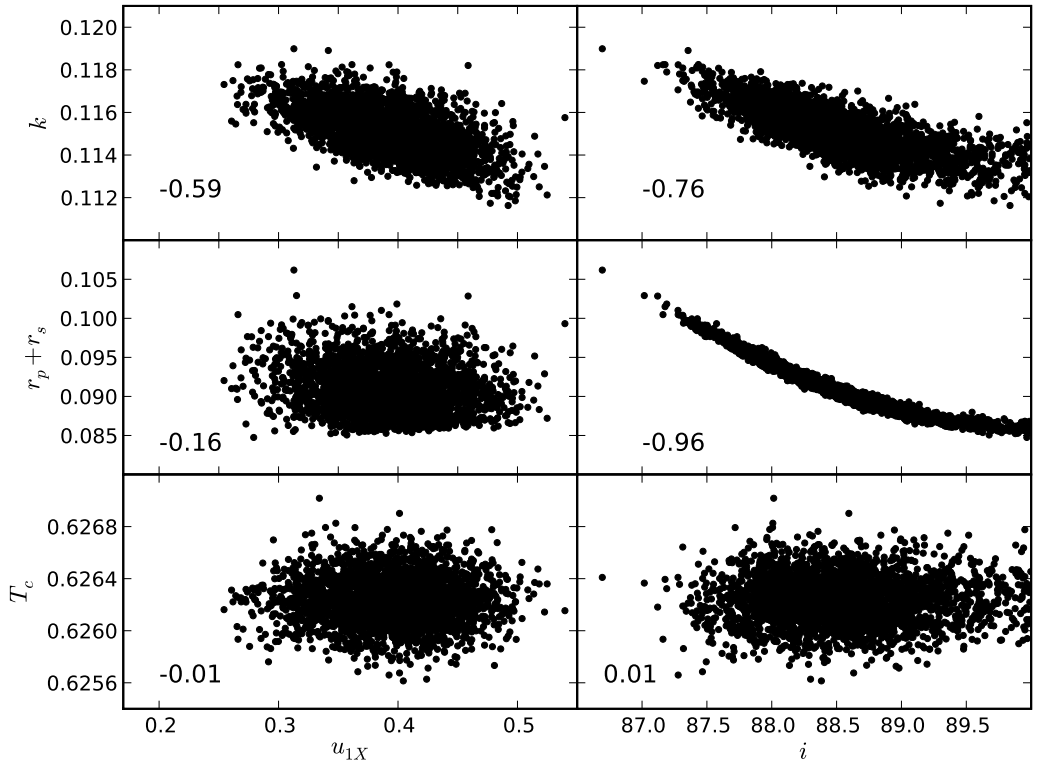

Figure 4.4 3000 results of 10000 Monte Carlo iterations (using JKTEBOP with the data of the night 2008-05-12) which show the correlation between the parameters fitted from the light curves: k, $r_p + r_s$, T_c, i and the linear coefficient u_{1X} of a quadratic limb darkening law, when all are left variable. The correlation coefficients between each variable are shown in the bottom left corner of each box.

Table 4.2. Summary of each step of the fitting process of the light curves of OGLE-TR-111b. See section 4.3 for details.

	Parameters		
Step	Free	Fixed	Reference[a]
I	k, $r_p + r_s$, T_c	i	A10
		u_{1x}	Claret
II	i, u_{1x}, T_c	k, $r_p + r_s$	Step I
III	T_c	k, $r_p + r_s$	Step I
		i, u_{1x}	Step II

[a]This column shows the origin of the adopted value of the fixed parameter.

These correlations can be minimized by fitting the parameters in three steps, also running 10^4 Monte Carlo simulations on each step. First, we fixed the inclination of the orbit to the value obtained by A10, $i = 88.3''$ together with the corresponding value of u_{1x} from the Claret tables and fitted k and $r_p + r_s$ for each light curve. Next, we fixed k and $r_p + r_s$ to the weighted average of the individual fits obtained in step I, and left i and u_{1x} as a free parameters. Finally, we adopted the weighted average of the resulting inclinations and the corresponding u_{1x} for each filter (because we have only one transit observed with *v-HIGH* and one with V we adopted directly the results of JKTEBOP for its u_{1x}), and fitted only for T_c. In Table 4.2 we summarized each step of the fitting process. An example of the histograms of the distribution of values for each parameter for the night 2008-05-12 are represented in Figure 4.5. The adopted values of each parameter for the individual light curves are summarize in Table 4.3. The average values for the system based on all light curves (Figure 4.1) are summarized in Table 4.4. To test the consistency of the Monte Carlo error estimates, we compared it to the results of the prayer-bead method (Bouchy et al. 2005). While the Monte Carlo method gives an idea of the white noise in the data, any level of red noise (time correlated noise,) is best characterized by the prayer-bead method. The errors obtained by the prayer-bead method were, in general, larger than the Monte Carlo errors, showing that red noise is the dominant factor in the light curves. In Table 4.3 we show the ratio R of the errors estimated by the Prayed-Bead and the Monte Carlo method. We adopted as 1σ errors of the parameters reported in Table 4.3, the larger values between these two error estimations.

The Levenberg-Marquardt Monte Carlo (LMMC) fitting method implemented by JKTEBOP, can present some disadvantages with respect to the Markov Chain Monte Carlo (MCMC), method used by several other recent TTVs studies. For example, LMMC can be trapped in a local mimima or/and can underestimate the errors of the fitted parameters (e.g. Fischer et al. 2009). Despite this, our results in Table 4.3 for the analysis of previously published light curves are fully consistent with the parameter fit values reported in Table 5 of A10 using MCMC. LMMC and MCMC are expected to yield similar results in well-behaved parameter space, i.e. with no multiple minima, as seem to be the case of our dataset. Even though, it is possible that the errors of LMMC best-fit parameters (provided by the parameter distribution of the Monte Carlo iterations) can be underestimated, but our adopted parameter errors are dominated/scaled by the red noise contribution (see the R values in Table 4.3), indeed our errors are very conservative in comparison with A10 estimations.

4.4 Timing Analysis

The mid-time for each transit derived in the previous section and listed in Table 2 was converted to Barycentric Julian Days, expressed in terrestrial time, i.e. BJD(TT), following the standard timing reference system recommendations by Eastman et al. (2010). Since our analysis includes data from different instruments/telescopes, spanning over four years, and reduced by different groups we checked carefully for any possible systematics. As example, A10 has already pointed out how previously published results on OGLE-TR-111b had not corrected the reported times for leap seconds (UTC to TAI) nor for the 31.184 second conversion between TAI and TT, where TAI is defined as the *International Atomic Time*. We have applied the same corrections to all the literature light curves used in our analysis.

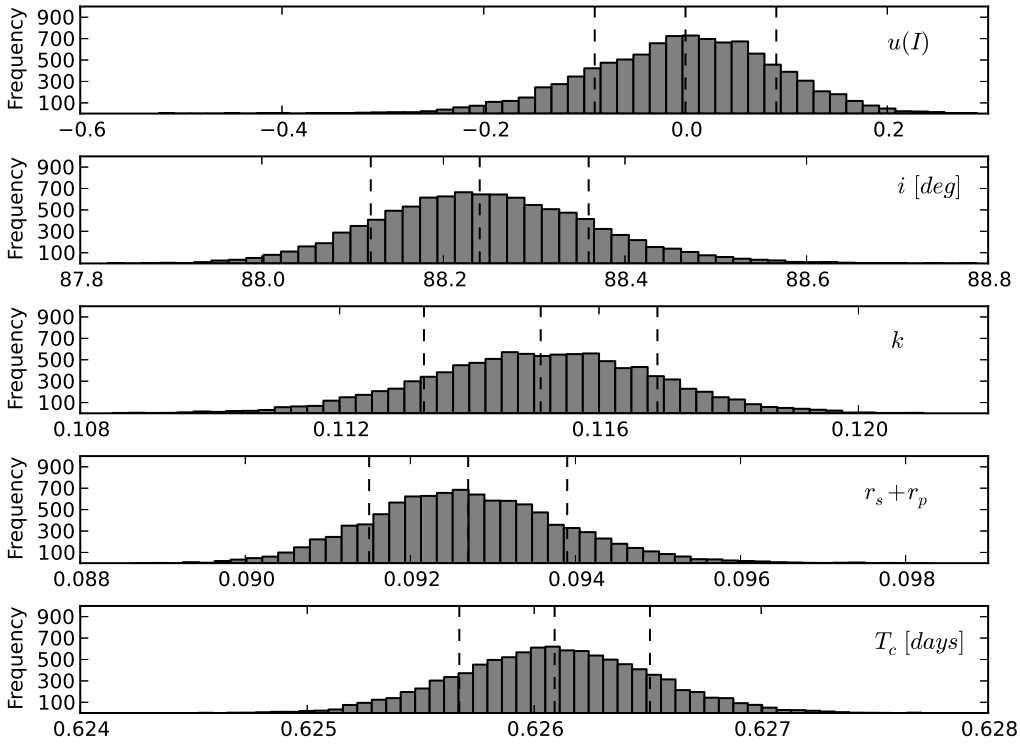

Figure 4.5 Histograms of the 10 000 Monte Carlo iterations (using JKTEBOP with the data of the night 2008-05-12) for the fitted parameters on each of the : T_c, $r_p + r_s$, k, i and the linear coefficient u_{1x} of a quadratic limb darkening law obtained after the steps I, II and III described in Section 4.3. The dashed lines show the fitted value and the $\pm 1\sigma$ errors which were compared with the red noise estimation using the prayer-bead method. The same analysis was performed on each of the 16 transits. The final value of k, $r_p + r_s$, i, $u_{1i'}$ and u_{1I} corresponds to the weighted average of these results, except for $u_{1v-HIGH}$ and u_{1V} where we adopted the results of JKTEBOP (see text).

Table 4.3. Adjusted parameters for each transit using JKTEBOP code.

Transit date[a]	k	R[b]	$r_p + r_s$	R	i [°]	R	u_{1x}	R	$T_c - 2450000$ (BJD)	R	χ^2_{red}
2008-04-26(122)	0.1203(23)	0.6	0.0926(17)	0.8	88.35(14)	0.4	0.81(05)	0.5	4582.56853(48)	0.5	0.17
2008-04-30(123)	0.1168(15)	1.1	0.0929(13)	1.3	88.22(12)	1.3	0.20(08)	1.3	4586.58288(72)	2.2	0.57
2008-05-04(124)	0.1169(21)	1.6	0.0947(19)	2.0	88.49(15)	1.5	0.22(05)	0.9	4590.59853(94)	3.0	0.69
2008-05-12(126)	0.1151(29)	1.7	0.0927(19)	1.6	88.24(27)	2.3	0.00(28)	3.0	4598.6261(18)	4.2	0.66
2008-05-20(128)	0.1265(24)	1.4	0.109(17)	1.2	89.37(99)	0.8	0.13(13)	2.0	4606.65482(89)	1.9	1.34
2005-04-09(-155)	0.1179(87)	1.1	0.0990(69)	1.2	88.89(53)	0.7	0.89(08)	1.5	3470.5684(11)	1.5	1.08
2006-02-21(-76)	0.1266(15)	0.8	0.0934(08)	0.8	88.70(36)	0.4	0.45(05)	0.9	3787.70928(56)	1.9	1.15
2006-03-05(-73)	0.1246(12)	0.8	0.0934(08)	1.2	88.78(16)	1.2	0.61(04)	1.1	3799.75213(81)	2.9	1.08
2006-12-19(-1)	0.1122(19)	0.8	0.0899(12)	1.0	87.85(17)	1.7	0.03(25)	2.4	4088.7922(19)	4.9	1.3
2006-12-23(0)	0.1139(26)	1.5	0.0910(11)	1.0	87.97(21)	2.1	0.06(22)	2.3	4092.8056(15)	3.7	1.14
2008-04-18(120)	0.1245(31)	2.1	0.098(16)	1.4	87.92(81)	17.3	0.26(12)	1.6	4574.54272(83)	2.3	0.99
2008-04-22(121)	0.1190(21)	0.8	0.0944(16)	1.0	88.54(17)	0.9	0.40(07)	0.8	4578.55497(43)	1.0	0.96
2008-05-12(126)	0.1183(13)	1.2	0.0915(09)	1.3	88.14(10)	1.4	0.26(07)	1.5	4598.62754(47)	1.9	1.02
2008-05-16(127)	0.1214(16)	1.5	0.0922(14)	1.8	88.38(13)	1.5	0.35(07)	1.7	4602.64167(47)	1.7	0.99
2009-02-17(196)	0.1187(15)	1.7	0.0926(15)	2.5	88.27(17)	3.0	0.27(09)	2.7	4879.63863(55)	2.7	1.01
2009-03-13(202)	0.1236(09)	1.0	0.0893(06)	0.9	88.13(13)	1.5	0.28(08)	1.4	4903.72566(26)	1.0	1.01

Note. — The values shown in parenthesis correspond to the errors in the last digits.

[a]The Epoch number is shown in parenthesis.

[b]R: Prayer-Bead and Monte Carlo errors ratio. See text for details.

Table 4.4. Final Parameter Values of OGLE-TR-111b

Parameter	Adopted Value	Error
k	0.1213	±0.0004
$r_p + r_s$	0.0917	±0.0003
i [°]	88.29	±0.04
Period [days]	4.0144477	±0.0000019
$T_o(BJD)$	2454092.80691	±0.00030
$u_{1v-HIGH}$	0.81	±0.05
u_{1I}	0.426	±0.024
$u_{1i'}$	0.313	±0.033
u_{1V}	0.89	±0.08

As an additional check to our reduction, light curve fitting and timing correction procedure, we compared our final BJD(TT) times to those published by A10. Particularly valuable for this test is the 2008-05-12 transit epoch, which was independently observed by us and A10. As illustrated in Figure 4.6, in spite of adopting completely different approaches to fit the light curves, all our derived transit mid-times agree well with the values obtained by A10. When comparing the T_c of our 2008-05-12 transit with A10's, both times agree within the 1σ error of our observation, although our mid-transit time occurs 124 seconds earlier. Four of the five transits we measure also produce mid-transit times on average 100 seconds earlier than the ephemerides predict (see Figure 4.6), although the differences are not statistically very significant. However, we have decided to further investigate the potential source of this discrepancy. First, we confirmed with the VLT staff that the times recorded in the image headers are the UTC times at the beginning of each exposure of our data (including all leap seconds). We further tested for any potential systematics between datasets by binning our data to 60 seconds, and removing the last ~ 50 points in our light curve to make it match the light curve sampling and phase coverage of A10. The result was only a 10 second time shift in the resulting T_c compared with the previous fit value. The two transits were observed in different filters, but we find no correlations between the limb darkening coefficients and T_c (see Figure 4.4) that could account for this mid-time discrepancy. We attributed this difference to the red noise in the FORS light curve, possibly due to weather (the R value of T_c of this transit in Table 4.3 is almost twice the value of A10 light curve).

Figure 4.7a shows the updated *Observed minus Calculated* (O-C) diagram with all the final BJD(TT) mid-time values calculated from the literature light curves and our five new transits. The data show a linear trend which can be attributed to the accumulation of timing uncertainties with respect to the adopted transit ephemerides (D08). After removing that linear trend (Figure 4.7b), the data are consistent with a constant period ephemeris equation of the form:

$$T_c = 2454092.80691(25)[BJD] + 4.0144477(16) \times N, \tag{4.1}$$

where T_c is the central time of a transit in N epochs since the reference time T_0. This fit has a reduced χ^2 of 1.8, so the errors in T_c have been rescaled by a factor of $\sqrt{\chi^2} = 1.18$ to make them consistent with $\chi^2 = 1$ (see errorbars in Figure 4.7b), The new period is fully consistent with the one obtained by A10.

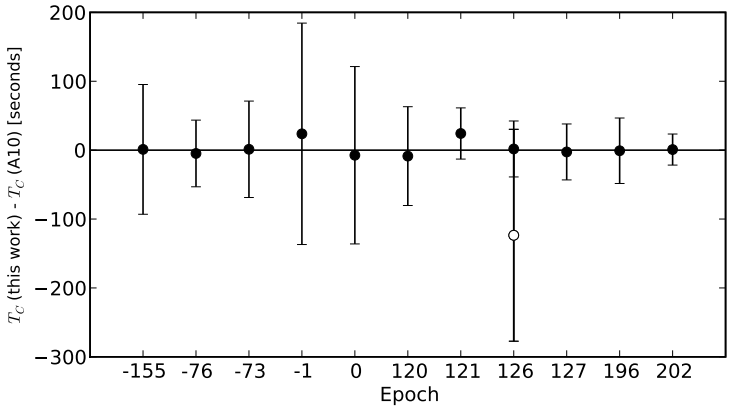

Figure 4.6 Comparison of the eleven mid-transit times, T_c, obtained by A10 and recomputed by us in this work. Solid circles show the difference between the T_c measured by each group. The open circle shows the T_c for the new transit we observed in 2008-05-12 UT, and coincides with one of the transits measured by A10. Although we find that the transit occurs 124 seconds earlier, both results are consistent within the errors.

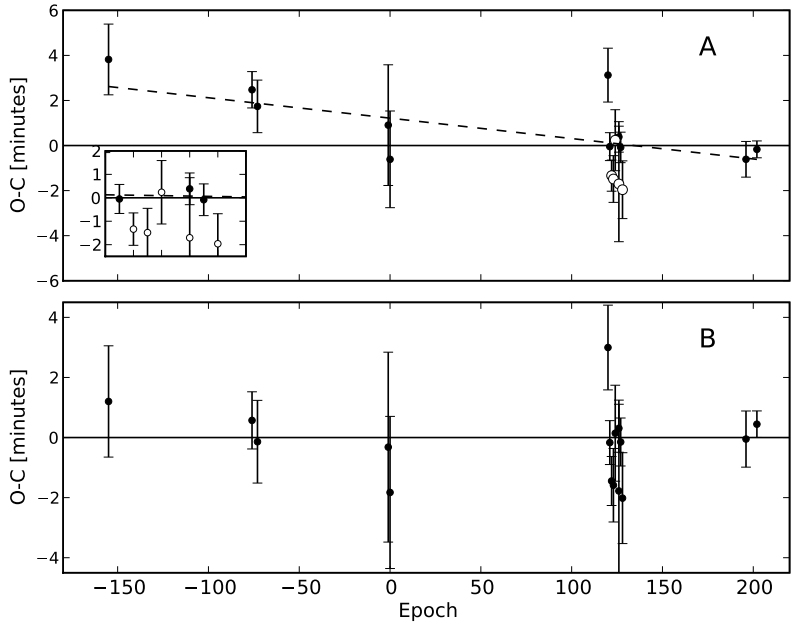

Figure 4.7 **Panel-A:** *Observed minus Calculated* diagram of the central times of the transits of OGLE-TR-111b. Black dots represent the times obtained with data from Pietrukowicz et al. (2010), Winn et al. (2007), Díaz et al. (2008) and Adams et al. (2010a), while the white dots are from the transits of this work. The dashed line represents a linear fit of the data. In the small box a zoom of the points between 110th and 120th epochs is shown. **Panel-B:** When the linear trend is removed no variations of more than 1.5 minutes are present. The errors were rescaled by $\sqrt{\chi^2} = 1.18$ to make them consistent with a linear fit with $\chi^2_{red} = 1$.

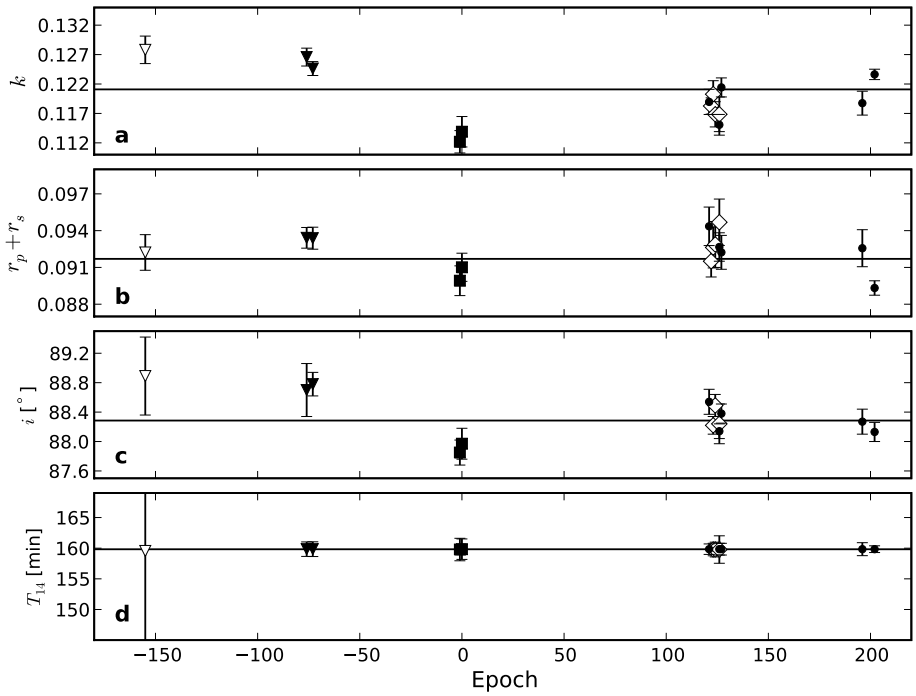

Figure 4.8 Resulting values for the ratio of the radii (**Panel a**), sum of the fractional radii (**Panel b**), orbit's inclination (**Panel c**) and duration of the transit (**Panel d**), defined as the time between the first and fourth contact, for each light curve using JKTEBOP. Open and solid triangles correspond to Pietrukowicz et al. (2010) and Winn et al. (2007) transits. Solid squares correspond to the two transits of Díaz et al. (2008) and solid dots represent the transits of Adams et al. (2010a). Open diamonds correspond to the new transits of this work.

4.5 Analysis of additional parameters of the light curves

We tested for possible variations of the physical parameters of the OGLE-TR-111 system using the values of the transit duration, T_{14}, the inclination, the planet to star radius ratio, and the sum of the fractional radii derived for each transit with JKTEBOP. The value of each of those parameters over time is represented in Figure 4.8.

There is no evidence of trends for any of the inspected parameters. However, it is noticeable that the results from the light curves observed by different groups appear clustered around the same values. We attribute that clustering to systematics introduced by the way the photometry is performed (i.e. aperture or PSF photometry, differential image analysis, and so on), and probably also by the way the light curve systematics are treated by the different groups. For example, D08 already pointed out that the depths of their transits were smaller than the average and that this was due to a reduction artifact of the differential image subtraction techniques previously noticed by Gillon et al. (2007). Although we used DIAPL instead of aperture photometry, our results are consistent with those of A10. Notice, however, that systematics in the transit depths have no effect in the determination of the transit midtimes.

4.6 Limits to additional planets

Based on the timing constrain of our $O-C$ diagram, i.e. no TTV variations with amplitudes larger that 1.5 minutes over a three year period, we run dynamical simulations to place limits on the mass and the semi-major axis of a possible orbital companion of the transiting planet using the *MERCURY* code (Chambers 1999). The first step was to explore stable orbital regions by assuming a massless point particle over a range of initial semi-major axes, and fixing all the other input variables to the known physical parameters of the system. The orbital evolution of the massless particle was integrated over 10^6 *days*. This test yields a strip of unstable orbits between $0.034 - 0.056$ AU, where encounters between the test particle and OGLE-TR-111b would occur. For all the other orbits we calculate TTVs of the transiting body with the hypothetical coplanar perturber using a wide range of masses ($0.1\ M_{\oplus} \leq M_{per} \leq 5000\ M_{earth}$), variable density (from Earth to Jupiter density depending on the mass) and semi-major axes ($0.02\ AU \leq a \leq 0.13\ AU$ in steps of $0.005\ AU$) with $\sim$ 4500 simulations over 7 years. All the initial relative angles were fixed to zero. Near resonances, the steps in the variables were reduced to increase precision. Only the last 5 years were used for the timing analysis, since that is about the same time span covered by the observations, and also to minimize any effects introduced by the choice of initial parameters. Then we calculated the central time of each transit during all the simulations. Similarly to what was done in section 4.4, we did a linear fit of these central times and we defined the TTV of each simulation as the standard deviation of the central times with respect to this linear fit. We checked that the final period of the transiting planet did not change by more than 3σ from its initial value due the gravitational interaction. With this method we were able to make a *mass* vs a diagram (Figure 4.9-A) where the solid line represents TTVs of 1.5 minutes. For comparison we also plot the mass limits of TTVs of 0.5 and 5 minutes (dotted and dash-point lines). The dashed line corresponds to the detectability limit placed by radial velocity observations (Santos et al. 2006). Our mass constrains are upper limits since for perturbers

with an orbital eccentricity different from zero, the mass necessary to produce TTVs of the same amplitude will be lower. We confirm this by performing a set of simulations with $e = 0.3$ and using as input parameters the values (M_{per}, a) which produced TTVs ~ 1.5 min in the case $e = 0$ (see Figure 4.9-B). With this configuration the unstable region becomes wider due to encounters between the orbital bodies and the TTVs produced for a given mass were larger than in the case of $e = 0$. Same results were obtained setting the initial values of the longitude of the periastron different from zero (90°, 180° and 270°) and $e = 0.3$. Combining TTV *RMS* and radial velocities we can rule out the presence of a perturber body with mass greater than 1.3, 0.4 and 0.5 M_{earth} at the 3:2, 1:2, 2:1 resonances with OGLE-TR-111b and lower the upper limit in the region exterior to the planet until ~ 0.08 AU to companions of less than ~ 30 $M_{\oplus}$.

4.7 Conclusions

We present 5 new transit light curves of OGLE-TR-111b. We homogeneously model all available light curves in the literature and search for any variation in the timing of the transits. With our updated ephemeris equation we find no TTVs with amplitudes larger than 1.5 minutes and therefore we rule out the presence of a companion in the 2:1, 3:2 and 1:3 orbital resonances. If the system has an additional orbiting body, its mass has to be lower than 30 $M_{\oplus}$ if is located between 3:2 and 1:2 resonances. The mass limits we place with our dynamical simulations based in the TTV data are lower than the limits obtained with radial velocities alone. We search for any trend in the duration, depth of the transit and inclination of the orbit but we do not see any clear evidence of variation with statistical significance. We point out that systematics of no evident source in the observations, reduction and/or analisys processes can induce differences in the values of the parameters obtained from the light curves and therefore a monitoring of transiting exoplanets carry out by the same group can contribute to reduce these differences.

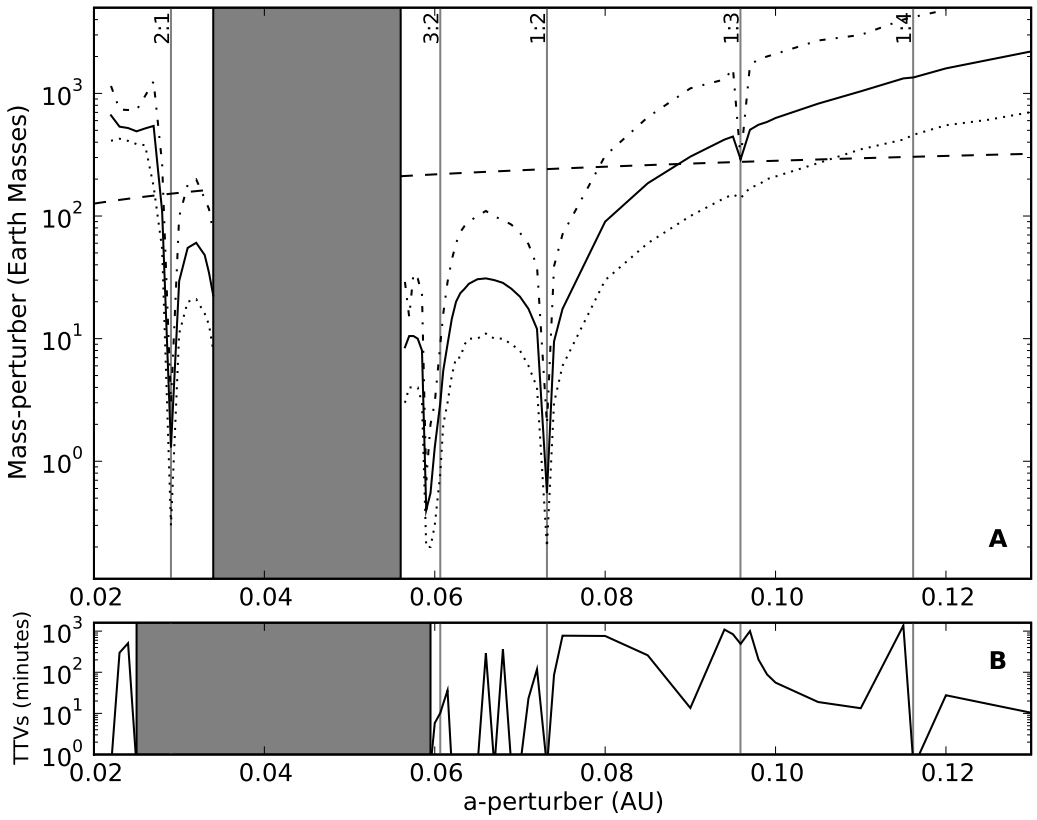

Figure 4.9 **Panel-A:** Upper mass limits of an orbital perturber. These simulations were computed using $e = 0$. The solid line represents transit timing variations of 1.5 minutes. The dotted line and dash-point line represent TTVs of 0.5 and 5 minutes, respectively. The dashed line corresponds to the limits due the radial velocities observations. Vertical lines and gray strip indicate the orbital resonances locations and the instability region respectively. An orbital companion of OGLE-TR-111b should have a mass in the region below the black solid line which corresponds to the mass limit imposed by the timing analysis. **Panel-B:** Transit Timing Variations with $e = 0.3$. If the eccentricity of the perturber represented by the solid line in Panel-A is increased, it will exhibit larger values than 1.5 minutes for its TTVs. Regions with TTVs below 1 minute correspond to unstable orbits with this new configuration.

Chapter 5

Analysis and Results of WASP5-b

Transit Monitoring in the South (TraMoS) project: Discarding Transit Timing Variations in WASP-5b

S. Hoyer[1], P. Rojo[1], M. López-Morales[2,3]
The Astrophysical Journal, Accepted

[1]: Astronomy Department, Universidad de Chile, Casilla 36-D, Santiago de Chile, Chile.

[2]: Institut de Ciencies de l'Espai (CSIC-IEEC), Campus UAB, Facultat de Ciencies, Torre C5, parall, 2a pl, E-08193 Bellaterra, Barcelona, Spain.

[3]: Carnegie Institution of Washington, Department of Terrestrial Magnetism, 5241 Broad Branch Rd. NW, Washington, D.C. 20015, USA.

Abstract

We report nine new transit epochs of the extrasolar planet WASP-5b, observed in the *Bessell I* band with SOAR at the Cerro Pachon Observatory and with the SMARTS 1-m Telescope at CTIO, between August 2008 and October 2009. The new transits have been combined with all previously published transit data for this planet to provide a new Transit Timing Variations (TTVs) analysis of its orbit. We find no evidence of TTVs *RMS* variations larger than 1 min over a 3 year time span. This result discards the presence of planets more massive than about 5 $M_{\oplus}$, 1 $M_{\oplus}$ and 2 $M_{\oplus}$ around the 1:2, 5:3 and 2:1 orbital resonances. These new detection limits exceed by $\sim 5-30$ times the limits imposed by current radial velocity observations in the Mean Motion Resonances of this system. Our search for the variation of other parameters, such as orbital inclination and transit depth also yields negative results over the total time span of the transit observations. This result supports formation theories that predict a paucity of planetary companions to Hot Jupiters.

Based on the work accepted in Hoyer et al. (2011a) and reproduced by permission of the AAS.

5.1 Introduction

In 2008, the WASP-South survey reported their second detection of an exoplanet, WASP-5b, transiting a relatively bright star ($V = 12.3$) in the Southern Hemisphere (Anderson et al. 2008, hereafter A08). This discovery paper, based on WASP photometry and two additional transit epochs plus radial velocities measurements, announced a Hot-Jupiter planet with a mass of $M_P = 1.58^{+0.13}_{-0.08}\ M_J$ and a density of $\rho_p = 1.22^{+0.19}_{-0.24}\ \rho_J$, orbiting a G4V star with a period of $P = 1.62$ days.

Gillon et al. (2009) did a reanalysis of the A08 data to produce the first timing study of WASP-5b and arrived to the conclusion of potential period variations, based on a $\sim$ 2-minute shift in the timing residuals of the most precise points.

Southworth et al. (2009a), hereafter S09, observed two new transits, for which they achieved very high photometric precision by defocusing the images at the 1.54-m Danish Telescope at La Silla Observatory, but at the expense of producing only 3-minute cadence. They refined the linear ephemeris of the system and concluded the high deviation of the timing residuals with respect to that straight line ($\chi^2_{red} = 5.7$) found by Gillon et al. (2009) was based on the divergence of only one point out of six. Smith et al. (2009) searched for signatures of additional planets in the residuals of WASP light curves after removing the transits of WASP-5b, and found no evidence of a transiting companion down to Saturn-size planets within periods of up to 20 days.

Other recent works have determined and refined several physical parameters of the system. For example, Triaud et al. (2010) determined the angle between the orbital plane of WASP-5b and the spin axis direction of its host star to be consistent with zero ($\lambda = 12^{\circ}{}^{+10}_{-8}$). This conclusion has been confirmed by the reanalysis of Fukui et al. (2011), hereafter F11, who obtain $\lambda = 7.2^{\circ} \pm 9.5$.

F11 additionally searched for TTVs of WASP-5b using seven new transit epochs, combined with all previously available observations. They find a RMS of about 68 seconds in their timing residuals despite of having an average of 41 seconds uncertainty per epoch, and proposed that such a large deviation from a linear fit ($\chi^2 = 32.2$ for 9 degrees of freedom) can be explained by an orbital perturber. Using dynamical simulations F11 constrained the masses of this hypothetical perturber to 2 $M_\oplus$ in the 1:2 and 2:1 mean motion resonances (MMRs) and set a mass of 43 $M_\oplus$ for a potential Trojan body.

Dragomir et al. (2011), hereafter D11, reported two new transits of WASP-5b with data of the 1-m telescope at Cerro Tololo Inter-American Observatory.

In this work we present nine additional transits of WASP-5b, observed between August 2008 and October 2009, and perform a new homogeneous timing analysis of all available epochs to further confirm or rule out the TTV signals previously proposed for this system.

In section 5.2 we describe the new observations and the data reduction. Section 5.3 details the modeling of the light curves and in section 5.4 we present the timing analysis. In Section 5.5 we discuss the mass limits for a *unseen* perturber. Finally, we present our conclusions in section 5.6.

Table 5.1. Observational information of each night.

Transit Date	Telescope/Instrument	Filter	Integration Time [s]	airmass range	Epoch
2008-08-21	SMARTS-1m/Y4KCam	Bessell I	13	1.7 - 1.01	199
2008-08-29[a]	SMARTS-1m/Y4KCam	Bessell I	10	1.05 - 1.02 - 1.06	204
2008-09-21[a]	SMARTS-1m/Y4KCam	Bessell I	10,7	1.9 - 1.01 - 1.07	218
2008-10-22[b]	SOAR/SOI	Bessell I	7,5,3	1.12 - 1.02	237
2008-11-04	SOAR/SOI	Bessell I	3	1.07 - 1.02 - 1.4	245
2008-11-17	SMARTS-1m/Y4KCam	Bessell I	10	1.02 - 1.4	253
2009-06-22	SOAR/SOI	Bessell I	7,5,3	1.95 - 1.02	387
2009-08-06[b]	SOAR/SOI	Bessell I	5,4	1.07 - 1.15	414
2009-10-25	SMARTS-1m/Y4KCam	Bessell I	15	1.06 - 1.02 - 1.97	463

[a]This transit was also observed by Southworth et al. (2009a).

[b]This transit has a incomplete phase coverage.

5.2 Observations and data reduction

In 2008 we started the Transit Monitoring in the South Project, which is a monitoring campaign of transiting planets observable from the Southern Hemisphere (Hoyer et al. 2011b), following the approach of using high-cadence observations and the same instruments and setups to try to minimize systematics and reduce uncertainties in the mid-transit times, as well as other transit parameters. For the TraMoS project we have already observed more than 60 transits of over 20 exoplanets.

As part of TraMoS we observed a total of nine transits of WASP-5b, between August 2008 and October 2009[1], with the Y4KCam on the SMARTS 1-m Telecope at Cerro Tololo Inter-American Observatory (CTIO) and with the SOAR Optical Imager (SOI) at the 4.2-meter Southern Astrophysical Research (SOAR) telescope in Cerro Pachón.

Y4KCam is a 4064×4064 CCD camera with a Field of View (FoV) of 20×20 squared arcminutes and a pixel scale of 0.289 arcsec pixel^{-1}. The standard readout time of the camera is 46 sec, which we reduce to $\sim$ 16 sec by binning 2x2. The SOI detector is composed of two E2V mosaics of 4096×4096 pixels with a scale of 0.077 arcsec pixel^{-1}, giving a FoV of 5.2×5.2 squared arcminutes. The instrument has a 20.6 sec standard readout, which becomes only ~ 11 sec after binning 2x2.

All nine transits were observed using a *Bessell I* filter ($\lambda_{\rm eff} = 8665$ $\AA$ and FWHM=3914 $\AA$) to reduce limb darkening effects in our light curves. Six of the transits were fully covered in phase. A fraction of the ingress of the 2008-11-03 transit was not observed because a telescope system crash as illustrated in Figure 5.1. Nevertheless, this transit was treated as a *complete* transit. Two other transits, 2009-08-05 and 2009-10-21, were only partially covered with data between phases $-0.034 \lesssim \phi \lesssim 0.01$ and $0.12 \lesssim \phi \lesssim 0.06$, respectively. Two of our transits, 2008-08-29 and 2008-09-21, coincide with the transit epochs published by S09. The observing log is summarized in Table 5.1.

[1]In the remaining of the text we refer to each individual transit by the UT date of mid-time of the transit, using the following notation YYYY-MM-DD

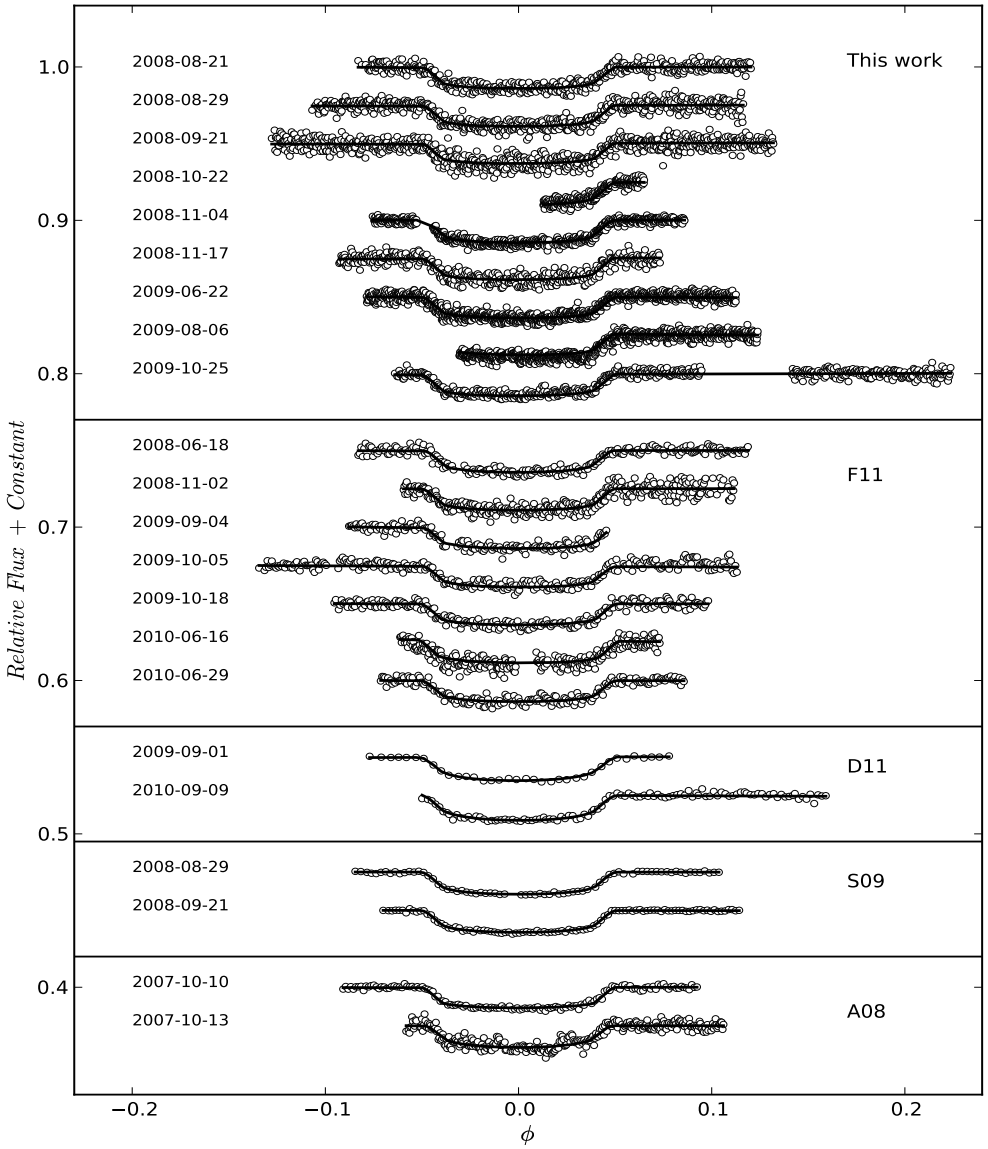

Figure 5.1 Light curves of the nine transits of WASP-5b presented in this work, the seven transits of F11, the two transits of D11, S09 and A08. The solid lines show our best model fits using TAP (see section 5.3.2). The UT date is indicated in the left of each light curve.

The initial trimming, bias and flatfield corrections of all the collected data were performed using custom-made pipelines specifically developed for each instrument. The times at the start of the exposure are recorded in the image headers, in particular we used the value of the *Modified Julian Day* (JD-2400000.5) field. In the SMARTS telescope, the time stamp recorded in the header of each frame is generated by a *IRIG-B GPS time synchronization protocol* connected to the computers that control the instrument. The SOAR telescope data use the time values provided by a time service connected to the instrument. We confirmed that these values have ~ 1 second precision. The time value assigned to each frame corresponds to the *Julian Day* at the start of the exposure plus 1/2 of the integration time of each image (see section 5.4 for details).

WASP-5 is located in a relative empty field, where both the target and several well suited comparison stars appear well isolated in our images. Therefore, we extracted the flux from the target and comparison stars via standard aperture photometry, and using our own python-based code. We used a range of stellar apertures between 8 and 12 pixels, and sky rings which extended between 25 and 35 pixels in radius.

For each sky-aperture combination, we generated differential light curves between the target and each comparison star to 1) optimize the apertures and 2) select the best comparison stars. The criterium used in both cases was *RMS* minimization for the out-of-transit and in-transit data (excluding the ingress and egress portions of the light curves). The final light curves were generated computing the ratio between target's flux and the best 2 to 5 comparison stars.

Finally, some systematics remaining after this step were removed by means of linear or quadratic regression fits to the out-of-transit light curve points using X-Y pixel position, time and/or airmass as free parameters. The final light curves present average photometric dispersions of the order of 0.2% - 0.45%.

5.3 Light Curve Modeling

5.3.1 Algorithm Comparison

We performed a comparison between algorithms that use different statistical uncertainty estimation techniques to the transit's parameters, in order to test potential systematics between them. There are different approaches to do that statistical error estimation analysis; for example, JKTEBOP[2] (Southworth et al. 2004a,b) uses the Levenberg-Marquardt Monte Carlo (LMMC) technique to compute errors (see e.g. Southworth 2010, Hoyer et al. 2011b), while several other studies have started to implement Monte Carlo Markov Chains (MCMC) techniques (e.g. Adams et al. 2010a, Fulton et al. 2011).

In Hoyer et al. (2011b) we proposed that the results of both, the LMMC and MCMC algorithms are equivalent if the parameter space lacks of local minima, where LMMC minimization can be trapped. Here we further test that proposal by comparing the results of both algorithms on the WASP-5b data used for this study. We compare the results of fitting

[2]http://www.astro.keele.ac.uk/ jkt/codes/jktebop.html

Table 5.2. Values obtained with Levenberg-Marquardt Monte Carlo (JKTEBOP) and Markov Chain Monte Carlo (TAP) algorithms with data of the 2008-08-21 transit of WASP-5b.

Parameter	JKTEBOP	TAP
R_p/R_s	0.0988 ± 0.0018	0.0988 ± 0.0026
i [°]	83.4 ± 1.5	83.7 ± 2.3
$\mu_1(I)$	0.22 ± 0.12	0.45 ± 0.11
$T_c - 2454699$ (UT)	$0.67690 \pm .00035$	0.67697 ± 0.00041
$(R_p + R_s)/a$	0.223 ± 0.015	$\cdots$
a/R_s	$\cdots$	5.01 ± 0.48

a light curve of WASP-5b with JKTEBOP and the Transit Analysis Package[3] (TAP; Gazak et al. 2011), which implements the MCMC method for the estimation of errors (more details in Fulton et al. 2011, and references therein).

Among the parameters that JKTEBOP allows to fit are: the planet-to-star radius ratio (R_p/R_s), the inclination (i) and eccentricity (e) of the orbit, the out-of-transit baseline flux (F_{oot}), the mid-time of transit (T_c), the quadratic limb darkening coefficients (μ_1 and μ_2), and the sum of the fractional radii, $R = R_p/a + R_s/a$, where R_p and R_s are the absolute stellar and planetary radii, and a is the orbital semi-major axis. TAP allows to fit for all those parameters except for the latter, which is replaced by a/R_s.

For the comparison we left free all the mentioned parameters except a/Rs and R in TAP and JKTEBOP, respectively, since they otherwise presented convergence problems. We also fixed $F_{OOT} = 1$, $e = 0$ and $\mu_2(I) = 0$ and the orbital period to $P = 1.62843142$ days from F11 since any variation in this parameter will be detected later in our timing analysis. We used 10^4 iterations in JKTEBOP and 10 chains of 10^5 steps each in TAP. We discarded the first 10% iterations on each chain to compute the final parameter's values and its respective errors. The results on each fit, shown in Table 5.2, reveal that the resultant fit values of all parameters common to the JKTEBOP and TAP algorithms agree within the error, except for $\mu_1(I)$.

Figure 5.2 shows the distribution of each parameter obtained using the LMMC and the MCMC techniques with data from 2008-08-21 transit (similar analysis was done with the other 6 complete light curves). From the three bottom panels in the Figure 5.2 it is evident that the 1σ errors (defined as the 68% of a Gaussian fit to the parameter value distributions) obtained with LMMC are generally smaller than those obtained using MCMC, since the latter does a more exhaustive exploration of the parameter space and therefore performs better error estimations. Also, from the top-panel of Figure 5.2, it can be seen that the LMMC results for certain parameters can appear biased towards their initial input values. That is the case for the linear limb-darkening coefficient, for which the value resulting from the LMMC analysis is $\mu_1(I) = 0.22 \pm 0.12$ (the initial value was 0.296). On the other hand, the distribution of values for this parameter on a single epoch as given by MCMC does not appear Gaussian,

[3] http://ifa.hawaii.edu/users/zgazak/ifA/TAP.html

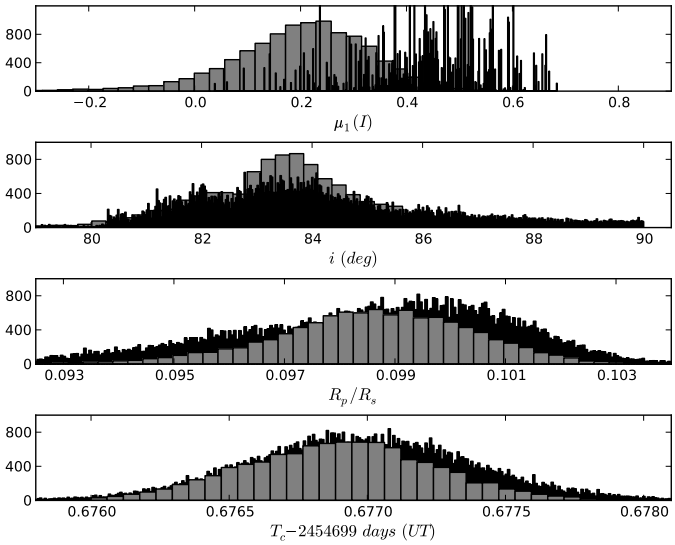

Figure 5.2 Histograms of the 10 000 LMMC iterations with JKTEBOP (gray histograms) and of the 10 chains with 10 000 links (after discarding the first 10% results on each chain) obtained with TAP (black histograms) for the 2008-08-21 epoch. For comparison, the binning factor of the TAP results histograms is 9 times the binning factor used for the JKTEBOP results. In both fittings, all the parameters were left free except for quadratic limb darkenning coefficients ($\mu_2(I) = 0$), eccentricity ($e = 0$) and the periastron longitude ($\omega = 0$).

revealing that the quality of a single transit in the current data does not allow to constrain the values of $\mu_1(I)$. Notice, however, that a Gaussian distribution is obtained when fitting several transits simultaneously (see Figure 5.4 and section 5.3.2).

From the test results above we conclude that the LMMC and MCMC techniques arrive to similar parameter results. However, because the apparent underestimation of the errors estimated by LMMC we have opted for using TAP for our analysis of the full WASP-5b transit dataset and the re-analysis of all the available data (see next section). This underestimation is due to lack of multi-parameter uncertainty estimator and failure to account for red noise in the minimization (Carter & Winn 2009) as TAP does. Other advantages of TAP include that the code can fit a greater number of parameters like linear systematics in the datasets, and it allows a simultaneous fitting of multiple transits.

5.3.2 Final Modeling

We used TAP to fit the nine new transit light curves presented in this paper and all the available light curves of the system (seven of F11, two of D11, two of S09 and the two of A08).

First, we attempted to model each of the new light curves independently, but ran into several problems. TAP had difficulties fitting the incomplete light curves. Also, when fitting individual light curves, parameters such as μ_1 did not clearly converge to a single value, as already mentioned in section 5.3.1 and illustrated in Figure 5.2. To avoid these problems

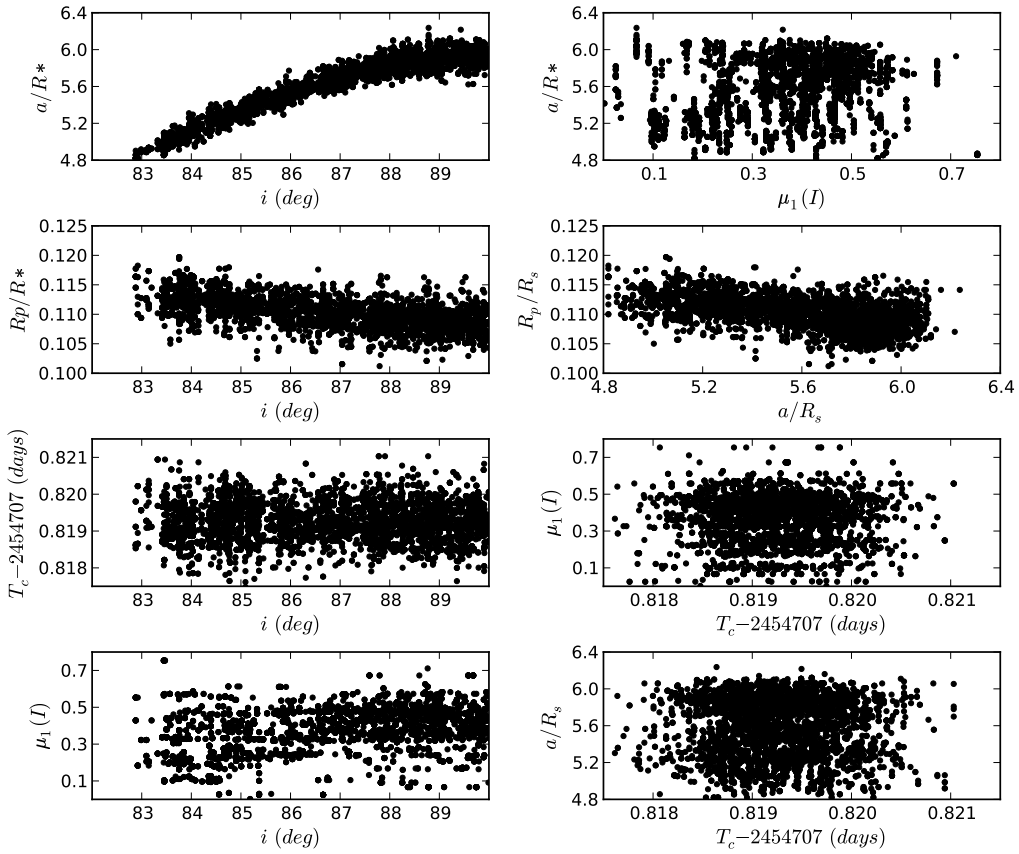

Figure 5.3 Results of the Markov Chain Monte Carlo iterations resulting of fitting the 2008-08-29 transit data with TAP, which show the correlation between the fitted light curve parameters a/R_s, R_p/R_s, T_c, i and $\mu_1(I)$.

we fit the seven complete light curves simultaneously, leaving as free parameters $\mu_1(I)$, i, R_p/R_s, T_c, F_{OOT}, in addition to possible linear trends to the light curves, F_{slope}, and white (uncorrelated) and red (correlated) noise components, σ_w and σ_r, respectively. The orbital period, the eccentricity, and the longitude of the periastron were fixed to the values P= 1.62843142 days (the value obtained by F11), $e = 0$ and $\omega = 0$.

We used a quadratic limb-darkening law, but found that the precision of the light curves was not enough to reliably fit the quadratic coefficient, so that value was also fixed to $\mu_2(I) = 0.32$, based on the tabulated results in Claret (2000).

As mentioned in Section 5.2, we initially corrected for systematic trends in the light curves using linear or quadratic regression fits. Altough slopes in the light curves are not clearly apparent, we leave F_{OOT} and F_{slope} as free parameters to ensure that any small residuals are properly fit. This might create concerns about wheter this two-step fitting of systematics can affect the results of the fits. To ensure we are not introducing any bias on the determination of the planetary parameters, we fit the two sets of data (i.e. the light curves with and without systematics trends removed) with TAP and arrive to consistent values of all derived planetary parameters.

We also searched for potential parameter correlations in the light curves using the fit results of the 2008-08-29 transit described in the previous section, where all the parameters were let to vary. The resultant parameter correlations are shown in Figure 5.3. This figure reveals a strong correlation between a/R_s and i. There is also evidence of weaker correlations between those two parameters and R_p/R_s. Therefore, to minimize the impact of those correlations in our results, we fixed a/R_s in all the light curves to 5.37 (from F11), while closely monitoring R_p/R_s and i for variations.

To fit the transits we ran 10 MCMC chains of 10^5 links each, discarding the first 10% results from each chain to avoid bias toward the initial input values of each fitted parameter. Because the resulting MCMC distributions for $\mu_1(I)$ are not Gaussian (see Figures 5.2 and 5.3), that parameter was fit simultaneously for all seven light curves, while for the other parameters we obtained one value per curve and combine them afterward via a weighted average. The resulting average values for each parameter are listed in Table 5.3, together with their 1σ errors. As an example, Figure 5.4 shows the resultant MCMC distributions of i, R_p/R_s, and T_c for the transit observed on 2008-08-29, while the distribution of $\mu_1(I)$ correspond to the results of the simultaneous seven transits fit. This distribution is now clearly Gaussian in contrast with the previously obtained.

Finally, we adopted the values of all the parameters that define the shape of the transit derived in the fit above and used them as fixed values in the two incomplete light curves (2008-10-22 and 2009-08-06 transits) to derive their mid-times of transit, T_c. The F_{OOT}, F_{slope}, σ_w and σ_r are still left variable in this case.

F11 used a procedure based on χ^2 minimization for modeling their light curves. We re-analyzed their data to do an homogeneous study of all the light curves, given that a multi-parameter minimization based on MCMC is statistically more robust. We modeled the seven light curves of F11[4], the two light curves of D11 (data provided by the author, private

[4]The data is available in the on-line material from the F11 publication on PASJ

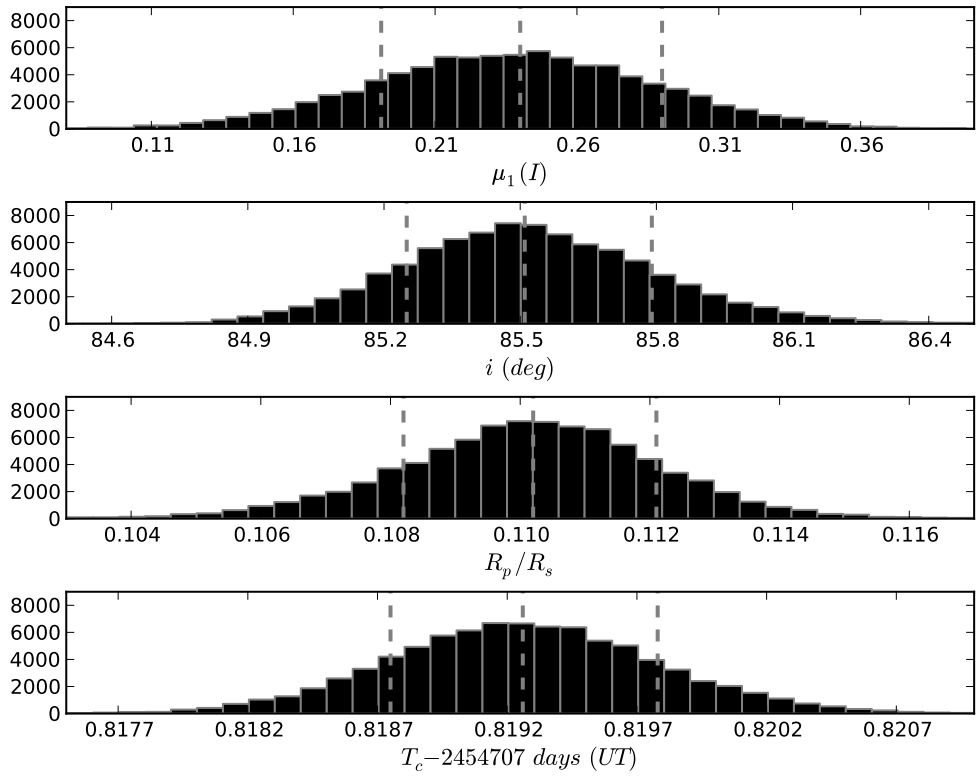

Figure 5.4 Histograms of the Markov Chain Monte Carlo iterations resulting of fitting the 2008-08-29 transit data with TAP, for their fitted parameters: $\mu_1(I)$, R_p/R_s, i and T_c. The dashed lines show the fitted value and the $\pm 1\sigma$ errors.

communication), the two light curves of S09[5] and the two of A08 (data provided by the author, private communication) in a similar manner to our complete light curves above. The F11 transits were observed with a *Bessel I* filter, the D11 and the S09 with a R filter, and the A08 with R and SDSS *i'* filter; therefore, we fit one $\mu_1(I)$ simultaneously for all F11 curves, one $\mu_1(R)$ for the D11 curves and one for the S09 curves, and separate $\mu_1(i)$ and $\mu_1(R)$ for the A08 curves. We fixed $\mu_2 = 0.32$ in all cases.

The obtained parameters are summarized Table 5.3. The resultant models to all 22 light curves are illustrated in Figure 5.1.

We point out that the errors of the F11's light curves estimated by us are, in average, 70 % larger than the reported by F11. We checked that the origin of this difference was not due only by the different red-noise estimator methods. Using the same red-noise factor estimated by F11, we have obtained errors consistent with those we present in Table 5.3. Carter & Winn (2009) found that time averaging and residual permutation methods underestimated the errors by $15-30\%$ compared with the wavelet-based method (implemented by TAP). We found that using a multi-parametric method for the error estimations with the light curves we analyzed in this work is critical to have reliable uncertainties contourns for the fitted

[5]The data is available at the CDS (http://cdsweb.u-strasbg.fr/)

Table 5.3. Adjusted parameters for each transit of WASP-5b using TAP.

Transit date	Epoch	R_p/R_s	i [°]	$\mu_1(X)$ [a]	$T_c - 2450000$ (BJD_{TT})	$\sigma_{red}/\sigma_{white}$
2008-08-21	199	$0.1112^{+0.0015}_{-0.0015}$	$85.60^{+0.25}_{-0.23}$	$0.237^{+0.05}_{-0.049}$	$4699.68303^{+0.00040}_{-0.00041}$	1.6
2008-08-29	204	$0.1102^{+0.0019}_{-0.0020}$	$85.51^{+0.28}_{-0.26}$	$0.237^{+0.05}_{-0.049}$	$4707.82465^{+0.00052}_{-0.00051}$	2.8
2008-09-21	218	$0.1080^{+0.0027}_{-0.0026}$	$85.76^{+0.46}_{-0.40}$	$0.237^{+0.05}_{-0.049}$	$4730.62301^{+0.00075}_{-0.00076}$	2.9
2008-10-22	237	0.1116^{b}	85.47^{b}	0.24^{b}	$4761.56356^{+0.00047}_{-0.00045}$	2.3
2008-11-04	245	$0.1148^{+0.0015}_{-0.0015}$	$85.17^{+0.17}_{-0.16}$	$0.237^{+0.05}_{-0.049}$	$4774.59093^{+0.00030}_{-0.00030}$	5.3
2008-11-17	253	$0.1115^{+0.0027}_{-0.0028}$	$85.45^{+0.36}_{-0.33}$	$0.237^{+0.05}_{-0.049}$	$4787.61792^{+0.00069}_{-0.00066}$	2.5
2009-06-22	387	$0.1101^{+0.0022}_{-0.0024}$	$85.62^{+0.21}_{-0.20}$	$0.237^{+0.05}_{-0.049}$	$5005.82714^{+0.00036}_{-0.00036}$	10.3
2009-08-06	414	0.1116^{b}	85.47^{b}	0.24^{b}	$5049.79540^{+0.00080}_{-0.00079}$	8.2
2009-10-25	463	$0.1114^{+0.0020}_{-0.0021}$	$85.71^{+0.26}_{-0.23}$	$0.237^{+0.05}_{-0.049}$	$5129.58759^{+0.00042}_{-0.00043}$	5.6
2008-06-18[c]	160	$0.1121^{+0.0032}_{-0.0032}$	$85.02^{+0.44}_{-0.41}$	$0.292^{+0.089}_{-0.089}$	$4636.17459^{+0.00079}_{-0.00082}$	2.9
2008-11-02[c]	244	$0.1109^{+0.0034}_{-0.0032}$	$85.62^{+0.50}_{-0.41}$	$0.292^{+0.089}_{-0.089}$	$4772.96212^{+0.00074}_{-0.00075}$	2.2
2009-09-04[c]	432	$0.1095^{+0.0048}_{-0.0047}$	$85.54^{+0.45}_{-0.38}$	$0.292^{+0.089}_{-0.089}$	$5079.10830^{+0.00075}_{-0.00079}$	2.0
2009-10-05[c]	451	$0.1091^{+0.0041}_{-0.0045}$	$85.44^{+0.50}_{-0.42}$	$0.292^{+0.089}_{-0.089}$	$5110.04607^{+0.00087}_{-0.00089}$	10.1
2009-10-18[c]	459	$0.1096^{+0.0030}_{-0.0031}$	$86.13^{+0.63}_{-0.47}$	$0.292^{+0.089}_{-0.089}$	$5123.07611^{+0.00079}_{-0.00079}$	2.5
2010-06-16[c]	607	$0.1121^{+0.0044}_{-0.0042}$	$87.30^{+1.5}_{-0.98}$	$0.292^{+0.089}_{-0.089}$	$5364.0815^{+0.0011}_{-0.0011}$	4.9
2010-06-29[c]	615	$0.1097^{+0.0040}_{-0.0044}$	$85.67^{+0.63}_{-0.48}$	$0.292^{+0.089}_{-0.089}$	$5377.10955^{+0.00091}_{-0.00093}$	5.2
2009-09-01[d]	430	$0.1111^{+0.0028}_{-0.0029}$	$86.16^{+0.59}_{-0.53}$	$0.51^{+0.11}_{-0.13}$	$5075.84947^{+0.00056}_{-0.00056}$	8.0
2010-09-09[d]	659	$0.1154^{+0.0041}_{-0.0043}$	$85.92^{+0.94}_{-0.68}$	$0.51^{+0.11}_{-0.13}$	$5448.75927^{+0.0010}_{-0.0011}$	4.6
2008-08-29[e]	204	$0.1109^{+0.0011}_{-0.0010}$	$85.78^{+0.20}_{-0.18}$	$0.367^{+0.052}_{-0.053}$	$4707.82523^{+0.00023}_{-0.00025}$	3.0
2008-09-21[e]	218	$0.1102^{+0.0014}_{-0.0015}$	$85.78^{+0.24}_{-0.25}$	$0.367^{+0.052}_{-0.053}$	$4730.62243^{+0.00031}_{-0.00031}$	3.7
2007-10-10[f]	5	$0.1095^{+0.0017}_{-0.0020}$	$85.61^{+0.37}_{-0.29}$	$0.37^{+0.11}_{-0.1}$	$4383.76750^{+0.00038}_{-0.00040}$	4.9
2007-10-13[f]	7	$0.1101^{+0.0061}_{-0.0066}$	$84.95^{+0.59}_{-0.49}$	$0.39^{+0.18}_{-0.21}$	$4387.0.2275^{+0.0010}_{-0.0010}$	11.7

[a] In the all the fits the quadratic coefficient was fixed to $\mu_2 = 0.32$.

[b] These parameters were fixed in the modeling and correspond to the weighted average of the results of the other seven full phase covered light curves presented in this work.

[c,d,e,f] Fitting results of the transits of Fukui et al. (2011) , Dragomir et al. (2011), Southworth et al. (2009a) and Anderson et al. (2008), respectively.

Table 5.4. Improved orbital values derived from the weighted average of the light curve's fits.

Parameter	Adopted Value	1σ Error
a/R_S [a]	5.37	± 0.15
R_p/R_s	0.1111	± 0.0005
i [°]	85.56	± 0.07
Period [days]	1.62842888	± 0.00000078
T_o $[BJD_{TT}]$	2454375.62549	± 0.00023

[a]Value adopted from Fukui et al. (2011).

parameters.

Using the model results is possible to look for variations in the most relevant parameters, in particular i and R_p/R_s, that can reveal the presence of an additional body in the system. In Figure 5.5, we plot R_p/R_s and i as a function of the transit epoch, based in the results of the twenty transit fits (our two incomplete light curves were not included). We do not see any significant variations in those parameters. The weighted average values of i and R_p/R_s based on all the light curves results are summarized in Table 5.4. We studied in detail the timing of the transits in the next section.

5.4 Timing Analysis

The times in our nine transit data and the D11 data were initially computed in Coordinated Universal Time (UTC) and then converted to Barycentric Julian Days, expressed in Terrestrial Time, BJD(TT), using the Eastman et al. (2010) online calculator [6]. The transit times of S09 and A08, which were initially expressed in HJD(UT) have also been converted to BJD(TT). No conversion was applied to the light curves reported by F11.

The times of the common transits, 2008-08-29 and 2008-09-21, derived from our light curves are consistent within the errors in the values derived by us and also by F11 from S09 data.

Using the F11's ephemeris equation, we calculated the residuals of the mid-times of the 22 transits of WASP-5b analyzed in this work. The top panel in Figure 5.6, shows the *Observed minus Calculated* $(O-C)$ diagram for our nine transits. In the middle panel of the figure we combine the $O-C$ values of our nine transits with the new values derived for the F11, D11, S09 and A08 (shown as open circles). As illustrated in that figure, a linear trend with a slope of 2.54×10^{-6} days is observed in the time residuals of all transits. That trend can be explained by the accumulation of errors in the current orbital period and T_0 of the transits over time, and therefore can be modeled out.

[6]http://astroutils.astronomy.ohio-state.edu/time/utc2bjd.html

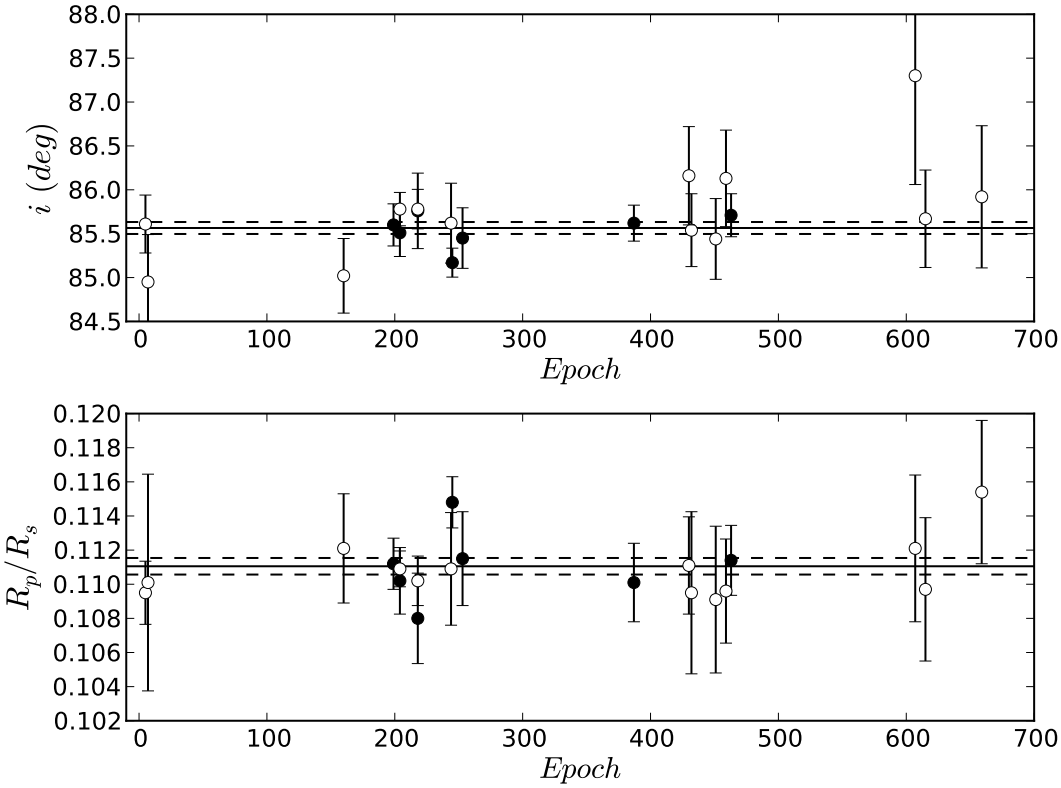

Figure 5.5 Derived values of the orbital inclination (**Top Panel**) and planet-to-star radii ratio, R_p/R_s (**Bottom Panel**) for all modeled transits. The solid circles correspond to our seven complete transits. The open circles correspond to the seven transits of F11 and the two transits of D11, S09 and A08. The weighted average to all points is represented by the solid line on each panel and the dashed lines show the $\pm 1\sigma$ errors of those fits. No significant variations are apparent for these parameters in the time span of the observations.

This linear regression of the points in the $O-C$ diagram has a $\chi^2_{red} = 1.22$ ($\chi^2 = 24.37$ for 20 degrees of freedom), which is significantly smaller than the value obtained for F11 of $\chi^2_{red} = 3.66$ ($\chi^2 = 32.2$ for 9 degrees of freedom). Additionally, we confirmed that with our results for the 11 epochs included in F11's analysis we also obtained an smaller χ^2 ($\chi^2 = 15.45$ that yields $\chi^2_{red} = 1.72$). This result lies in the fact that our T_c uncertainties are larger than those estimated by F11.

Once the linear trend is removed the updated ephemeris equation is:

$$T_c = 2454375.62459(23)[BJD_{TT}] + 1.62842888(78) \times E, \tag{5.1}$$

where T_c is the central time of a transit in the epoch E since the reference time T_0. The errors of the last digits are shown in parenthesis. The bottom panel in Figure 5.6 shows the resulting $O-C$ values of all available transits using the updated ephemeris equation. The resultant $O-C$ diagram is consistent with a constant period, and we conclude that the observed TTV residuals (with a *RMS* of ~ 0.00073 days $\simeq 63$ seconds), are most likely introduced by data uncertainties and systematics rather than due by gravitational perturbations of an orbital companion. This newly obtained precision permits to place strong constraints in the mass of an hypothetical companion, particularly in MMR's, as we discuss in the next section.

5.5 Limits to additional planets

To place upper limits to the potential perturbers in the WASP-5 system based in the derived TTV *RMS* of about 60 sec we use *Mercury* (Chambers 1999) N-body simulator. The input parameters to *Mercury* include the mass and the radius of both the star and the transiting planets, the planet-to-star orbital separation, as well as the inclination, eccentricity and periastron longitude of the system. The values for all these parameters were adopted from S09. In addition, all the initial relative angles between the perturber and WASP-5b were set to zero.

We explored a wide range of perturber masses between 1 $M_\oplus$ and 4000 $M_\oplus$ in initial steps of 50 $M_\oplus$, which are subsequently refined as described below. For the semi-major axis distances we explore a range between 0.001 and 1.2 AU in steps of 0.001 AU, which was further reduce near resonances. The density of the perturber was kept constant to that of Earth for $M_p \leq 10M_\oplus$ and to that of Jupiter for $M_P \geq 200M_\oplus$, it was varied linearly for masses in between. Also, we assumed the perturber to be in a circular orbit and coplanar to WASP-5b, since this configuration provides the most strict limit to the amplitude of the TTVs for a given perturber's mass. Non-zero eccentricities and non-coplanar orbits produce larger TTVs as already pointed out by e.g. Bean (2009), Hoyer et al. (2011b) and Fukui et al. (2011). For each model configuration we let the system relax for five years, and then we used the next five years to obtain our fit results, which in total is more than 3 times the time span of the observations. These 5 years of relaxation time permits to minimize the effect of any initial bias (e.g. the relative angles). We found orbits between 0.02 and 0.035 AU to be unstable due to the presence of WASP-5b. For all other (stable) orbits we recorded the central times of each transit of WASP-5b and computed the predicted TTVs for each configuration, assuming an average constant period. Additionally, we checked that

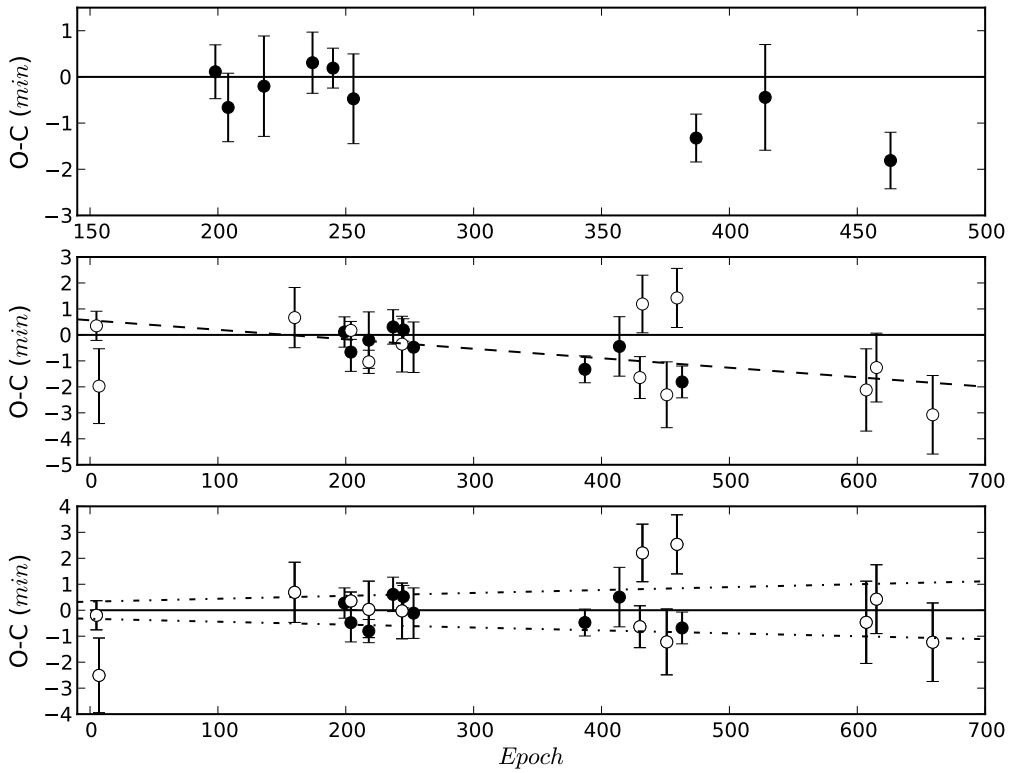

Figure 5.6 **Top-panel:** *Observed minus Calculated* diagram of the central times of the nine transits reported in this work. **Middle-panel:** $O-C$ residuals of our nine transits (solid circles) combined with the $O-C$ residuals of the new fits to the F11, D11, S09 and A08 transits (open circles). The dashed line shows the linear trend found in the data. **Bottom-panel:** $O-C$ residuals of all available data after removing the linear trend. The solid and point-dashed lines in this figure correspond, respectively, to our new ephemeris equation fit and its associated $\pm 1\sigma$ errors.

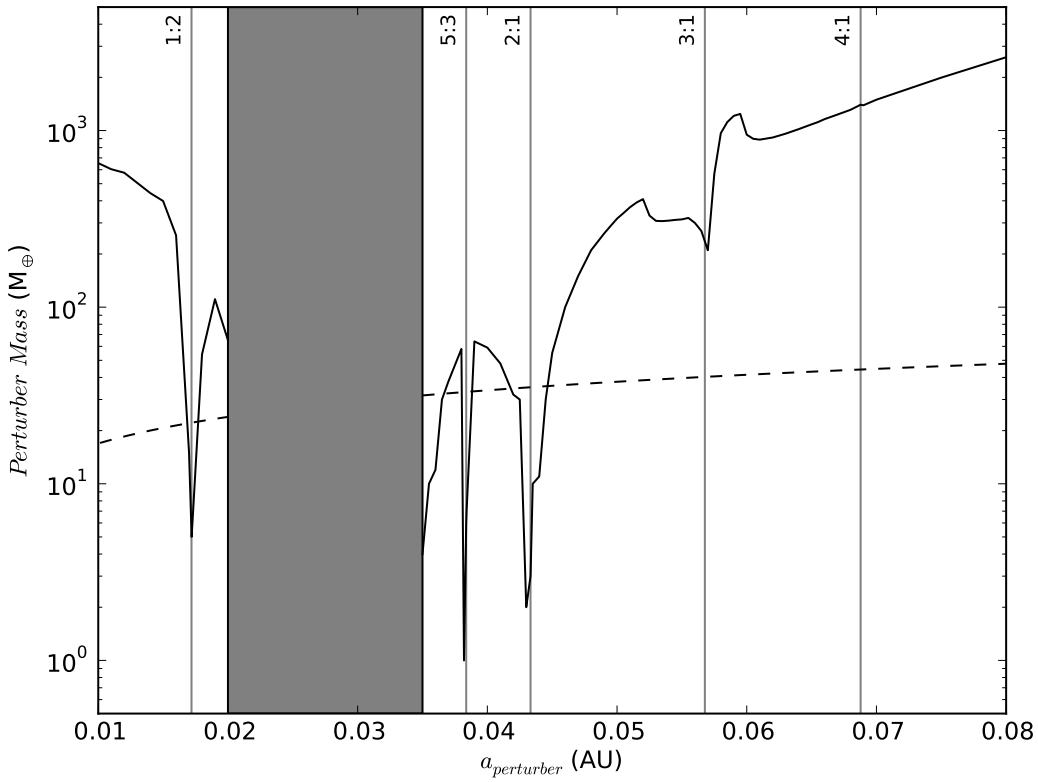

Figure 5.7 Upper mass limits of an orbital perturber derived by dynamical simulations done with *Mercury* code (Chambers 1999). The solid line represents transit timing variations limits with a *RMS* of 1 minute. The dashed line corresponds to the limits imposed by the current radial velocities observations. Vertical lines indicate the location of the MMR distances with WASP-5b for orbital separations of less than 0.08 AU. The gray band indicates the range of distances in which any other object would be in a unstable orbit.

the fitted average period did not deviate by more than 3 σ from the obtained orbital period of WASP-5b. Also, to ensure a good sampling of the potential perturber's mass, we reduced the steps in M_{pert} to $1M_\oplus$ whenever the TTVs approached 60 sec.

The results of our model simulations is illustrated in Figure 5.7, where we show the M_{pert} ($M_\oplus$) versus $a(AU)$ diagram that places the mass limits to potential perturbers in the system. The solid line in the diagram indicates the derived upper limits to the mass of the perturbers that would produce TTVs *RMS* of 60 sec at different orbital separation. The dashed line shows the perturber mass upper limits imposed by the most recent radial velocity observations of the WASP-5 system, for which we have adopted a precision of 15 m/s (A08 and Triaud et al. 2010, report RV precision of 14 m/s and $12 - 18$ m/s, respectively).

Figure 5.7 thus shows that the perturber would have been detected by RV measurements in all areas except around the 1:2, 5:3 and 2:1 MMRs, where it could have a maximum mass of 5, 1 and 2 $M_\oplus$, respectively.

5.6 Conclusions

We present nine new transit light curves of WASP-5b. We homogeneously model these light curves together with all available transit data of this system. Based in these fits we search for any variation in the timing of the transits.

Using 22 transit epochs we updated the ephemeris equation and we find a TTVs *RMS* of 63 seconds. All the transit times are consistent with a constant orbital period within 2σ.

Our linear fit of the transit times has a $\chi^2_{reduce} = 1.22$, which is considerably lower than the value found by Fukui et al. (2011) used to implied the presence of an perturber body.

Despite obtaining a similar TTV *RMS* than Fukui et al. (2011) ($\sim$ 1 min), we conclude a much smaller significance to deviations from a constant period due to our larger per-epoch uncertainties as obtained by the MCMC algorithm. We thus emphasize the need to use a multi-parametric uncertainty estimator for these studies.

If the system has an additional orbiting body, its mass has to be lower than 5, 1 and 2 $M_{\oplus}$, in the 2:1, 5:3 and 1:2 resonances. In any other location the perturber would have been detected by RVs.

We search for any trend in the depth of the transit and inclination of the orbit but we do not see any clear evidence of variation with statistical significance.

Chapter 6

Analysis and Results of WASP4-b

TraMoS PROJECT: IMPROVING PHYSICAL PARAMETERS AND A STELLAR SPOTS MODELING WITH TWELVE NEW TRANSIT EPOCHS OF THE EXOPLANET WASP-4b

S. Hoyer[1], M. López-Morales[2,3], P. Rojo[1], V. Nascimbeni[4,5], S. Hidalgo[6], N. Astudillo[1], F. Concha[1],Y. Contreras[1],E. Searvajean[1],

Montly Notices of the Royal Astronomical Society, Submitted

[1]: Astronomy Department, Universidad de Chile, Casilla 36-D, Santiago de Chile, Chile.

[2]: Institut de Ciencies de l'Espai (CSIC-IEEC), Campus UAB, Facultat de Ciencies, Torre C5, parall, 2a pl, E-08193 Bellaterra, Barcelona, Spain.

[3]: Carnegie Institution of Washington, Department of Terrestrial Magnetism, 5241 Broad Branch Rd. NW, Washington, D.C. 20015, USA.

[4]: Dipartamento di Astronomia, Università degli Studi di Padova, Vicolo dell'Osservatorio 3, 35122 Padova, Italy.

[5]: INAF - Osservatorio Astronomico di Padova, Vicolo dell'Osservatorio 5, 35122 Padova, Italy.

[6]: Instituto de Astrofísica de Canarias, Via Láctea s/n, E38200 La Laguna, Tenerife, Canary Islands, Spain

[7]: Department of Astrophysics, University of La Laguna, Via Láctea s/n, E38200 La Laguna, Tenerife, Canary Islands, Spain

Abstract

For the Transit Monitoring in the South Project (*TraMoS*), we report twelve new transit epochs of the extrasolar planet WASP-4b. These transits were observed in the *Bessell I* band with SOAR and in the *Cousins R* and *I* with the SMARTS 1-m Telescope at CTIO, between August 2008 and September 2011. The new transits of this object have been combined with all previously published transit data to provide a new and homogeneous Transit Timing Variations (TTVs) analysis of its orbit. For WASP-4b, we find no evidence of TTVs *RMS* variations larger than 40 seconds over a 4 year time span. With the twelve new epochs we refined the ephemeris equation. This result discards the presence of planets more massive than about 6.5 $M_{\oplus}$, 4.0 $M_{\oplus}$ and 2.0 $M_{\oplus}$ around the 1:2, 5:3 and 2:1 orbital resonances. Our

Based on the submitted work Hoyer et al. (2011c)

search for the variation of other parameters, such as orbital inclination and transit depth also yields negative results over the total time span of the transit observations. We found evidence of stellar spot occultations by the planet in four of our light curves. Using this information it is possible to estimate the stellar rotation period and the relative angle between the stellar rotation axis and the orbital axis of the planet.

6.1 Introduction

Among the wide variety of studies that can be conducted with transiting exoplanets, it has been proved that the presence of *unseen* orbital companions can produce changes in the orbital period of transiting exoplanets (Miralda-Escudé 2002, Agol et al. 2005, Holman & Murray 2005). Detection of additional planets in the system can be done by monitoring for this Transit Timing Variations (TTVs).

In addition, Silva-Valio (2008) and Sanchis-Ojeda et al. (2011) have pointed out that observations of star-spot occultations during closely-spaced transits can be used to not only estimate the stellar rotation period, but also to measure alignment differences between the rotation axis of the star and the orbital axis of the planet.

We are conducting a careful and homogeneous photometric monitoring of transits observable from the Southern Hemisphere: Transit Monitoring in the South (*TraMoS*) Project. The aim of this project is to perform a careful and homogeneous monitoring of the exoplanet transits trying to minimize systematics and reduce uncertainties in the transit parameters, such as the transit mid-time, following the approach of using high-cadence observations and the same instruments and setups.

In the framework of the *TraMoS* project we present twelve new transit observations of the exoplanet WASP-4b, observed between August 2008 and September 2011.

WASP-4b was the first exoplanet detected by the WASP-South survey in 2008. At that time, Wilson et al. 2008 (hereafter W08) reported a Hot-Jupiter ($P = 1.34$ days) with a mass of $M_P = 1.22^{+0.09}_{-0.08}\ M_J$ and a planetary radius of $R_p = 1.42^{+0.07}_{-0.04}\ R_J$ orbiting a G7V southern star. This discovery paper included WASP photometry, two additional transit epochs (observed in September 2007) plus radial velocities measurements.

Gillon et al. (2009), hereafter G09, added to the follow-up of this exoplanet a *VLT/FORS2* light curve observed in October 2007 with a *z-GUNN* filter. Using a reanalysis of the W08 data they found no evidence of period variability. Winn et al. (2009), hereafter W09, presented two new high-quality transits observed in 2008 with the Baade Telescope (one of the twin 6.5-m Magellan telescopes at Las Campanas Observatory) using a *z-filter*. Four new transit epochs were reported shortly after by Southworth et al. (2009b), hereafter S09, with the 1.54-m Danish Telescope at La Silla Observatory using a *Cousins-R* filter during 2008. Sanchis-Ojeda et al. (2011) (hereafter SO11), using four new transit light curves (observed during 2009), interpreted two anomalies in the photometry as starspot occultations by the planet and concluded from that result that the stellar rotation axis is nearly with the planet's rotation axis. This results agrees with the observations of the Rossiter-Mclaughlin effect for this system by Triaud et al. (2010). Most recently, two new transits of WASP-4b were reported by Dragomir et al. (2011), hereafter D11, with data of the 1-m telescope at Cerro Tololo Inter-American Observatory (*V*- and *R-filter*).

In Sections 6.2 and 6.3 we describe the new observations and the data reduction, respectively. Section 6.4 details the modeling of the light curves and in Section 6.5 we present the timing analysis and discuss the mass limits for a *unseen* perturber for the system. Finally, we present a summary in Section 6.6.

6.2 Observations

The observations we present in this work were performed with the Y4KCam on the SMARTS 1-m Telecope at Cerro Tololo Inter-American Observatory (CTIO) and with the SOAR Optical Imager (SOI) at the 4.2-m Southern Astrophysical Research (SOAR) telescope in Cerro Pachón.

We have taken advantage of the 20×20 squared arcminutes of Field of View (FoV) of the Y4KCam, which is a 4064×4064 CCD camera with a pixel scale of 0.289 arcsec pixel^{-1}. Despite its large dimensions, this camera allows to use a readout time of only $\sim 16/5$ sec using the 2x2/4x4 binning mode (comparing with the 46 sec of the standard readout time). The SOI detector is composed of two E2V mosaics of 4096×4096 pixels with a scale of 0.077 arcsec pixel^{-1}. SOI has FoV of only 5.2×5.2 squared arcminutes, which allows a readout time of only ~ 11 sec after binning 2x2 (20.6 sec is its standard readout time).

As part of the *TraMoS* project we have observed a total of 12 transits of WASP-4b, between August 2008 and September 2011[1]. Three transits were observed with SOI at SOAR telescope and the remaining nine were observed with the Y4KCAM at the 1-m CTIO telescope.

To reduce limb darkening effects in our light curves, the ten first transits were observed using a *Bessell I* or *Cousins I* filter. For the observations of the 2011 transits we used the 4x4 binning mode of the Y4KCam and a *Cousins R* filter. The observing log is summarized in Table 6.1.

All the transits were observed entirely with the exception of the 754th, 482th and -62th transits where some portions of the transits that were lost due technical failures (see Figure 6.1). The before-transit and the ingress portions of the -71th transit was not observed, but after the $phase = -0.034$ (where $phase = 0$ is defined as the phase of the mid-transit) the observation of the transit was done without interruption.

6.3 Data Reduction

The trimming, bias and flatfield corrections of all the collected data were performed using custom-made pipelines specifically developed for each instrument.

The times at the start of the exposure are recorded in the image headers, we used the value of the *Modified Julian Day* (JD-2400000.5) field. In the SMARTS telescope, the time stamp recorded in the header of each frame is generated by a *IRIG-B GPS time synchronization protocol* connected to the computers that control the instrument. The SOAR telescope data use the time values provided by a time service connected to the instrument. We confirmed that these values have $\lesssim 1$ second precision. The time stamp assigned to each frame corresponds to the *Julian Day* at the start of the exposure plus 1/2 of the integration time of each image. For the photometry and light curve generation we use the same procedure than Hoyer et al. (2011a). That is, we perform a standard aperture photometry where the optimal sky-aperture combination was chosen based on the *RMS* minimization of the differential light curves of the

[1] In the remaining of the text we refer to each individual transit by the epoch number transit, using the ephemeris equation of D11: $T_c(N) = 2454823.591767^{+0.000019}_{-0.000019} + N \times 1.33823326^{+0.00000011}_{-0.00000011}$

Table 6.1. Information for each of the new transit epoch observations presented in this work.

UT date	Epoch	Telescope/Instrument	Filter	binning	average exptime
2008-08-23[a]	-91	1-mt SMART/Y4KCam	Cousins I	2x2	20 sec
2008-08-23[a]	-91	SOAR/SOI	Bessell I	2x2	7 sec
2008-08-27	-88	1-mt SMART/Y4KCam	Cousins I	2x2	20 sec
2008-09-19	-71	1-mt SMART/Y4KCam	Cousins I	2x2	20 sec
2008-09-23[a]	-68	1-mt SMART/Y4KCam	Cousins I	2x2	20 sec
2008-10-01[a]	-62	1-mt SMART/Y4KCam	Cousins I	2x2	26 sec
2009-07-29	163	SOAR/SOI	Bessell I	2x2	8 sec
2009-09-22	204	SOAR/SOI	Bessell I	2x2	10 sec
2009-10-28	231	1-mt SMART/Y4KCam	Bessell I	2x2	14 sec
2010-09-29	482	1-mt SMART/Y4KCam	Cousins I	2x2	14 sec
2011-09-24	751	1-mt SMART/Y4KCam	Cousins R	4x4	20 sec
2011-09-28	754	1-mt SMART/Y4KCam	Cousins R	4x4	20 sec

[a]These epochs have also been observed by other authors.

target and the reference stars. For this analysis we excluded the ingress and egress portions of the light curves, i.e. we use the out-of transit and in-transit data. The final light curves were generated computing the ratio between target's flux and the average of the best 1 to 3 comparison stars. In order to detrend the light curves, we search for correlations of the out-of-transit Flux (F_{OOT}) with the X-Y CCD coordinates of the target, airmass and/or time. To remove the trends we found, we applied linear or quadratic regressions fits, which were subtracted from the light curve.

6.4 Light Curve Modeling

We used the TAP package (Gazak et al. 2011) to fit all the available light curves of WASP-4. This package allows to fit the analytical models of Mandel & Agol (2002) based on the Markov Chain Monte Carlo (MCMC) method which have proved to give the most reliable results compared with other approaches, particularly in the uncertainties estimations of the fitted parameters. This point is critical especially for the timing analysis of the transits. TAP also implements the wavelet-based method (Carter & Winn 2009) to account for the red-noise in the light curve fitting. This method helps impose more confident uncertainty estimates compared with other red-noise calculators such as 'time averaging' or 'residual permutation' methods (see Carter & Winn 2009).

We fitted the twelve new transit light curves presented in this work and the other twelve available light curves of the system from W09, S09, D11 and SO11[2].

[2]W09 and S011 data is available in the on-line material from the S011 publication on ApJ, S09 data is available at the CDS (http://cdsweb.u-strasbg.fr) and D11 data was provided by the author (private communication)

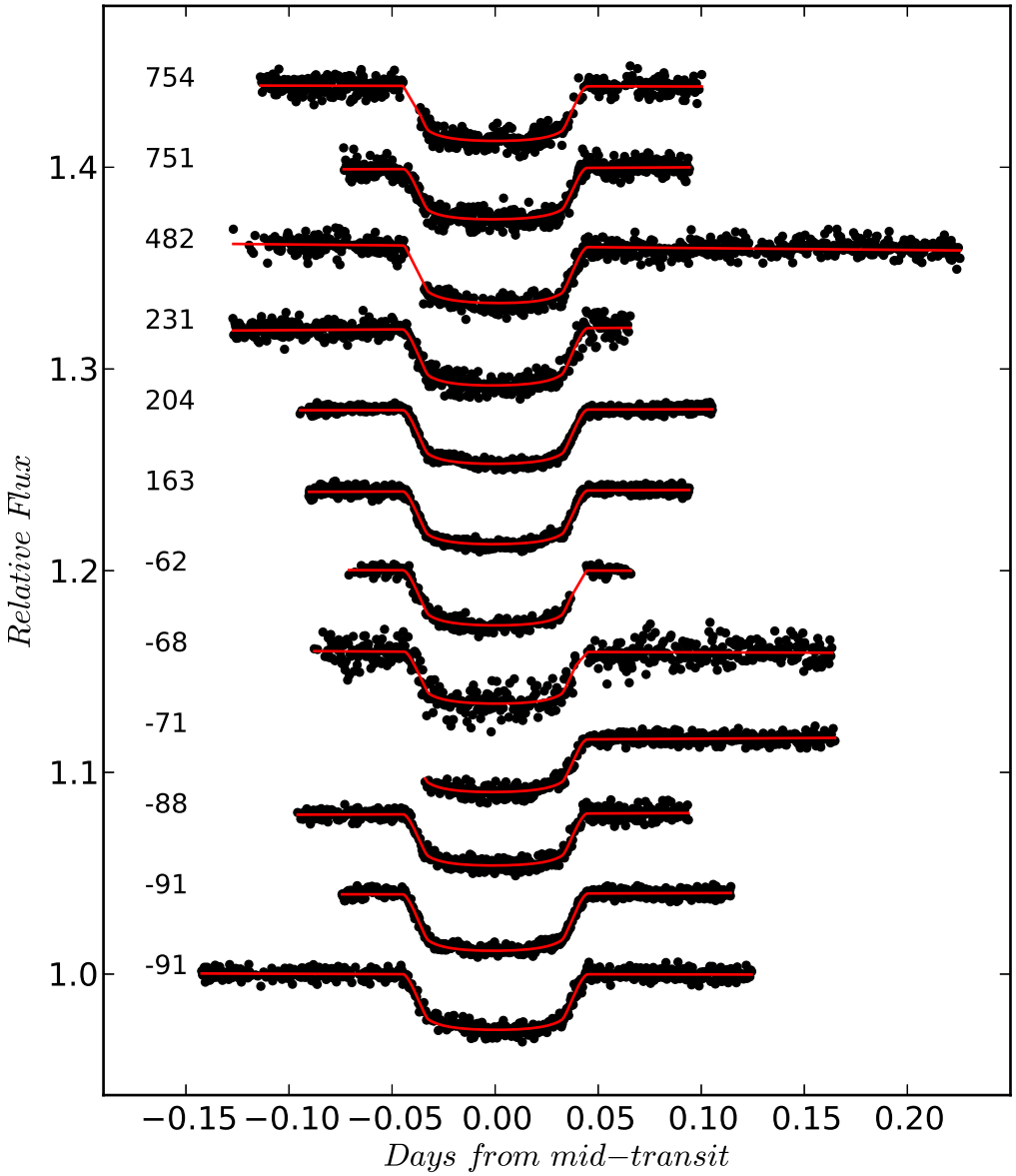

Figure 6.1 Light curves of the twelve transits of WASP-4b presented in this work. The solid red lines show our best model fits using TAP. The epoch is indicated in the left of each light curve.

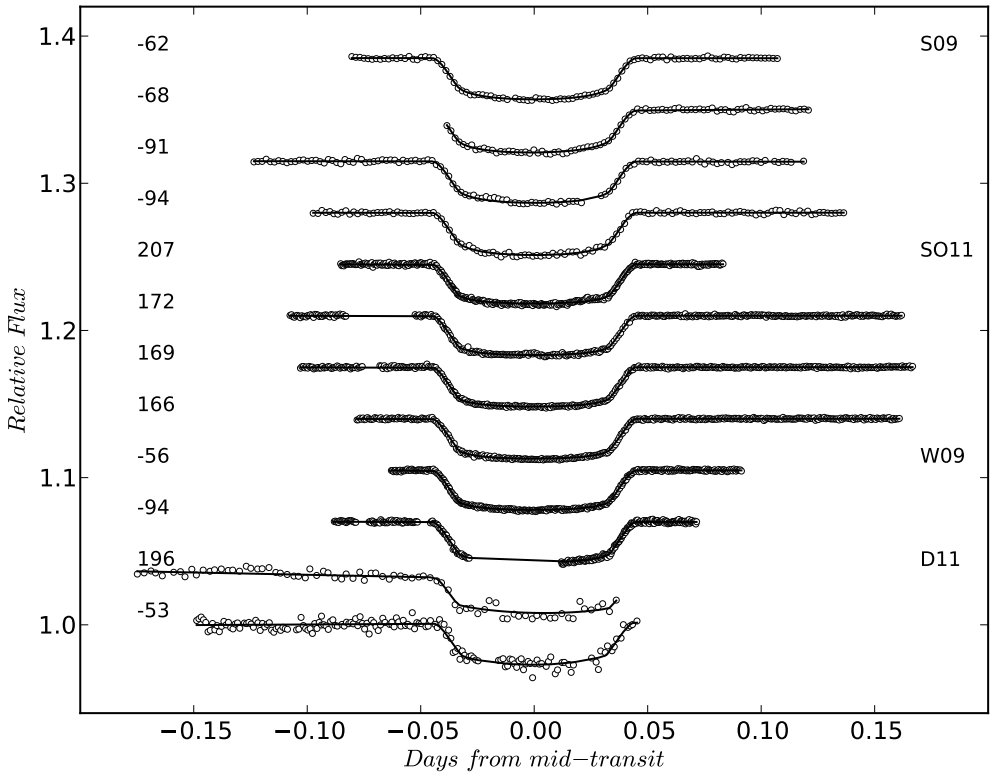

Figure 6.2 Light curves of the twelve transits of WASP-4b available in the literature. The solid lines show our best model fits using TAP. The epoch is indicated on the left of each light curve. The author of each serie of light curves is indicated in the right.

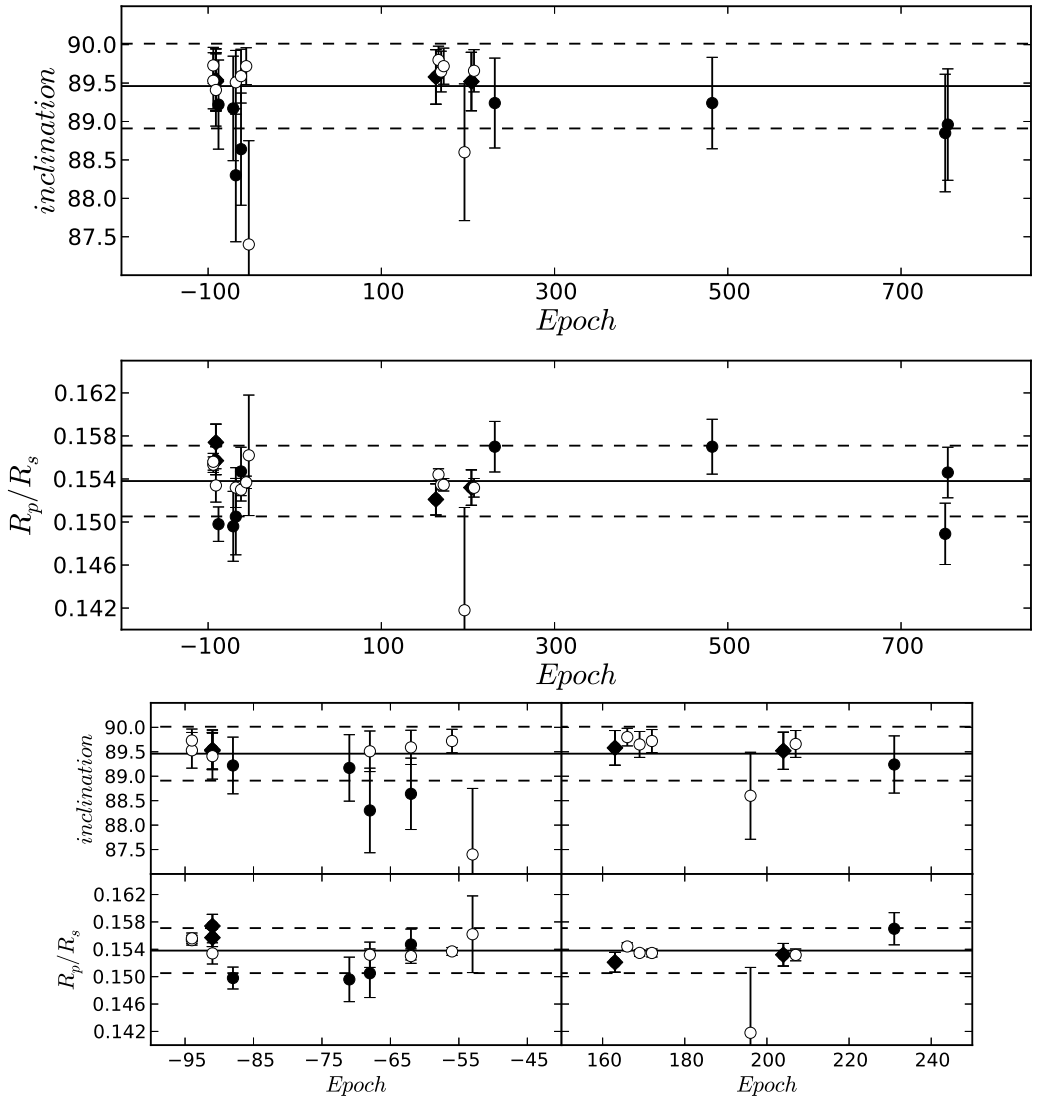

Figure 6.3 The orbital inclination (top panel) and the planet-to-star radii ratio (middle panel) we derived for the twelve transit we present in this work (solid symbols) and for the twelve transits available in the literature (open symbols), as a function of the transit epoch. The parameters derived from our transits with evidence of star-spot occultations are shown with solid diamonds. In general, for these transits we obtained higher inclination values. The solid and dashed horizontal lines represent the weighted average and its $\pm 1\sigma$ errors, respectively. There is no evidence of variations on these parameters for the time span of the observations. In the bottom panels we show a zoom of the diagrams around the -70th and 200th epochs.

We grouped the light curves with the same filter/telescope to perform the modeling. As we describe below, this allows us to fit for the linear limb-darkening coefficient (μ_1) with all the light curves simultaneously as was done in Hoyer et al. (2011a). Therefore, the first group is composed by our ten *I-filter* light curves (from 2008 to 2010) and the second by our two *Cousins-R* light curves (the 2011's transits). Third group is formed by the six SO11's *z-filter* light curves (which includes the two transits observed by W09) and the S09's light curves form the fourth group (*Cousins-R*). Finally, we fitted the V- and R-light curves of D11 separately.

We fit each group independently, leaving as free parameters for each light curve the orbital inclination (i), the planet-to-star radii ratio (R_p/R_s) and the central time of the transit (T_c). The orbital period, the eccentricity, and the longitude of the periastron were fixed to the values P= 1.33823326 days (from D11), $e = 0$ and $\omega = 0$.

We search for possible linear trend residuals in the light curves, fitting for the out-of-transit flux (F_{OOT}) and for a flux slope (F_{slope}). The ratio between the semi-major axis and the star radius, a/R_s, usually presents strong correlations with i and R_p/R_s. To break these correlations and their effects in our results, we fixed a/R_s in all the light curves to 5.53 (from D11). We checked that doing this we are not introducing any bias/effect to the rest of the parameters fitted and its errors (for details, see Hoyer et al. 2011a). We also fitted for a white and red noise component, σ_w and σ_r, respectively.

The coefficients of a quadratic limb-darkening law (μ_1 and μ_2) in our light curves are strongly correlated. We fixed μ_2 to 0.32 (based in the results of Claret 2000) and fitted simultaneously μ_1 on each light curve group. As summary, for each group fit we obtained a single value of μ_1 and a value of i, R_p/R_s, σ_w, σ_r and T_c for each light curve belonging the group.

To fit the transits we ran 10 MCMC chains of 10^5 links each, discarding the first 10% results from each chain to avoid bias toward the initial results of each fitted parameter. We use a jump rate of 25% for all the fitted parameters.

Resulting values for each parameter of the 24 light curves together with their 1σ errors are shown in Table 6.2. The resultant models to all the new 12 light curves presented in this work are illustrated in Figure 6.1, while Figure 6.2 shows the light curves from the literature.

Variations in transit parameters, in particular in i and R_p/R_s, can be attributed to the perturbations produced by an additional body in the system. In Figure 6.3, we plot R_p/R_s and i as a function of the transit epoch, based in the results of the 24 transit fits. We do not see any significant variations in those parameters. The weighted average values of i and R_p/R_s based on all the light curves results are summarized in Table 6.3. We studied in detail the timing of the transits in section 6.5.

In the -91, 163 and 204 light curves, we noticed a bump feature during the transit (Figure 6.4). As in SO11, we interpreted these features as star-spot occultations done by the exoplanet while is crossing in front the star disk. We noticed that the model fits in these light curves is affected by the presence of this protuberance, in particular in the estimation of the transit's depth and/or the inclination. In Figure 6.3 we show with solid diamonds the light curves where we found these bumps. While in R_p/R_s we found no any systematic trend, we noticed the inclinations values we derived for these light curves are, in general, higher than those

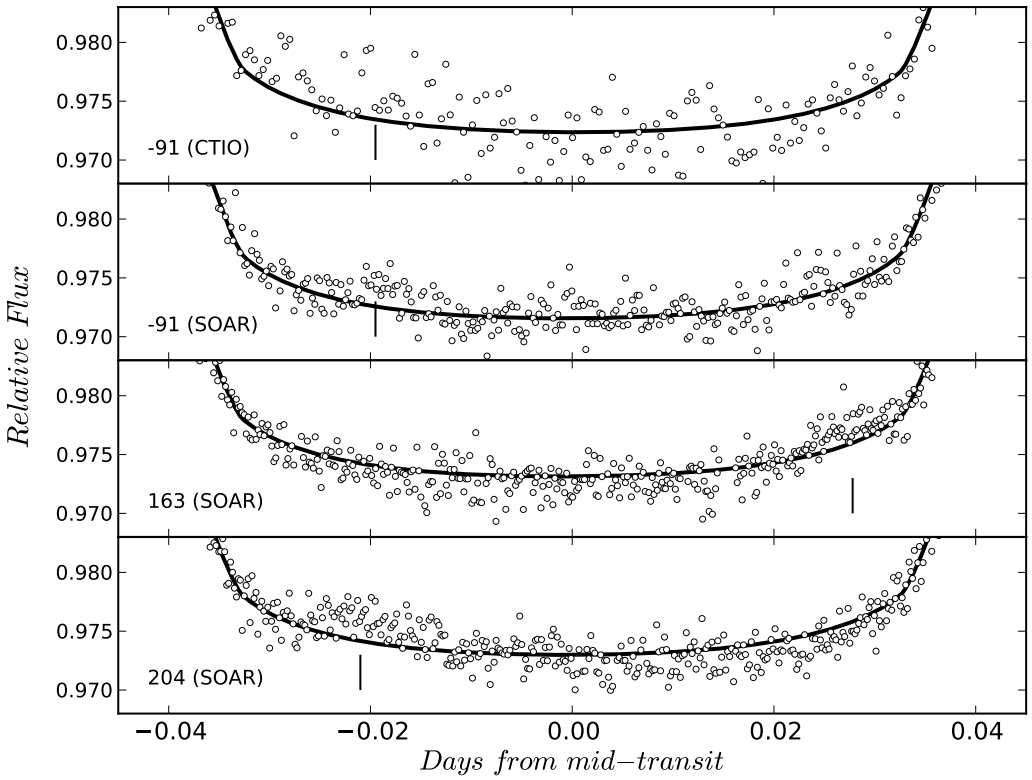

Figure 6.4 Four of our light curves present 'bumps' in the photometry during the transit, which can be interpreted as evidence of star-spot occultations. The location of the 'bump' is marked with a small vertical line. The epoch and the telescope of the light curve is indicated in the left-bottom corner of each panel. The fitted model is shown by the solid line. In some cases, there is an understimation on the derived transit's depth.

without bumps. To properly account for these bumps in the light curves fits we need to modeled out the star-spot occultation, which is beyond the scope of this work.

Table 6.2. Adjusted parameters for each transit of WASP-4b using TAP. In the last column we show the red-to-white noise ratio estimated in the light curves.

Epoch	$T_c - 2450000$ (BJD_{TT})	i [°]	R_p/R_s	μ_1	σ_{red}	$\frac{\sigma_{red}}{\sigma_{white}}$
-91	$4701.8128^{+0.00025}_{-0.00024}$	$89.54^{+0.32}_{-0.49}$	$0.1557^{+0.0013}_{-0.0013}$	$0.216^{+0.020}_{-0.021}$	0.0017	4.6
-91	$4701.81303^{+0.00019}_{-0.00019}$	$89.52^{+0.34}_{-0.41}$	$0.1574^{+0.0017}_{-0.0017}$	”	0.0011	9.2
-88	$4705.82715^{+0.00030}_{-0.00028}$	$89.22^{+0.53}_{-0.63}$	$0.1498^{+0.0016}_{-0.0016}$	”	0.0022	2.3
-71	$4728.57767^{+0.00046}_{-0.00046}$	$89.17^{+0.56}_{-0.80}$	$0.1496^{+0.0030}_{-0.0035}$		0.0021	3.3
-68	$4732.59197^{+0.00057}_{-0.00053}$	$88.3^{+1.0}_{-0.73}$	$0.1505^{+0.0035}_{-0.0036}$	”	0.0034	5.8
-62	$4740.62125^{+0.00038}_{-0.00039}$	$88.64^{+0.81}_{-0.65}$	$0.1547^{+0.0022}_{-0.0023}$	”	0.0019	3.5
163	$5041.72377^{+0.00018}_{-0.00017}$	$89.58^{+0.3}_{-0.41}$	$0.1521^{+0.0014}_{-0.0015}$	”	0.0012	7.3
204	$5096.59148^{+0.00022}_{-0.00022}$	$89.52^{+0.32}_{-0.44}$	$0.1532^{+0.0016}_{-0.0017}$	”	0.001	10.5
231	$5132.7231^{+0.00040}_{-0.00043}$	$89.24^{+0.52}_{-0.65}$	$0.1570^{+0.0023}_{-0.0024}$	”	0.0033	2.6
482	$5468.61943^{+0.00046}_{-0.00045}$	$89.24^{+0.53}_{-0.66}$	$0.1570^{+0.0025}_{-0.0026}$	”	0.0027	6.4
751	$5828.60375^{+0.00042}_{-0.00041}$	$88.85^{+0.75}_{-0.78}$	$0.1489^{+0.0028}_{-0.0029}$	$0.212^{+0.066}_{-0.067}$	0.0021	7.8
754	$5832.61815^{+0.00041}_{-0.00042}$	$88.96^{+0.69}_{-0.76}$	$0.1546^{+0.0024}_{-0.0023}$	”	0.0023	6.1
-94 [a]	$4697.79788^{+0.00013}_{-0.00013}$	$89.53^{+0.32}_{-0.41}$	$0.15533^{+0.00072}_{-0.00072}$	$0.333^{+0.017}_{-0.017}$	0.0017	1.8
-91 [a]	$4701.81234^{+0.00026}_{-0.00026}$	$89.41^{+0.41}_{-0.53}$	$0.1534^{+0.0016}_{-0.0015}$	”	0.0011	5.6
-68 [a]	$4732.59188^{+0.00027}_{-0.00027}$	$89.51^{+0.34}_{-0.49}$	$0.1532^{+0.0017}_{-0.0020}$	”	0.0022	4.8
-62 [a]	$4740.62118^{+0.00016}_{-0.00016}$	$89.59^{+0.29}_{-0.41}$	$0.153^{+0.0010}_{-0.0011}$	”	0.0021	4.3
-94 [b]	$4697.79817^{+0.00008}_{-0.00009}$	$89.73^{+0.19}_{-0.28}$	$0.1556^{+0.00077}_{-0.00079}$	$0.2027^{+0.0076}_{-0.0076}$	0.0034	5.6
-56 [b]	$4748.65111^{+0.00007}_{-0.00007}$	$89.72^{+0.20}_{-0.28}$	$0.15369^{+0.00057}_{-0.00058}$	”	0.0019	7.2
166 [c]	$5045.73853^{+0.00008}_{-0.00008}$	$89.8^{+0.14}_{-0.22}$	$0.15441^{+0.00053}_{-0.00055}$	”	0.0012	6.5
169 [c]	$5049.75325^{+0.00007}_{-0.00007}$	$89.65^{+0.24}_{-0.29}$	$0.15347^{+0.00049}_{-0.00047}$	”	0.001	4.9
172 [c]	$5053.76774^{+0.00009}_{-0.00009}$	$89.72^{+0.19}_{-0.28}$	$0.15346^{+0.00058}_{-0.00058}$	”	0.0033	6.2
207 [c]	$5100.60595^{+0.00012}_{-0.00012}$	$89.66^{+0.23}_{-0.32}$	$0.15318^{+0.00086}_{-0.00087}$	”	0.0027	10.0

Table 6.2 (cont'd)

Epoch	$T_c - 2450000$ (BJD_{TT})	i [°]	R_p/R_s	μ_1	σ_{red}	$\frac{\sigma_{red}}{\sigma_{white}}$
-53 [d]	$4752.66576^{+0.00067}_{-0.00069}$	$87.4^{+1.6}_{-1.1}$	$0.1562^{+0.0053}_{-0.0059}$	$0.50^{+0.18}_{-0.16}$	0.0021	4.8
196 [d]	$5085.88418^{+0.00084}_{-0.00086}$	$88.6^{+0.79}_{-0.99}$	$0.1418^{+0.0092}_{-0.0099}$	$0.42^{+0.20}_{-0.19}$	0.0023	11.5

[a,b,c,d]Transits from Southworth et al. (2009b), Winn et al. (2009), Sanchis-Ojeda et al. (2011) and Dragomir et al. (2011), respectively.

Table 6.3. New derived parameters using the weighted average of the fits of all available light curves of WASP-4b.

Parameter	Derived Value	error
$P(days)$	1.3382319	±0.0000018
T_0 (BJD)	2454823.59194	±0.00030
i (°)	89.46	±0.55
R_p/R_s	0.1538	±0.0033
a/R_s	5.53[a]	
e	0.0 [a]	

[a]From Dragomir et al. (2011). These values were fixed in the light curve modeling.

6.5 Timing Analysis and Limits to Additional Planets

The times of our twelve transit data and the D11 data were initially computed in Coordinated Universal Time (UTC) and then converted to Barycentric Julian Days, expressed in Terrestrial Time, BJD(TT), using the Eastman et al. (2010) online calculator[3]. The time stamps of the S09's light curves were initially expressed in HJD(UT) and have also been converted to BJD(TT). No conversion was applied to the light curves reported by SO11 (which includes the two transits of W09). We use the reported transit mid-times by G09 of their *VLT* observation and their revisited T_c of the two W08's transits (see G09, Table 2) and converted it to BJD(TT). As they suggested we use their reported 'prayer bead' errors estimations. We do not included the T_c derived from the 2006 and 2007 WASP data due that information is based in the folded transits of the entire WASP observational seasons, and therefore lacks for the precision required for our timing analysis.

We use the D11's ephemeris equation to calculate the residuals of the mid-times of the 24 transits of WASP-4b analyzed in this work plus the three epochs published by G09. The panel A in Figure 6.5, shows the *Observed minus Calculated* $(O-C)$ diagram of the times for our twelve transits. In the panel B of the figure we combine the $O-C$ values of twelve

[3]http://astroutils.astronomy.ohio-state.edu/time/utc2bjd.html

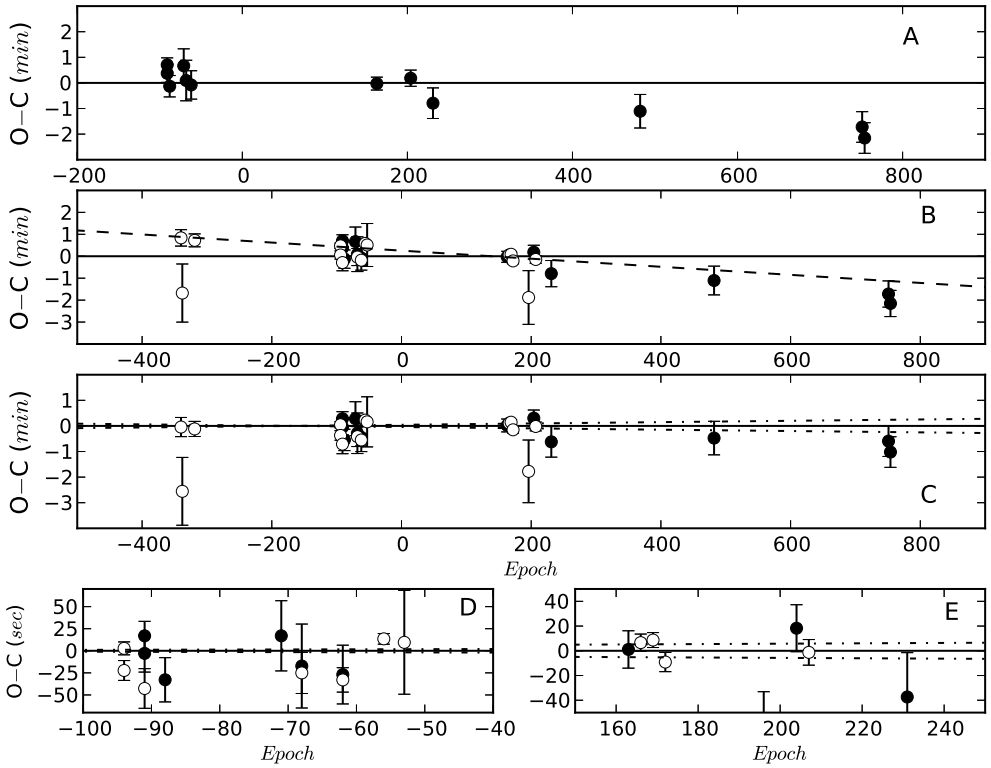

Figure 6.5 *Observed minus Calculated* diagrams of the WASP-4b's transits. **Panel A:** Timing residuals of the observed new twelve transit midtimes presented in this work compared with the predicted ephemerides from D11. **Panel B:** Our twelve T_c (solid circles) combined with the new times derived from W09, S09, SO11 and D11(open circles). We also include three epochs from G09 (open diamonds). A linear trend in the residuals is evident. **Panel C:** If the linear trend is removed, the transit times present a RMS of only 38 seconds with respect to the updated ephemeris equation shown by the horizontal solid line. The $\pm 1\sigma$ levels are shown by the point-dashed lines. **Panel D** and **E:** we shown a close view centered in the -70th and 200th epochs, respectively. The lines are as Panel C. An excellent agreement is found in the mid-times derived from the common epoch transits and with the updated ephemeris equation.

transits with the new values derived for the W09, S09, SO11 and D11 (shown as open circles). A linear trend is evident in the residuals of all the transits (represented by a dashed line in panel B). If that trend is removed (panel C), the RMS of the residuals of the transits times is only of 38 seconds, while the average deviation from a linear ephemeris equation is of ~ 16 seconds.

Despite this linear regression of the points in the $O-C$ diagram has a relative large reduced-χ^2 of $\chi^2_{red} = 1.6$ ($\chi^2 = 40.14$ for 25 degrees of freedom) there is enough evidence to conclude that WASP-4b follows a constant orbital period.

Once the linear trend is removed the updated ephemeris equation is:

$$T_c = 2454823.59194(30)[BJD_{TT}] + 1.3382319(18) \times E, \tag{6.1}$$

where T_c is the central time of a transit in the epoch E since the reference time T_0. The errors of the last digits are shown in parenthesis.

The panel C in Figure 6.5 shows the resulting $O-C$ values of all available transits using the updated ephemeris equation. Almost all the transits coincide with it within the ± 1 σ errors represented by the point-dashed lines. We show in panels D and E a close-up of the $O-C$ diagram around the -70th and 200th epochs, were the transit observations are more clustered. All the T_c of the common transits analyzed in this work are in excellent agreement within the errors.

We attributed to observational/modeling systematics the origin of remaining deviations from a constant orbital period. This newly obtained precision permits to place strong constraints in the mass of an hypothetical companion, particularly in MMR's, as we discuss below.

We use *Mercury* N-body simulator (Chambers 1999) to place upper limits to the mass of a potential perturber in the WASP-4 system, based in our timing analysis of the transits of section 6.5. A detailed description of the setup we used for running the dynamical simulations can be found in Hoyer et al. (2011b) and Hoyer et al. (2011a). As a summary, for the simulated perturber body we use circular ($e = 0$) and coplanar orbits with WASP-4b. We explore a wide range of perturber masses ($0.1\ M_\oplus \leq M_{pert} \leq 5000 M_\oplus$) and distances between 0.1 AU and 0.06 AU. The semi-major axis steps were reduced near MMRs with the respective transiting body. For WASP-4b, we reduced the mass sampling when the calculated TTV *RMS* approached to 60 seconds.

We identified a region of unstable orbits where any orbital companion, in principle, experimented close encounters with the transiting body in the time of the integrations we studied. For all the other stable orbits we recorded the central times of the transits, which were compared with predicted times assuming an average constant orbital period for each system. This period do not deviate by more than 3 σ from the derived period of each transiting body.

The results of our dynamical simulations are illustrated in Figure 6.6, where we show the mass of the hypothetical perturber as a function of the star distance. The solid line in this Figure represents upper limits on the mass of a perturber that would produce a TTV *RMS* of 60 seconds in the transits of WASP-4b.

For WASP-4b, we found that the upper limits in the mass of an unseen orbital companion

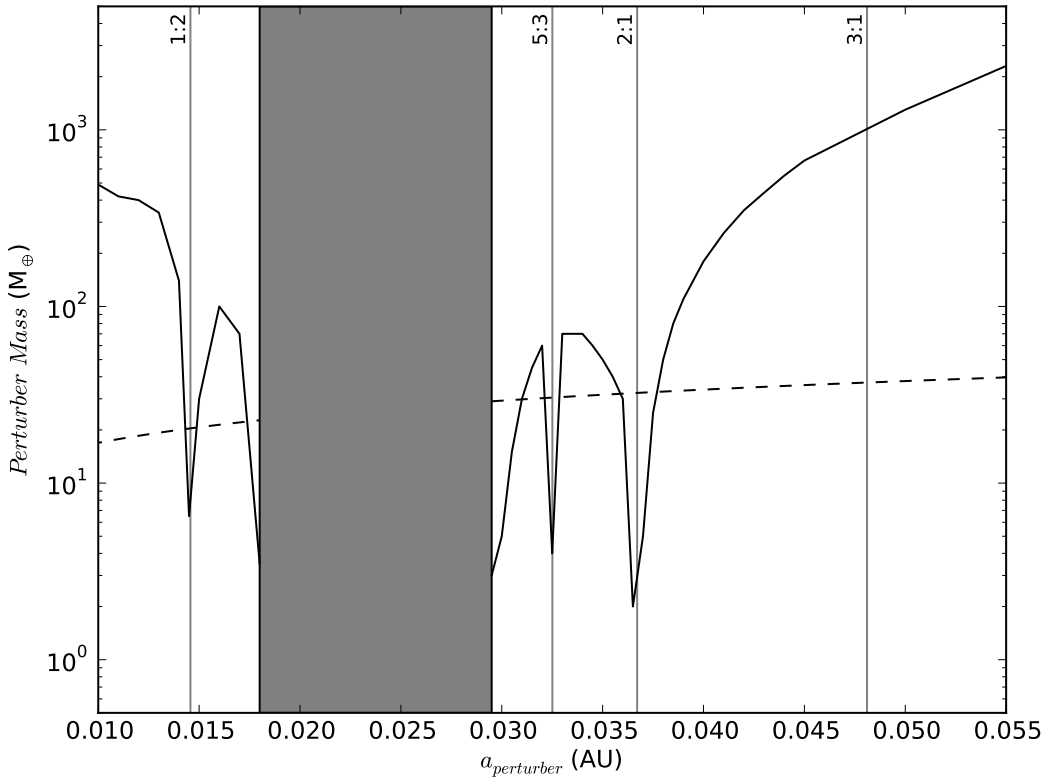

Figure 6.6 Upper mass limits as function of the orbital semi-major axis of an hypothetical perturber of the exoplanet WASP-4b, based on dynamical simulations done with the Mercury N-body simulator (Chambers et al. 1999). The solid line corresponds to perturber masses which produce TTVs RMS of less than 1 minute, as we measure in our timing analysis (see section 5). The dashed line shows the limits imposed by the radial velocity measurements. Vertical lines mark the MMRs with WASP-4b locations and the gray bar indicates the region of orbital unstabilities for any other object in the system.

are 6.5, 4.0 and 2.0 $M_{\oplus}$ in the 1:2, 5:3 and 2:1 MMRs respectively (vertical lines in figures 6.6). These limits are more strict compared with the radial velocities constraints (see the dashed line in Figure 6.6), specially in the MMRs.

6.6 Summary

We present twelve new transit epoch observations of the WASP-4b exoplanet. The number of the transit observed by the *TraMoS* project almost equals the available data in the literature. With the modeling of all this data we performed a timing analysis of the transits confirming that WASP-4b orbits its host star by a linear orbital period, based in the RMS of the O−C diagram of about 40 seconds in four years span observations. We updated the ephemeris equation of this planet and also we refined the values of the inclination of the orbit and the planet-to-star radii ratio. By inspection of the light curves and based in the work of Sanchis-Ojeda et al. (2011) we detected small anomalies in the relative flux of four of the transits presented in this work. We identified this bumps as stellar spots occultations by the planet. Further modeling of these occultations will permit to confirm the relative direction of the stellar rotation and the axis of the orbital motion of the planet.

Chapter 7

Analysis and Results of WASP7-b

TraMoS PROJECT: NEW PHYSICAL PROPERTIES OF WASP-7b BASED IN THREE NEW TRANSIT OBSERVATIONS

S. Hoyer[1], M. López-Morales[2,3], P. Rojo[1], N. Astudillo[1], E. Servajean[1]

Montly Notices of the Royal Astronomical Society, Submitted

[1]: Astronomy Department, Universidad de Chile, Casilla 36-D, Santiago de Chile, Chile.

[2]: Institut de Ciencies de l'Espai (CSIC-IEEC), Campus UAB, Facultat de Ciencies, Torre C5, parall, 2a pl, E-08193 Bellaterra, Barcelona, Spain.

[3]: Carnegie Institution of Washington, Department of Terrestrial Magnetism, 5241 Broad Branch Rd. NW, Washington, D.C. 20015, USA.

Abstract

We present three new transit epochs of the WASP-7b exoplanet, observed between June 2009 and July 2011 with the Y4KCam at the CTIO SMARTS 1mt Telescope which we combined with the two epochs previously reported to perform an homogeneous analysis of all the available data. Despite the large uncertainties we obtained for the mid-times of the transits we measured a dispersion of 2.6 minutes with respect to the updated ephemeris equation. The values we derived for the transit's depth of our light curves are closer to the presented by Hellier et al. (2009) and differs by about a 30% with the value derived by Southworth et al. (2011) which indicated that the radius of WASP-7b corresponds to a more inflated planet. More data are necessary to clarify this disagreement and to confirm or rule-out the presence of a perturber in the system. Additionally, with the timing information we could exclude the presence of a perturber of mass larger than $2M_{\oplus}$, $10M_{\oplus}$ and $2M_{\oplus}$ in the 1:2, 5:3 and 2:1 MMRs.

Based on the submitted work Hoyer et al. (2011c)

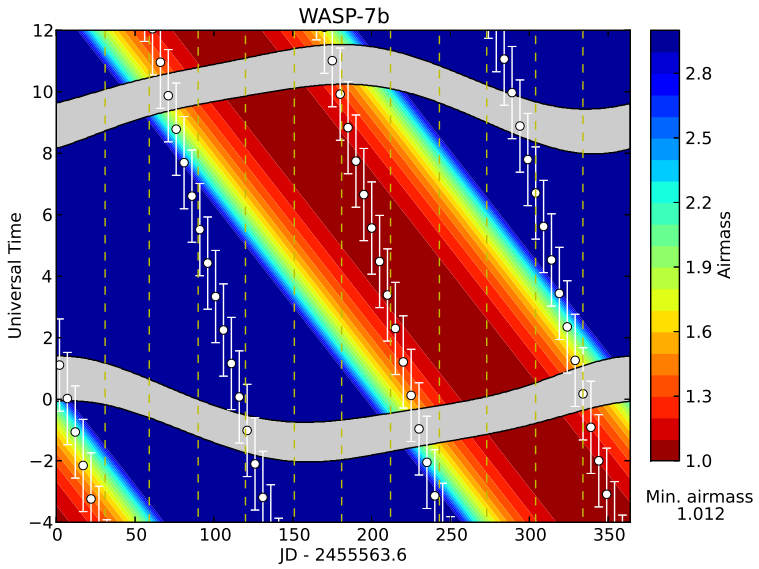

Figure 7.1 Observability of the transits of WASP-7b during 2011 as seen by CTIO telescopes. The symbols are as in Figure 3.1. Only few complete transits were observable during July 2011.

7.1 Introduction

Unlike of other WASP planets (e.g. WASP-3b, WASP-4b or WASP-5b), the transits of WASP-7b have not been intensively observed. Besides the discovery paper where this exoplanet was reported orbiting a bright F5V star (V=9.5 mag) with an orbital period of 4.95 days (Hellier et al. 2009, hereafter H09) only one other transit observation has been reported (Southworth et al. 2011, hereafter S11). This transit was observed with a *Gunn I* filter using the 1.54m Danish Telescope at La Silla. Based in this high quality data they calculated a much lower mean density of the planet ($\rho_p = 0.41 \pm 0.10\ \rho_J$).

Among the reasons that can explain why this exoplanet is poorly followed are the long duration of the transit ($\sim$ 4 hours) and its relative long orbital period ($\sim$ 5 days). This two properties makes it very difficult to allocate complete transits during one night. See for example Figure 7.1) where the observability of the transits of WASP-7b during 2011 as seen in CTIO is shown. Also, the lack of good reference stars in the nearby, principally due to the brightness of the host star, imposes the use of telescopes with wide field of views.

We present 3 new light curves of WASP-7b observed in June 2009 and July 2011. In Section 7.2 we describe the *TraMoS* observations of this exoplanet and we summarize the reduction of the data. In Section 7.3 we describe the light curve fitting and in Section 7.4 we discuss our results. Finally in Section 7.5 we present our conclusions.

Table 7.1. Information of the new transit epoch observations of WASP-7b presented in this work.

UT date	Epoch	Telescope/Instrument	Filter	binning	$RMS(F_{OOT})$
2009-06-08	-92	1-mt SMART/Y4KCam	Cousins I	2x2	0.0970
2009-06-13	-91	1-mt SMART/Y4KCam	Cousins I	2x2	0.0160
2011-07-21	64	1-mt SMART/Y4KCam	Cousins I	2x2	0.0095

7.2 Observations and Reduction

The observations we present in this work were performed with the Y4KCam on the SMARTS 1-m Telecope at Cerro Tololo Inter-American Observatory (CTIO). To reduce overheads we use the 2×2 binning mode. We used a *Bessell I* filter.

The two 2009's transits were observe entirely but with very poor Signal-to-Noise (SN) due to the extreme short exposure time (between 1 and 4 seconds) set to avoid saturation of WASP-7. We did not use the defocusing technique employed usually in these cases. The transit of 2011 has a better SN (10 seconds of integrations), and only a small fraction of the transit was lost due to technical failures. In Table 7.1 we summarize the observation log of each night. In the 20×20 arcmin^2 FoV (pixels scale of 0.289 arcsec pixel^{-1}) of the SMARTS 1-m telescope we could fit only two comparison stars of the same relative brightness. Unfortunately,one of them saturated in almost all the frames. Aperture photometry was performed over the target and the comparison stars. Based in the RMS of the out-of-transit flux (F_{OOT}) we chose the best values of the aperture and/or sky radii. We searched for correlations of the F_{OOT} with with the X-Y CCD coordinates of the target, airmass and/or time. To remove the trends we found, we applied linear or quadratic regressions fits, which were subtracted from the light curve. In Table 7.1 we show the final RMS values of each light curve.

7.3 Light Curve Fitting

To fit our three light curves and the one of S11 we use Transit Analysis Package, TAP (Gazak et al. 2011). In a first attempt to fit we noticed that because of the poor quality of the 2009's light curves the fitting did not converge. The large dispersion in the ingress/egress prevented TAP minimization to converge, in particular the mid-times of the transit. It is very likely, that the high dispersion in the light curves prevented the code to differentiate between the in- and the out- points of the transit. To avoid this behavior in the parameter space we fixed some parameter values and imposed some limits in the modeling of others as we explain below. We fixed the orbital period to $P = 4.9546416$ *days* and the semi-major and star radius ratio to $a/R_s = 9.26$ as was determined by S11. We left free the orbital inclination (i), the ratio of the planet and star radii (R_p/R_s), the central time of the transit (T_c), the red and white noise estimations (σ_R, σ_W). We also searched for any linear residual trend that can still be present in our light curve despite the systematic removal we perform before the fitting process. Therefore we left free the F_{OOT} and F_{slope}. We fitted for a quadratic limb

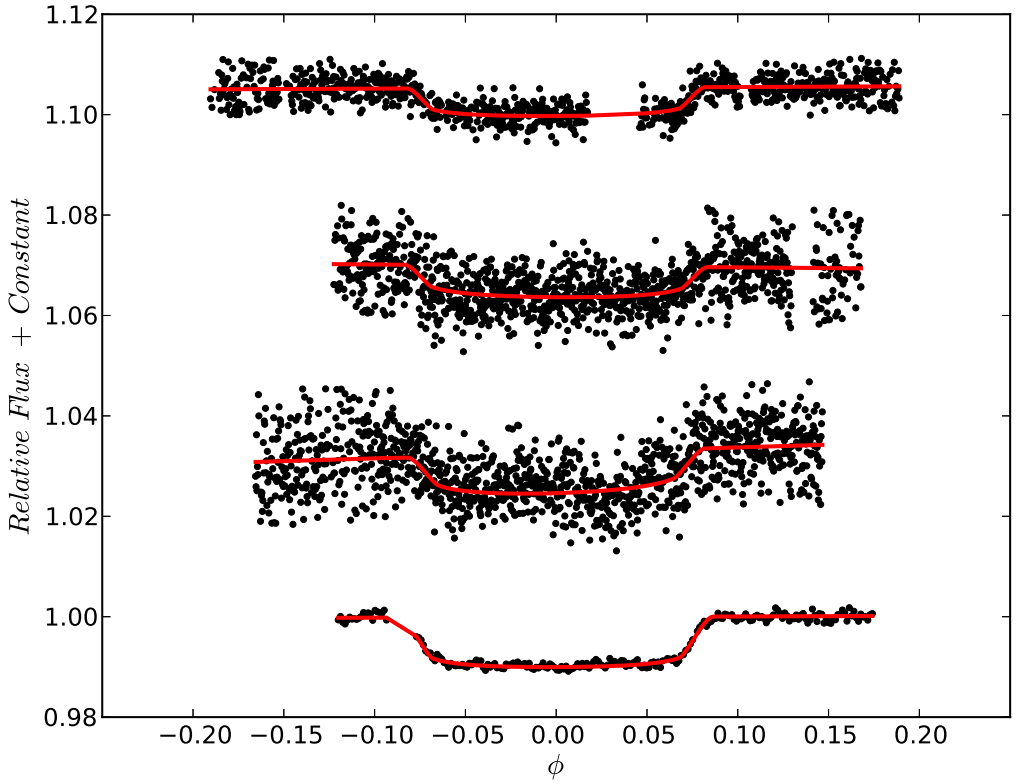

Figure 7.2 The three light curves of WASP-7b presented in this work and observed (from top to bottom) during : 21 July 2011, 13 June 2009 and 08 June 2009. The bottom light curve is the transit reported by S11. The best fitted model are represented by the solid red lines.

Table 7.2. Adjusted parameters for each transit of WASP-7b using TAP. In the last column we show the red-to-white noise ratio estimated in the light curves.

Epoch	$T_c - 2450000$ (BJD_{TT})	i [°]	R_p/R_s	μ_1	σ_{red}	$\frac{\sigma_{red}}{\sigma_{white}}$
-91	$4990.8039^{+0.0022}_{-0.0023}$	$86.88^{+0.36}_{-0.29}$	$0.0843^{+0.0048}_{-0.0052}$	$0.32^{+0.19}_{-0.16}$	0.0243	
-92	$4995.7614^{+0.0018}_{-0.0020}$	$87.19^{+0.40}_{-0.29}$	$0.0740^{+0.0037}_{-0.0037}$	$0.31^{+0.20}_{-0.22}$	0.0135	
64	$5763.7297^{+0.0013}_{-0.0012}$	$87.03^{+0.21}_{-0.17}$	$0.0713^{+0.0025}_{-0.0026}$	$0.21^{+0.09}_{-0.17}$	0.0057	
0[a]	$.63507^{+0.00085}_{-0.00087}$	$87.36^{+0.20}_{-0.15}$	$0.0956^{+0.0024}_{-0.0026}$	$0.13^{+0.240}_{-0.099}$	0.00548	

[a]Transit from Southworth et al. (2011).

darkening law but fixing the quadratic term to $\mu_2(I) = 0.32$ using as reference the values of Claret (2000). The eccentricity and the longitude of the periastron were fixed to zero. By visual inspection of the light curves we imposed limits in the modeling to R_p/R_s, T_c, μ_1, but these limits were not very strict.

In Table 7.2 we show the derived values of each light curve's parameters, using 10 MCMC chains of 10^5 links each, discarding the first 10% results from each chain. Figure 7.2 shows the four light curves and the best models we obtained using TAP.

7.4 Analysis

With the derived values of the central times of the transits and the value reported by H09, we built the O−C diagram using the ephemeris equation of S11. We fitted a linear regression to the residuals of the times represented by the dashed line in the Panel A of Figure 7.3. After correcting the residuals for this linear regression we obtained a *RMS* of 2.6 minutes (Panel B in Figure 7.3). We also plot with point-dashed lines the $\pm 1\sigma$ contours of the updated equation ephemeris. More data is needed to confirm if these deviations correspond to perturbation of an orbital companion or if they are consequence of the poor quality of the data and/or unsuccessful removal of systematics in the data. The *goodness of the fit* of the linear regression is $\chi^2 = 7.7$ with 3 degrees of freedom, which corresponds to a $\chi^2_{red} = 2.56$.

The updated ephemeris equation of the WASP-7b exoplanet is:

$$T_c(N) = T_0 + P \times N = 2455446.63631(63) + 4.9546473(40) \times N, \tag{7.1}$$

where the errors are shown in parenthesis and N represents the epoch when the central time of the transit T_c is predicted.

Based in the TTV *RMS* we estimated, we place upper limits in the mass of a perturber in the system. In Figure 7.4 we plot the results of the dynamical simulations we obtained using the *Mercury* Code. We can ruled-out the presence of a perturber of $2M_\oplus$ in the 1:2 and 2:1 MMRs and of a $10M_\oplus$ in the 5:3 MMR.

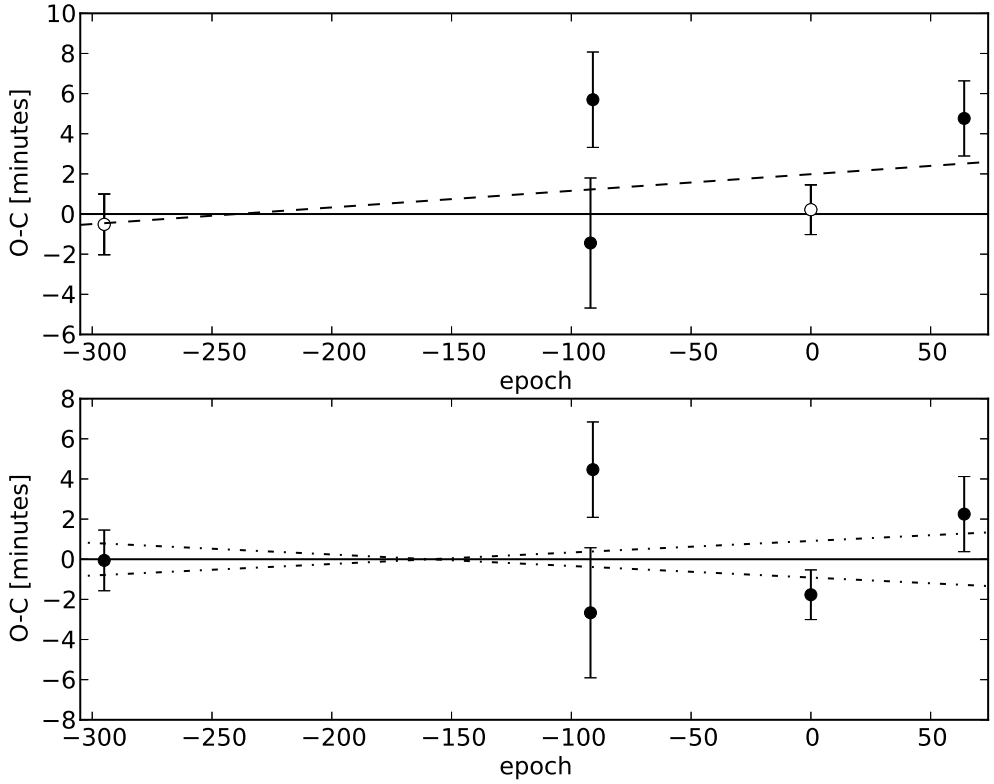

Figure 7.3 Observed *minus* Calculated Diagram of the WASP-7b's transits. **Top Panel:** The open symbols correspond to Hellier et al. (2009) and Southworth et al. (2011) transits. Solid symbols represent the epochs presented in this work. Using the S11's ephemeris equation as reference we calculated a linear trend in the residuals of the transit times ($\chi^2_{red} = 2.67$). **Bottom B:** After removing the linear trend, the *RMS* of the T_c is of 2.6 minutes. The $\pm 1\sigma$ of the updated ephemeris equation are represented by the point-dashed lines.

Table 7.3. The final derived values obtained by the weighted average of the modeling results of section 7.3. For comparison we also show the derived parameters of H09 and S11.

Parameter	This work	H09	S11
i (°)	87.03 ± 0.18	$89.6^{+0.4}_{-0.9}$	87.03 ± 0.93
R_p/R_s	0.0724 ± 0.0096	0.0761 ± 0.0008	0.0956 ± 0.0016
μ_1	0.24 ± 0.078	$\cdots$	0.059 ± 0.064
P (days)	4.9546473(40)	4.9546416(35)	$4.954658^{+0.000055}_{-0.000043}$

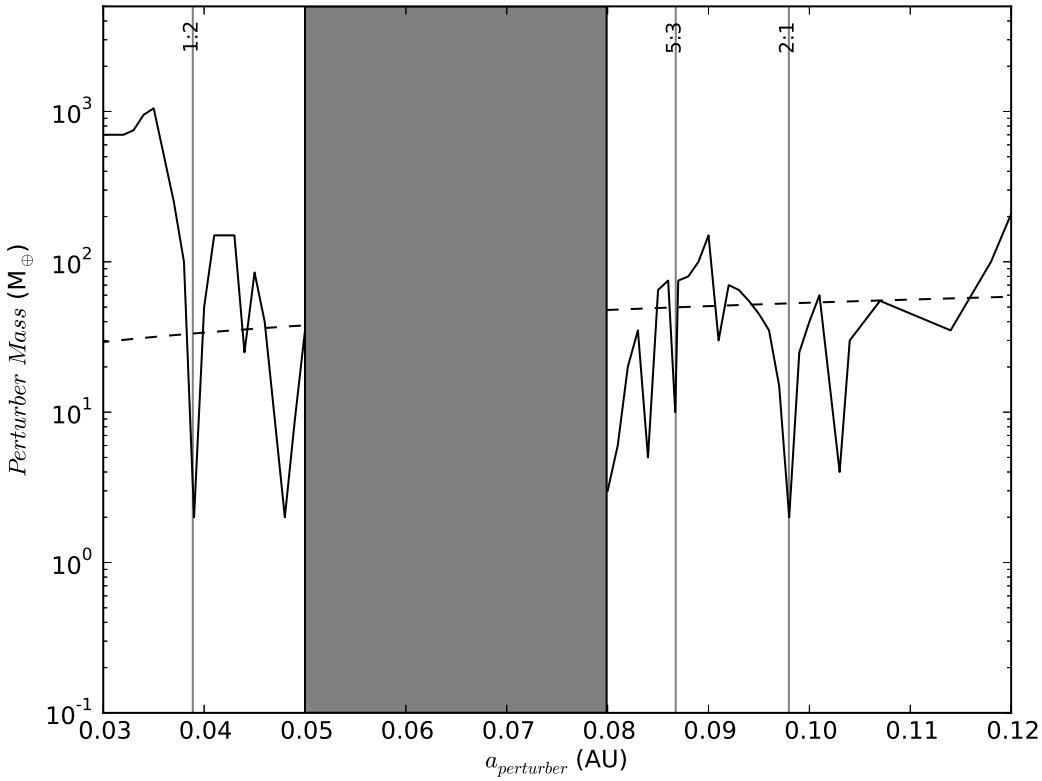

Figure 7.4 Upper mass limits as function of the orbital semi-major axis of an hypothetical perturber of the exoplanet WASP-7b, based on dynamical simulations done with the Mercury N-body simulator (Chambers et al. 1999). The solid line corresponds to perturber masses which produce TTVs RMS of less than 3 minutes, as we measure in our timing analysis. The dashed line shows the limits imposed by the radial velocity measurements. Vertical lines mark the MMRs with WASP-7b locations and the gray bar indicates the region of orbital unstabilities for any other object in the system.

We plot in the top panel of Figure 7.5 the derived values of the orbital inclination of the four fitted light curves. All of them are consistent within the errors. On the contrary, the fitted values of the depth of the transits (R_p/R_s) of our three light curves do not match the S11's value (solid and open symbols in Figure 7.5 respectively). The values from the our second and third transit light curves present the lowest values of R_p/R_s. The weighted average of the transit depth from our three light curves ($R_p/R_s = 0.0724 \pm 0.0096$) is consistent within the errors with the reported value by H09 (see Table 7.3) but differs in $\sim 30\%$ with the value reported by S11. Our derived value from S11's light curve is the same obtained by S11 ($R_p/R_s = 0.0956 \pm 0.0016$).

We investigated if the origin of this discrepancy is due to that the counts in the science images reached the non-linearity or saturation regime of the detector, resulting in a problem in the normalization of the light curves. Figure 7.6 shows the maximum number of counts within the aperture of each frame of the three transit observations (after bias subtraction, and therefore there is a $\sim 3500 - 3800$ *counts* offset present). We notice that despite the count levels were closer to the non-linearity regime (42000 ADUs above bias) in the first and third night, it can not explain the discrepancy in the depth of the transit with respect to the value derived by S11. Actually, the second night is far below the non-linearity regime and we also calculated a low value in R_p/R_s. Our most precise estimate we assessed correspond to the 2011's transit, which is also our best light curve in terms of *RMS*. This transit gives the lower value of the depth.

Another possibility of the source of this inconsistency can be explained by the different methods used for the photometry. S11 used a DAOPHOT aperture to reduce their data, and it is known that the depth of the transits can change depending on the use of image subtraction or aperture photometry (e.g. Gillon et al. 2007, Pont et al. 2007). Therefore this effect can not be ruled-out in the explaining of the apparent transit depth disagreement.

To test how the values in the inclination and/or the limb darkening can influence the estimates of R_p/R_s we investigate the correlation between the variable we fitted using the results of the MCMC iterations (Figure 7.7). We observed some correlation, as was expected, between i ,μ_1 and R_p/R_s. To quantify how this correlations can influence the results, we ran the same fits but now fixing the values of both limb darkening coefficients ($\mu_1 = 0.21$ and $\mu_2 = 0.32$). Doing this we break the correlation between i and R_p/R_s but the values derived for these variables are consistent with the previous results within the errors.

Despite the indications of R_p/R_s variations, we emphasize that further follow-up of additional transits of WASP-7b exoplanet is needed in order to clarify this discrepancy in the values of the transit's depth. We expect that if these variations are originated by an astrophysical source, i.e, some type of orbital precession or gravitational perturbation, we would find evidence of variations in the orbital inclination (related with the transit duration) as well. More precise data, in particular in the ingress and egress of the transit will constrain in a better way these variables and therefore a more detailed inspection of their evolution will illuminated the discussion.

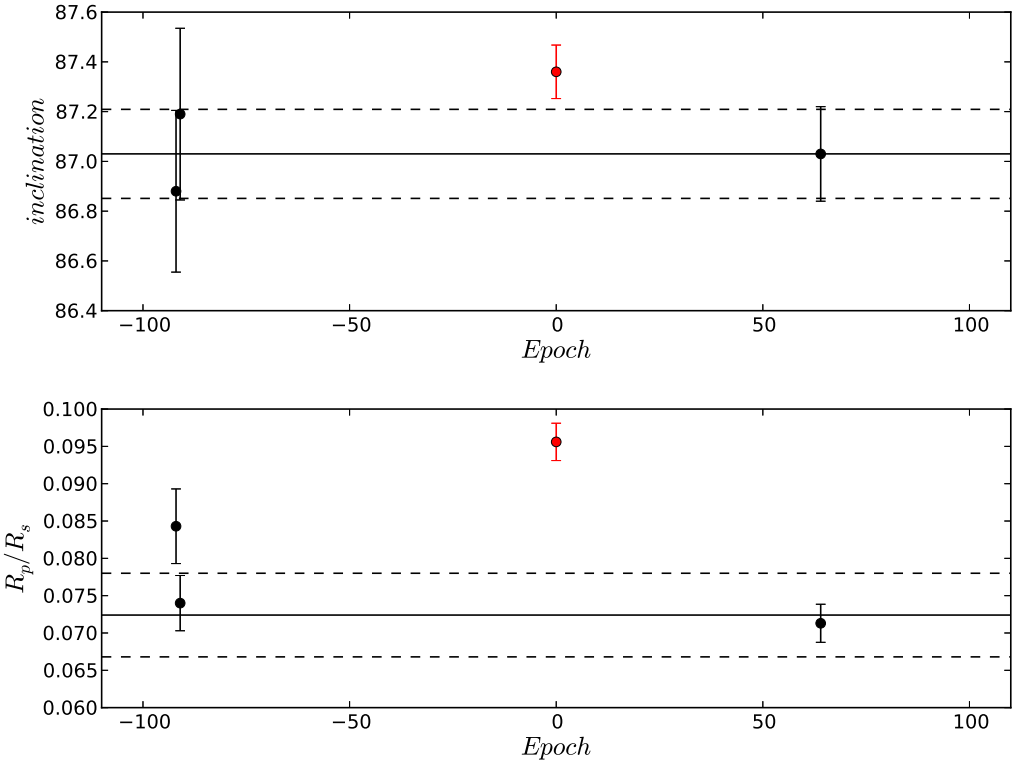

Figure 7.5 Orbital inclination values (Top panel) and Planet-to-Star radii ratio (Bottom panel) derived with TAP. The black points correspond to the three transits presented in this work and the red point corresponds to the value derived from S11's light curve. The weighted average and its $\pm 1\sigma$ limits are represented by the solid and dashed lines respectively. The value of S11's light curve was discarded when computing the average to emphasize the disagreement between the all the points.

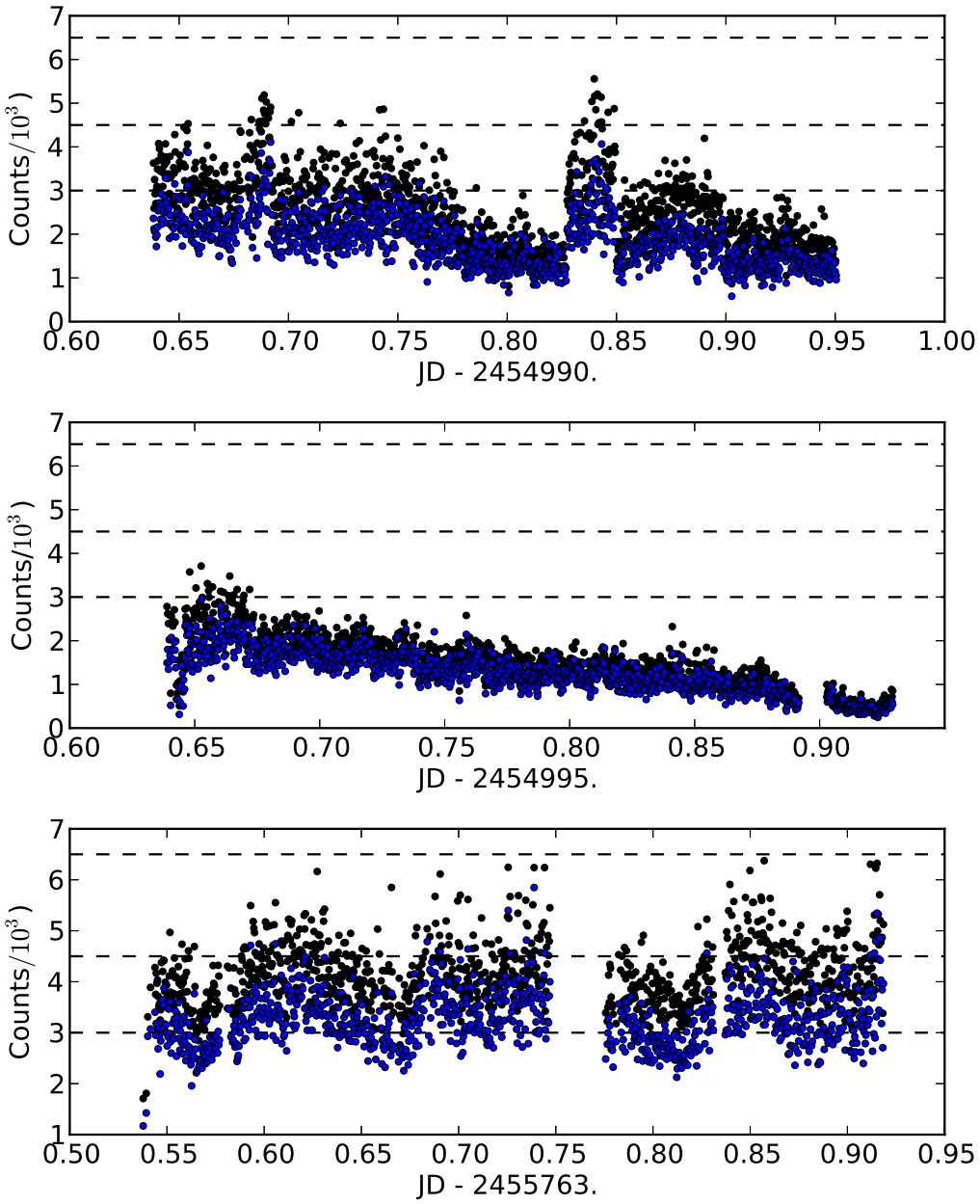

Figure 7.6 Pixel peaks of within the photometry aperture for the target (black points) and the comparison star (blue points) for the three nights presented in this work. We marked the 30K, 45K and 65K count levels with the dashed lines. Several frames in the first and third night reached the non-linearity regime of the detector but that can not account for the lower values of R_p/R_s we derived.

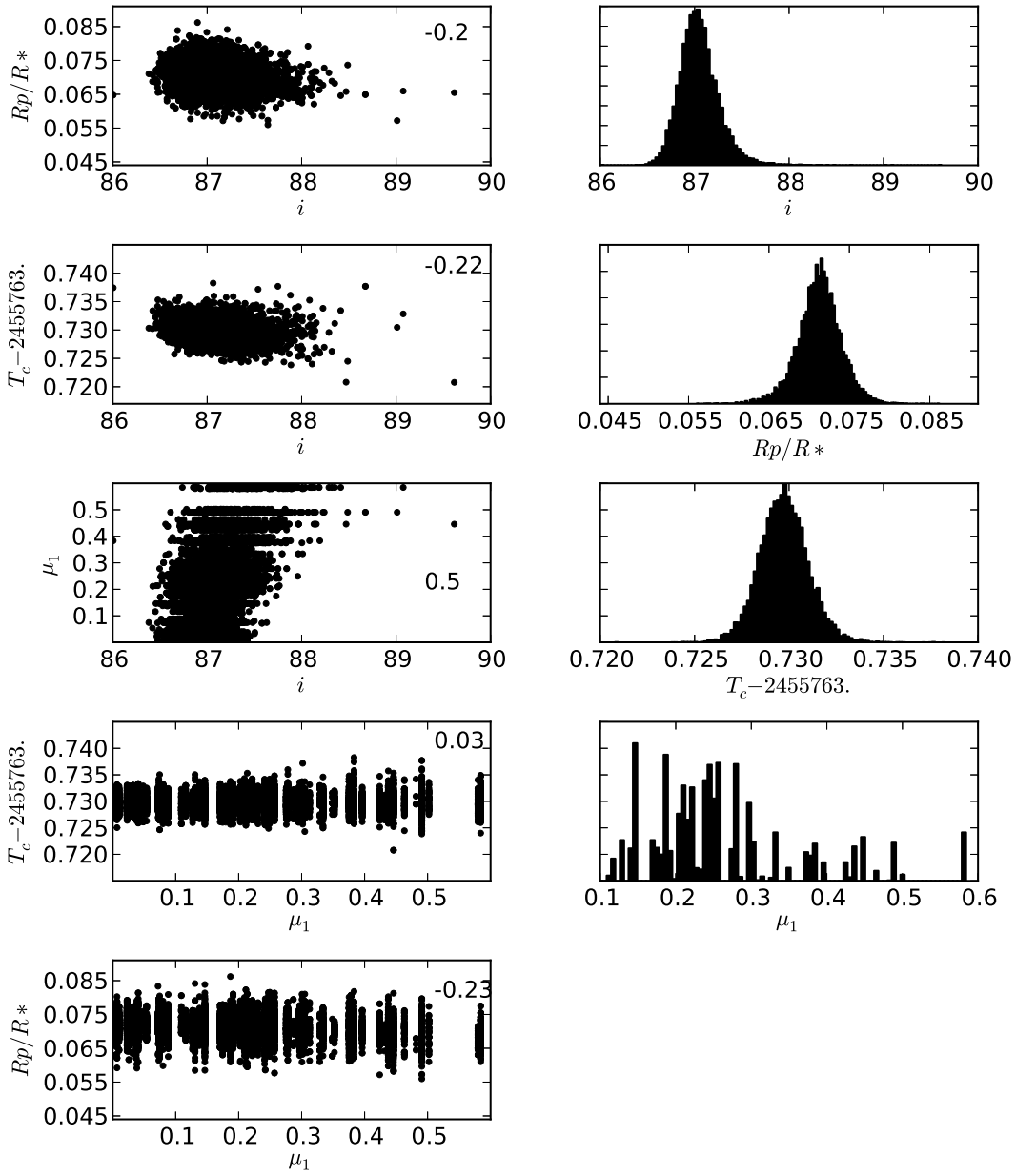

Figure 7.7 A subset of 20 000 of the 10×10^5 Markov Chain Monte Carlo iterations (picked randomly) resulting of fitting the 2011's transit data with TAP. In the left panels we show the correlations between i, R_p/R_s, T_c and μ_1. The correlation coefficients between each variable are shown on each panel. In the right panels we show the histograms of these variables. It is clear that μ_1 do not follows a Gaussian distribution because data quality is not enough to constrain the successfully the quadratic limb darkening coefficient.

7.5 Summary

We presented three new transit observations of WASP-7b. After modeling these light curves and the one of S11 we derived the T_c, i, R_p/R_s among other light curve parameters. After a linear regression fit of the residuals of the transit mid-times we found a TTV RMS of 2.6 minutes. The transits are consistent with the updated ephemeris equation. Only the -92th transit is beyond the $\pm 1\sigma$ uncertainties. We see a lack of variations in the derived orbital inclinations. All the parameter values are within the $\pm 2\sigma$ limits. On the other hand, the transit's depths of our light curves differ clearly from the value of the S11's transit. The weighted average obtained from our light curves is consistent with the value reported in the discovery paper of this exoplanet. We have investigated various possible sources of the difference without any positive results. We emphasize the need of further data of higher precision to disentangle the difference in the R_p/R_s values.

Chapter 8

Summary

The Transit Timing Variation technique has demonstrated to be a powerful tool to detect orbital companions of transiting planets even in the Earth-mass regime. Careful photometric monitoring of the transit events permits to search for variations in the central times of the transit that can be attributed to gravitational perturbations induced by an orbital companion in the system.

For this PhD project, I have developed the required tools and methods to conduct a monitoring of transiting planets observable from the Southern Hemisphere. This PhD thesis have led to establishing a long-term monitoring program of transiting planets using a wide variety of telescope/instrument available in Chilean observatories. To date, *TraMoS* is a unique dedicated project of its kind in the Southern Hemisphere.

Besides the TTV studies that can be undertaken under the *TraMoS* project, the accumulation of light curves permits to derived accurate physical parameters of the transiting systems, which are critical to constrain models of interiors and evolution of exoplanets.

In the framework of *TraMoS* we have observed more than 70 transit's light curves of 20 exoplanets. These data is being reduced and analyzed by custom-made pipelines especially developed for each instrument used.

The results of the analysis of most sampled targets are the bulk of this thesis (results that have been published or submitted to referee journals as is indicated in the text). I presented in this Thesis five new light curves of OGLE-TR-111b, nine of WASP-5b, twelve of WASP-4b and three of WASP-7b. For each case, these new data equals or doubles all the already published transits for those WASP planets.

Based on the measurement of the central times of the transits of the planets analyzed in this thesis, I have discarded TTVs (previously suggested in the literature) in the cases of OGLE-TR-111b and WASP-5b, and I have confirmed the linear periodicity of WASP-4b. Besides the scatter in the T_c of WASP-7b of 2.6 minutes, and taking into account the large time uncertainties, it is premature to suggest that the observed variations are originated by an orbital companion. Further observations are also needed to clarify the disagreement in the depth of the transits of WASP-7b. The R_p/R_s derived from the light curves I analyzed refutes the value reported by Southworth et al. (2011). The derived R_p/R_s is 30% smaller

than the value previously reported.

Additionally, we have identified stellar spot features in some of the light curves of WASP-4b. Modeling of these spot occultations will provided valuable insights for the determination of the star's rotation angle and period.

Despite the lack of clear evidence of TTVs in the exoplanets studied in this thesis, the performed timing analysis allowed me to place strong limits in the mass of hypothetical perturbers in the systems, overcoming the constraints imposed by radial velocities measurements.

In summary, the limits on the perturber's masses for each planet are

- OGLE-TR-111b: 1.3 $M_{\oplus}$, 0.4 $M_{\oplus}$ and 0.5 $M_{\oplus}$ in the 3:2, 1:2 and 2:1 MMRs. Also there is an upper limit of ~ 30 $M_{\oplus}$ in the region between the 3:2 and 1:2 MMRs.
- WASP-5b: $5M_{\oplus}$, $1M_{\oplus}$ and $3M_{\oplus}$ in the 1:2, 5:3 and 2:1 MMRs,
- WASP-4b: 6.5 $M_{\oplus}$, 4.0 $M_{\oplus}$ and 2.0 $M_{\oplus}$ in the 1:2, 5:3 and 2:1 MMRs,
- WASP-7b: 2 $M_{\oplus}$, 10 $M_{\oplus}$ and 2 $M_{\oplus}$ in the 1:2, 5:3 and 2:1 MMRs.

This information sets strong insights in the manner how these Hot Jupiters were formed. Such type of accurate determination of the architecture of more transiting systems will provide the numbers to establish a clear picture of the formation and evolution of exoplanets.

8.1 Collaborations

One or two transits of an exoplanet are not enough to perform a complete TTV analysis. For this reasons I have established collaborations with other groups in order to exploit the data of the less sampled targets. These data are of high interest in order to complement the observations made for other groups. That is the case of OGLE-TR-56b, where the 2009-04-28 transit observed with GEMINI-South was included in a work where new 21 light curves of this exoplanet were presented (Adams et al. 2011b). With this large number of new observed transits it was possible to refine the values of the planetary radius, the inclination, transit duration and the orbital semi-major axis. No indications of TTVs were also reported for this exoplanet.

Also, another collaboration was started with a European group. I included in my analysis of WASP-4b (see Chapter 6) two light curves observed by this group with the CTIO SMARTS 1-m Telescope in the R band during 2011. These transits extended the span coverage of the observations resulting in a more accurate estimation of the ephemeris equation of this planet.

In the case of GJ-1214b, I am joining efforts with researchers of the European Southern Observatory (ESO), Pontificia Universidad Católica (PUC) and Universidad de Chile, to finish the analysis of new photometric data of this planet. The principal goal of this group is to characterize exoplanets atmospheres by mean of transmission spectroscopy and/or photometric measurements of primary and secondary transits. We plan to submit the results of

the analysis of two transits (one observe in a K band and other in a z' band) by the end of January 2012. This work will complement the wavelength coverage of the transits of this planet (see for example Bean et al. 2010).

8.2 Future Work

As I mentioned before, I have observed 70 transits of 20 exoplanets. I have started a preliminary/fast analysis of the data of all of them and its O−C diagrams will be ready to be inspected in brief to search for TTV indications. The most sampled objects (OGLE-TR-113b, WASP-2b and WASP-18b) will be our priority targets to be analyzed and its results to be published.

The results of the less sampled targets are planned to be published together in order to make them available in the literature for future follow-up of other groups or for establishing collaborations like the case of OGLE-TR-56b.

In the near future I also will focus in the *TraMoS* data obtained with the use of the small telescopes in order to analyze the data of the new discovered planets searching for TTVs signals.

Is worth mentioning that many students of the Astronomy Department of Universidad de Chile were/are involve directly in this project, either performing observations and/or reducing and analyzing the data of the telescopes recently used in the *TraMoS* project. Observational programs like *TraMoS* are also very valuable due the academic and observational training opportunities that open up for students at the Astronomy Department.

Appendix A

A brief description of the Pipeline Codes

A.1 Brief description of the pipeline tasks

The task performed by the Reduction Pipelines are:

- Overscan and Trimming: The code implements overscan corrections when is needed. Depending on the detectors size and the CHIPS placement, the code cuts overscan regions and removes gaps between individual CCDs. creating a mozaiced frame of all the images of the night. Resulting images are named with a *t.* prefix
- Bias Correction: The code reads a list with the names of the bias images of the night to perform a median combination to create a MASTER-BIAS image. This MASTER-BIAS is substracted on each flat and science image. Resulting images are named with a *b.* prefix.
- Flatfield Correction: The code reads a list with the names of the flats images of the night to perform a median combination to create a MASTER-FLAT image (normalized to its median value). Each science image is then divided by the normalized MASTER-FLAT frame. Resulting images are named with a *f.* prefix.
- Photometry: I have implemented single and multi-aperture photometry tasks. The multi-aperture was created to allow to use a series of different apertures but reducing the running time of the code (since the frames are openned, read and closed only once). Photometry task reads the CCD X-Y coordinates of the stars, search for its centroids and sums the counts of the pixels inside a circle of a indicated radius. The sky or background value is calculated using a median value of the pixels located in a ring around the centroid. A single file with the values of the photometry of each star per frame is created. The JD and the phase (time from-to the T_c) of the half of the exposure are also recorded. This values are calculated based in the respective header's time stamps.

- Light Curve Generation: This task reads the output file from the photometry and creates different type of light curves used to test the suitability of the aperture/sky chosen based in the RMS of the out of transit flux. The task generates a plot of the relative flux of the target with every stars for separated and also a plot of the differential photometry of the target versus the average of all star's fluxes. It is possible to indicate which stars will not be included for a 'clean average'. Light curves using this 'clean average' and a binning factor are also created. All the statistics is recorded in a output file. File with both the 'clean' and the binned light curves are also outputs of this task.
- Detrending task: A number of correlations between the Flux and several parameters can be tested in order to estimated its influence in the light curve shape and/or RMS.

A.2 Parameters Configuration File

Edit a configuration file for each observation night is required to run the pipelines. Critical parameters used by the different task are specified in this file. A template of the configuration file is shown in what follows (the line numbers are shown in the left for the readability of the code):

```
1
2  [PHOTPARS]                  #  Parameters of the Photometry
3
4  auto: 1                     #  The photometry is executed in automatic mode?
5  gain : 1.5                  #  Gain of the instrument
6  ron : 14                    #  Readout noise of the instrument
7  rad : 7                     #  Aperture radius
8  ann : 20                    #  smaller radius of the sky ring
9  dan : 5                     #  Width of the sky ring
10 stampsize : 20              #  Scale of the STAMP size (see apphot.py)
11 outphot : phot.7.data       #  Name of the output file
12 coofile : estrellas.coo     #  Name of the file with the coordinates list
13 filelist : images.list      #  Name of the file with the list of the frame names
14
15
16 [NIGHTPARS]                 # Parameter of the specific night
17
18 date : 20080823             # Used to titled the plots
19 planet : WASP-4
20 nstars : 2                  # number of stars used to created the LCs
21 nframes : 787               # number of frames used to created the LCs
22 photfile:  phot.7.data      # Name of the file with the photometric measurements
23 plotdir: plots              # Where to save the plots
24 outfile: lc.out.7.data      # Output file with the LCs statistics
25
26 [PLOTS]                    # Parameters used to generate the plots
27
28 script: 1                  # Automatic mode?
29 saveplots : 0               # Do you want to save the plots?
30 phasecurve : 0              # Do you want to used the phase in the x-axis
31                             # instead of the frame number?
32 growplot : 0                # Do you want to create a Growing Curve?
```

```
33 growframe : 450              # Number of the last frame used in the GC
34 LCall : 1                    # Do you want to plot the flux of every star?
35 nsubx: 2                     # to create a proper plot (nsubx x nsuby = nstars)
36 nsuby: 6
37 LCdiff : 1                   # Do u want to plot the relative flux of the target
38                              # and every star?
39 LCaver : 1                   # Do u want to plot the relative flux of the target
40                              # and the average flux?
41 LCclean : 1                  # Do u want to plot the relative flux of the target
42                              # with the 'clean' average flux?
43 stars2clean : 4 5            # Which stars do u want to discard?
44 LCbin : 1                    # Do you want to plot the binned LC ?
45 bin : 4                      # Number of consecutive frames to bin
46
47 [LIMITS]                     # Limits to plot and to do statistics
48
49 jdlim: 2454701.9             # What is the JD of the last frame?
50 jd0 : 2454697.7975           # T0 of the planet
51 period : 1.33823             # Period of the planet
52 epochs : 1000                # number of maximum orbits use to calculate Tc
53 b1end : 100                  # baseline 1 limit (in terms of frame number)
54 bottom1: 200                 # time of the 2nd contact
55 bottom2: 340                 # time of the 3rd contact
56 b2start: 440                 # baseline 2 limit (in terms of frame number)
57 p1: -.05                     # baseline 1 limit (in terms of phase)
58 p2: -.025                    # phase of the 2nd contact
59 p3: .025                     # phase of the 3rd contact
60 p4: .05                      # baseline 2  limit (in terms of phase)
61
62 [DETREND]                    # Parameters for the detrending tasks
63
64 airmass : 0                  # Do u want to correlate Flux vs the airmass ?
65 seczfile : secz.data         # Name of the file with the airmass of each frame
66 flux : 0                     # Do u want to fit Flux vs time ?
67 poldegree : 1                # degree of the polynomial used to fit
68 background : 0               # Do u want to fit Flux vs background values ?
69 backfile : back.data         # Name of file with the background values
70 xycorr : 1                   # Do you want to correlate with the X-Y position?
71 xyfile : xycentroids.data    # Name of the file with the XY coo (centroids)
```

Bibliography

Adams, E. R., López-Morales, M., Elliot, J. L., Seager, S., & Osip, D. J. 2010a, *ApJ*, 714, 13

—. 2010b, *ApJ*, 721, 1829

—. 2011a, *ApJ*, 728, 125

Adams, E. R., et al. 2011b, *ApJ*, 741, 102

Agol, E., Steffen, J., Sari, R., & Clarkson, W. 2005, *MNRAS*, 359, 567

Agol, E., & Steffen, J. H. 2007, *MNRAS*, 374, 941

Alard, C., & Lupton, R. H. 1998, *ApJ*, 503, 325

Alonso, R., et al. 2004, *ApJ*, 613, L153

Anderson, D. R., et al. 2008, *MNRAS*, 387, L4

Appenzeller, I., et al. 1998, The Messenger, 94, 1

Bakos, G. Á., et al. 2009, *ApJ*, 707, 446

Ballard, S., et al. 2011, ArXiv e-prints

Barge, P., et al. 2008, *A&A*, 482, L17

Bean, J. L. 2009, *A&A*, 506, 369

Bean, J. L., Miller-Ricci Kempton, E., & Homeier, D. 2010, *Nature*, 468, 669

Borucki, W. J., et al. 2010, Science, 327, 977

—. 2011, *ApJ*, 728, 117

Bouchy, F., Pont, F., Melo, C., Santos, N. C., Mayor, M., Queloz, D., & Udry, S. 2005, *A&A*, 431, 1105

Cáceres, C., Ivanov, V. D., Minniti, D., Naef, D., Melo, C., Mason, E., Selman, F., & Pietrzynski, G. 2009, *A&A*, 507, 481

Cáceres, C., et al. 2011, *A&A*, 530, A5

Carter, J. A., & Winn, J. N. 2009, *ApJ*, 704, 51

Chambers, J. E. 1999, *MNRAS*, 304, 793

Chan, T., Ingemyr, M., Winn, J. N., Holman, M. J., Sanchis-Ojeda, R., Esquerdo, G., & Everett, M. 2011, *AJ*, 141, 179

Charbonneau, D., Brown, T. M., Latham, D. W., & Mayor, M. 2000, *ApJ*, 529, L45

Charbonneau, D., et al. 2005, *ApJ*, 626, 523

—. 2009, *Nature*, 462, 891

Claret, A. 2000, *A&A*, 363, 1081

—. 2004, *A&A*, 428, 1001

Cochran, W. D., et al. 2011, *ApJS*, 197, 7

Coughlin, J. L., Stringfellow, G. S., Becker, A. C., López-Morales, M., Mezzalira, F., & Krajci, T. 2008, *ApJ*, 689, L149

Csizmadia, S., et al. 2010, *A&A*, 510, A94

Deming, D., Seager, S., Richardson, L. J., & Harrington, J. 2005, *Nature*, 434, 740

Deming, D., et al. 2011, *ApJ*, 740, 33

Désert, J.-M., et al. 2011, *ApJS*, 197, 11

Díaz, R. F., Rojo, P., Melita, M., Hoyer, S., Minniti, D., Mauas, P. J. D., & Ruíz, M. T. 2008, *ApJ*, 682, L49

Doyle, L. R., et al. 2011, Science, 333, 1602

Dragomir, D., et al. 2011, ArXiv e-prints

Eastman, J., Siverd, R., & Gaudi, B. S. 2010, *PASP*, 122, 935

Fernandez, J. M., Holman, M. J., Winn, J. N., Torres, G., Shporer, A., Mazeh, T., Esquerdo, G. A., & Everett, M. E. 2009, *AJ*, 137, 4911

Fischer, D., et al. 2009, *ApJ*, 703, 1545

Ford, E. B., & Holman, M. J. 2007, *ApJ*, 664, L51

Ford, E. B., et al. 2011, ArXiv e-prints

Fukui, A., et al. 2011, *PASJ*, 63, 287

Fulton, B. J., Shporer, A., Winn, J. N., Holman, M. J., Pál, A., & Gazak, J. Z. 2011, *AJ*, 142, 84

García-Melendo, E., & López-Morales, M. 2011, *MNRAS*, 417, L16

Gazak, J. Z., Johnson, J. A., Tonry, J., Eastman, J., Mann, A. W., & Agol, E. 2011, ArXiv e-prints

Gibson, N. P., et al. 2009, *ApJ*, 700, 1078

—. 2010, *MNRAS*, 401, 1917

Gillon, M., et al. 2007, *A&A*, 466, 743

—. 2009, *A&A*, 496, 259

Haghighipour, N., & Kirste, S. 2011, Celestial Mechanics and Dynamical Astronomy, 111, 267

Hebb, L., et al. 2009, *ApJ*, 693, 1920

Hellier, C., et al. 2009, *ApJ*, 690, L89

Henry, G. W., Marcy, G. W., Butler, R. P., & Vogt, S. S. 2000, *ApJ*, 529, L41

Heyl, J. S., & Gladman, B. J. 2007, *MNRAS*, 377, 1511

Holman, M. J., & Murray, N. W. 2005, Science, 307, 1288

Holman, M. J., et al. 2010, Science, 330, 51

Hoyer, S., Rojo, P., & López-Morales. 2011a, *ApJ*, accepted

Hoyer, S., Rojo, P., López-Morales, M., Díaz, R. F., Chambers, J., & Minniti, D. 2011b, *ApJ*, 733, 53

Hoyer, S., et al. 2011c, *MNRAS*, submitted

Jordán, A., & Bakos, G. Á. 2008, *ApJ*, 685, 543

Kipping, D., & Bakos, G. 2011, *ApJ*, 733, 36

Kipping, D. M. 2009a, *MNRAS*, 392, 181

—. 2009b, *MNRAS*, 396, 1797

Knutson, H. A., Charbonneau, D., Noyes, R. W., Brown, T. M., & Gilliland, R. L. 2007, *ApJ*, 655, 564

Kozai, Y. 1962, *AJ*, 67, 591

Lin, D. N. C., Bodenheimer, P., & Richardson, D. C. 1996, *Nature*, 380, 606

Lissauer, J. J., et al. 2011, *Nature*, 470, 53

Maciejewski, G., Errmann, R., Raetz, S., Seeliger, M., Spaleniak, I., & Neuhäuser, R. 2011a, *A&A*, 528, A65

Maciejewski, G., Raetz, S., Nettelmann, N., Seeliger, M., Adam, C., Nowak, G., & Neuhäuser, R. 2011b, *A&A*, 535, A7

Maciejewski, G., Seeliger, M., Adam, C., Raetz, S., & Neuhäuser, R. 2011c, ACA, 61, 25

Maciejewski, G., et al. 2010, *MNRAS*, 407, 2625

—. 2011d, *MNRAS*, 411, 1204

Mandel, K., & Agol, E. 2002, *ApJ*, 580, L171

Mayor, M., & Queloz, D. 1995, *Nature*, 378, 355

McLaughlin, D. B. 1924, *ApJ*, 60, 22

Meschiari, S., & Laughlin, G. P. 2010, *ApJ*, 718, 543

Miller-Ricci, E., et al. 2008a, *ApJ*, 682, 593

—. 2008b, *ApJ*, 682, 586

Minniti, D., et al. 2007, *ApJ*, 660, 858

Miralda-Escudé, J. 2002, *ApJ*, 564, 1019

Nascimbeni, V., Piotto, G., Bedin, L. R., Damasso, M., Malavolta, L., & Borsato, L. 2011, *A&A*, 532, A24

Nesvorný, D. 2009, *ApJ*, 701, 1116

Nesvorný, D., & Beaugé, C. 2010, *ApJ*, 709, L44

Nesvorný, D., & Morbidelli, A. 2008, *ApJ*, 688, 636

Pál, A., Sárneczky, K., Szabó, G. M., Szing, A., Kiss, L. L., Mező, G., & Regály, Z. 2011, *MNRAS*, 413, L43

Payne, M. J., & Ford, E. B. 2011, *ApJ*, 729, 98

Pietrukowicz, P., et al. 2010, *A&A*, 509, A4

Pont, F., Zucker, S., & Queloz, D. 2006, *MNRAS*, 373, 231

Pont, F., et al. 2007, *A&A*, 465, 1069

Rasio, F. A., & Ford, E. B. 1996, Science, 274, 954

Rojo, P. M. 2006, PhD thesis, Cornell University

Rossiter, R. A. 1924, *ApJ*, 60, 15

Sanchis-Ojeda, R., Winn, J. N., Holman, M. J., Carter, J. A., Osip, D. J., & Fuentes, C. I. 2011, *ApJ*, 733, 127

Santos, N. C., et al. 2006, *A&A*, 458, 997

Sartoretti, P., & Schneider, J. 1999, *A&AS*, 134, 553

Seager, S., & Mallén-Ornelas, G. 2003, *ApJ*, 585, 1038

Silva-Valio, A. 2008, *ApJ*, 683, L179

Sing, D. K., & López-Morales, M. 2009, *A&A*, 493, L31

Smith, A. M. S., et al. 2009, *MNRAS*, 398, 1827

Southworth, J. 2010, *MNRAS*, 408, 1689

Southworth, J., Maxted, P. F. L., & Smalley, B. 2004a, *MNRAS*, 351, 1277

Southworth, J., Zucker, S., Maxted, P. F. L., & Smalley, B. 2004b, *MNRAS*, 355, 986

Southworth, J., et al. 2009a, *MNRAS*, 396, 1023

—. 2009b, *MNRAS*, 399, 287

—. 2011, *A&A*, 527, A8

Steffen, J. H., & Agol, E. 2005, *MNRAS*, 364, L96

Steffen, J. H., et al. 2010, *ApJ*, 725, 1226

Stetson, P. B. 1987, *PASP*, 99, 191

Szabó, G. M., et al. 2010, *A&A*, 523, A84

Triaud, A. H. M. J., et al. 2010, *A&A*, 524, A25

Udalski, A., Kubiak, M., & Szymanski, M. 1997, *AcA.*, 47, 319

Udalski, A., et al. 2008, *A&A*, 482, 299

Vidal-Madjar, A., et al. 2004, *ApJ*, 604, L69

Wilson, D. M., et al. 2008, *ApJ*, 675, L113

Winn, J. N. 2010, Exoplanet Transits and Occultations, ed. Seager, S., 55–77

Winn, J. N., Holman, M. J., Carter, J. A., Torres, G., Osip, D. J., & Beatty, T. 2009, *AJ*, 137, 3826

Winn, J. N., Holman, M. J., & Fuentes, C. I. 2007, *AJ*, 133, 11

Wozniak, P. R. 2000, *AcA.*, 50, 421